ANALYSIS OF REQUIRED SUPPORTING SYSTEMS FOR THE SUPERCRITICAL CO_2 POWER CONVERSION SYSTEM

By

Rosemary M. Freas

B.S. Electrical Engineering
Old Dominion University, 2003

B.S. Computer Engineering
Old Dominion University, 2003

SUBMITTED TO THE DEPARTMENT OF NUCLEAR SCIENCE AND ENGINEERING IN PARTIAL FULFILLMENT OF THE REQUIREMENTS FOR THE DEGREE OF

MASTER OF SCIENCE IN NUCLEAR SCIENCE AND ENGINEERING
AND
NUCLEAR ENGINEER'S DEGREE
AT THE
MASSACHUSETTS INSTITUTE OF TECHNOLOGY

SEPTEMBER 2007

Signature of Author: _____
Department of Nuclear Science and Engineering
August 10, 2007

Certified by: _____
Dr. Michael J. Driscoll -Thesis Supervisor
Professor Emeritus of Nuclear Science and Engineering

Certified by: _____
Dr. Pavel Hejzlar -Thesis Reader
Principal Research Scientist; Director, Advanced Reactor Technology Program,
Center for Advanced Nuclear Energy Systems (CANES)

Accepted by: _____
Dr. Jeffrey A. Coderre
Chairman, Department Committee on Graduate Students

ANALYSIS OF REQUIRED SUPPORTING SYSTEMS FOR THE SUPERCRITICAL CO_2 POWER CONVERSION SYSTEM

By

Rosemary M. Freas

Submitted to the Department of Nuclear Science and Engineering on August 10, 2007 in partial fulfillment of the requirements for the degree of Master of Science in Nuclear Science and Engineering, and the Nuclear Engineer's Degree

Abstract

Recently, attention has been drawn to the viability of using S-CO_2 as a working fluid in modern reactor designs. Near the critical point, CO_2 has a rapid rise in density allowing a significant reduction in the compressor work of a closed Brayton Cycle. Therefore > 45% efficiency can be achieved at much more moderate temperatures than is optimal for the helium Brayton cycles. An additional benefit of the S-CO_2 system is its universal applicability as an indirect secondary Power Conversion System (PCS) coupled to most GEN-IV concept reactors, as well as fusion reactors. The United States DOE's GNEP is now focusing on the liquid Na cooled primary as an alternative to conventional Rankine steam cycles. This primary would also benefit from being coupled to an S-CO_2 PCS.

Despite current progress on designing the S-CO_2 PCS, little work has focused on the principal supporting systems required. Many of the required auxiliary systems are similar to those used in other nuclear or fossil-fired units; others have specialized requirements when CO_2 is used as the working fluid, and are therefore given attention in this thesis.

Auxiliary systems analyzed within this thesis are restricted to those specific to using CO_2 as the working fluid. Particular systems discussed include Coolant Make-up and Storage, Coolant Purification, and Coolant Leak Detection. Concepts discussed include: potential forms of coolant storage, including cryogenic and high pressure gas, with some "back of the envelope" methods which can be used for estimating the coolant transferred; possible coolant contaminants and their sources; options for the procurement of the CO_2 from potential distributors, including available purities and estimated cost; the purity of CO_2 for the S-CO_2 system and purification methods; various methods of coolant leak detection using both in-situ analyzers and portable devices for maintenance personnel, and instrumentation for the monitoring of compartmental CO_2 and CO concentrations to meet OSHA standards. A conceptual design is presented for coolant storage. Systems are discussed in terms of basic functionality, system requirements, desired features, basic safety and design concerns, and identification of issues to be resolved by future research.

Thesis Supervisor: Michael J. Driscoll
Title: Professor Emeritus of Nuclear Science and Engineering

Thesis Reader: Pavel Hejzlar
Title: Principal Research Scientist; Director, Advanced Reactor Technology Program, Center for Advanced Nuclear Energy Systems (CANES)

Acknowledgements

As with any thesis prepared about a system with a substantially developed background, collaboration between colleagues and professors proves to be an invaluable and essential tool. The author would like to recognize the technical assistance and support provided from individuals involved with this thesis' development.

Thanks to my advisor, Prof. Mike Driscoll, whose patience and support are largely responsible for the contributions contained within this thesis. His continuous stream of ideas and references were highly instrumental.

Dr. Pavel Hejzlar's strong technical understanding of the S-CO_2 PCS dynamics, and his never failing dedication to the subject were a valuable resource. Most days he could be found in his office in the late evenings still plugging away at his work; so he was usually pretty easy to find when questions arose.

Jon Gibbs' understanding of Solid Edge [2005], and numerous hours of effort resulted in most of the three dimensional drawings included within this thesis.

Thanks to Dr. Nate Carstens, a recent PhD graduate of MIT, for providing S-CO_2 PCS specifications as the system was in development.

And finally, thanks to Yunzhi Wang, an MIT undergraduate student whose work on cryogenic system design led to the conceptual cryogenic storage calculations provided in this thesis.

THIS PAGE INTENTIONALLY LEFT BLANK

Table of Contents

List of Figures

List of Tables

List of Abbreviations

AC	Alternating Current
ACGIH	American Conference for Governmental Industrial Hygienists
AFM	Atomic Force Microscopy
AGR	Advanced Gas-cooled Reactor
ANP	Advanced Nuclear Power technology program
ASME	American Society of Mechanical Engineers
CANES	Center for Advanced Nuclear Energy Systems
CEP	Chemical Engineering Progress
CFC	chlorofluorocarbon
CFR	Code of Federal Regulations
CGA	Compressed Gas Association
CNS	Central Nervous System
CRC	Chemical Rubber Company
CVR	Coolant Void Reactivity
CVS	Cardiovascular System
DC	Direct Current
DID	Discharge Ionizing Detector
DOE	Department Of Energy
DOL	Department Of Labor
EGCR	Enhanced Gas-Cooled Reactor
EPA	United States Environmental Protection Agency
EPDM	Ethylene-Propylene Diene Monomer
EPMA	Electron Probe Micro-Analysis
ETGBR	Existing Technology Gas Breeder Reactor
FID	Flame Ionization Detector
GC	Gas Chromatography
GEN-IV	Generation-IV
GFR	Gas-cooled Fast Reactor
GIF	Generation-IV International Forum
GNEP	Global Nuclear Energy Partnership
hazmat	Hazardous Material
He	Helium
HP	Hewlett-Packard
HPG	High Pressure Gas
HTR	High Temperature Reactor
ICAPP	International Congress on Advanced Nuclear Power Plants
ICONE	International Conference on Nuclear Engineering
IDLH	Immediately Dangerous to Life and Health
IG	Intergranular

INEEL	Idaho National Engineering and Environmental Laboratory
INL	Idaho National Laboratory
IR	Infrared
ISO	International Organization for Standardization
ISOPE	International Society of Offshore and Polar Engineers
ISP	Infrared Spectrophotometers
LEPC	Local Emergency Planning Committee
LFR	Lead-cooled Fast Reactor
MIT	Massachusetts Institute of Technology
MSR	Molten Salt Reactor
NDT	Nil Ductility Temperature
NERAC	U.S. DOE Nuclear Research Advisory Committee
NERI	Nuclear Energy Research Initiative
NIOSH	National Institute for Occupational Safety and Health
NIST	National Institute of Standards and Technology
O	Oxygen
OSHA	Occupational Safety and Health Administration
PEL	Permissible Exposure Limit
PHYSOR	Physics of Reactors
PSA	Pressure Swing Adsorption
PTFE	polytetrafluoroethylene
QVL	Quality Verification Levels
REFPROP	Reference Properties
REL	Recommended Exposure Limit
RGA	Residual Gas Analyzer
RPV	Reactor Pressure Vessel
SARA	Superfund Amendments and Reauthorization Act
SCWR	Supercritical-Water-Cooled Reactor
SEFOR	Southwest Experimental Fast Oxide Reactor
SEI	Safety Equipment Institute
SEM	Scanning Electron Microscope
SERC	State Emergency Response Commission
SFR	Sodium-cooled Fast Reactor
SNL	Sandia National Laboratories
STEL	Short-Term Exposure Limit
STP	Standard Temperature and Pressure (25°C / 0.1 Mpa)
TCD	Thermal Conductivity Detector
THC	Total Hydrocarbons
TID	Tube-In-Duct
TLV	Threshold Limit Value
TWA	Total Weight Average

U.S.	United States
UIG	Universal Gases Inc.
UK	United Kingdom
VHTR	Very-High-Temperature Reactor
XPS	X-ray photoelectron spectroscopy

Nomenclature

(n,p)	neutron absorption followed by proton decay
(v) or (v/v)	by volume
(w)	by weight
amu	atomic mass unit
atm	atmospheres
C	Celsius or Carbon
cfm	cubic feet per minute
cm	centimeters
CO	Carbon Monoxide
CO_2	Carbon Dioxide
CPS	Coolant (or Carbon Dioxide) Purification System
cryo	cryogenic
eff.	effective
eq	equivalent
Equil	Equilibrium
f	fraction of ICV inventory that is injectable into the PCS
g	grams
GPa	Gigapascals
h	specific enthalpy
H	Enthalpy or Hydrogen
H_2	Hydrogen Gas
H_2O	Water
hrs	hours
HTR	High Temperature Recuperator
ICV	Inventory Control Volume
ID	Inner Diameter
IHX	Intermediate Heat Exchanger
K	Kelvin
kcal	kilocalories
kg	kilograms
kPa	kilopascals
kW	kilowatts
L	liter
lb	pound
liq	liquid
LTR	Low Temperature Recuperator
m	mass or meters
mg	milligrams

min	minute
mL	milliliters
mm	millimeters
MPa	Megapascals
MW_e	Megawatts, Electric
MW_{th}	Megawatts, Thermal
OD	Outer Diameter
P	Pressure or Phosphorus
PCIV	Prestressed Cast Iron Vessel
PCS	Power Conversion System
pH	reverse logarithmic representation of relative hydrogen proton (H^+) concentration
Po_2 or ppO_2	Partial Pressure of Oxygen Gas
ppb	parts per billion
ppm	parts per million
ppt	parts per trillion
PRE	Pre-Cooler
Press	Pressure
psi	pounds per square inch
psia	pounds per square inch, absolute
psig	pounds per square inch, gauge
r	radius
s	specific entropy
S	Entropy or Sulfur
scf	standard cubic foot
S-CO_2	Supercritical Carbon Dioxide
sec	seconds
T	Temperature
t	thickness
u	specific internal energy
V or vol	Volume
vap	vapor
w/	with
w/o	without
xfer	transfer
yr	year
γ	heat capacity ratio c_P/c_V
Δ	"change in"
ΔG	Gibbs Free Energy
μm	micrometers
ρ	density

THIS PAGE INTENTIONALLY LEFT BLANK

1 Introduction

1.1 Motivation

There is a revival of interest in nuclear power for highly efficient "green" power generation. The interest is driven in part by a desire to reduce dependency on fossil fuels for both economic and environmental reasons. By the late nineties, the challenges in meeting the growing energy demand worldwide while minimizing the effect of greenhouse emissions on the planet were being widely recognized; and some countries began laying a framework for action. Seeing an opportunity for further development, nine countries entered into the Generation-IV International Forum (GIF) in January 2000: Argentina, Brazil, Canada, France, Japan, South Africa, South Korea, the United Kingdom, and the United States of America. The original nine countries in the GIF were joined by Switzerland in 2002, EURATOM in 2003, and China and Russia in late 2006. The primary GIF goals are to improve nuclear safety and proliferation resistance, minimize waste and natural resource utilization, and to optimize the profit-to-cost ratio in building and running new plants [GIF, 2007].

Pursuant to the goal of finding new nuclear energy systems for meeting future energy challenges, six designs (of approximately 100 reviewed) have been selected for concept screening by the GIF. The technologies under evaluation for future service in the GEN-IV program are diverse and include thermal neutron spectrum systems (Very-High-Temperature Reactor (VHTR) and Supercritical-Water-Cooled Reactor (SCWR)) with coolants and temperatures that enable hydrogen or electricity production with high efficiency, and fast neutron spectrum systems (Gas-Cooled (GFR), Lead-Cooled (LFR), and Sodium-Cooled (SFR) fast reactors) that will enable more effective management of actinides through

recycling of most components in the discharged fuel. Although not currently being pursued in the US, the GIF is also reviewing the Molten Salt Reactor (MSR) [GIF[(b)], 2007].

Until recently, the predominant GFR design screened has been a direct helium-cooled cycle with a desired thermal power output of 600-2400MW_{th}. In order to make the design more economically attractive, the efficiency had to be improved from the 35-39% seen in the previous GFR designs. By raising the operating point within the high temperature reactor (HTR) thermal spectrum, 850°C at 5-7MPa, the PCS gained about 10% in net efficiency – a remarkable increase. However, the allowable stress limitations at such high core outlet temperatures added impetus to the search for a cooler alternative [Handwerk, 2007].

Recently, attention has been drawn to the viability of using supercritical carbon dioxide (S-CO_2) as a working fluid in modern reactor designs. Near the critical point (T_C = 31°C, P_C = 7.29MPa), CO_2 has a rapid rise in density (see appendix B for the Mollier diagram) and reduction in compressibility, allowing a significant reduction in the compressor work of a closed Brayton Cycle. Therefore a high efficiency (> 45%) can be achieved at much more moderate temperatures (550°C) than is optimal for the helium Brayton cycles (≥850°C) [Handwerk, 2007]. By operating the S-CO_2 at a slightly higher temperature (650°C), it has been shown that efficiencies as high as 48% can be achieved [Pope, 2006]. Dostal et al. [2004] have proposed that a temperature as high as 700°C could even yield a thermal efficiency as high as 53%. An additional benefit of S-CO_2 as a working fluid is the compactness (by a factor of ~5) of the turbo-machinery due to the increased density and the non-ideal nature of CO_2 [Carstens, 2007]. Accordingly, the GIF has expanded their review to direct and indirect S-CO_2 systems. The work reported in this thesis is in support of S-CO_2 power conversion systems development.

The use of CO_2 as a working fluid in a direct system is not a new concept. Over fifty years of commercial operating experience had been obtained in England using CO_2 as the primary coolant in their thermal spectrum Magnox Reactors and Advanced Gas Cooled Reactors (AGR). In 1998, Britain and Japan banded together to evaluate a more efficient 3600MW_{th} CO_2 cooled fast reactor with enhanced passive safety features (such as a negative void coefficient) called the Enhanced Gas-Cooled Reactor (EGCR). The EGCR was an

evolved version of the UK's ETGBR, which incorporated up-to-date lessons learned into the licensing and operating process, and had a lower breeding gain (better for non-proliferation).

An additional benefit of the S-CO_2 system is its universal applicability as an indirect secondary Power Conversion System (PCS) coupled to most GEN-IV concept reactors. Table 1.1.1 shows the estimated temperatures and efficiencies for S-CO_2 cycle use in conjunction with GEN-IV concept reactors. The United States Department of Energy's (DOE) Global Nuclear Energy Partnership (GNEP) is now focusing on the liquid sodium cooled primary as an alternative to conventional Rankine steam cycles [DOE, 2007].

Table 1.1.1 Applicability of S-CO_2 Indirect Cycle to GEN-IV Reactors [Gibbs et al, 2006]

Concept	Reactor Outlet Temp	S-CO_2 Turbine Inlet T	Estimated S-CO_2 Cycle Thermal Efficiency
GFR	850°C (He)	800°C	53%
LFR	550-800°C	530-780°C	43-52%
SFR	550°C	530°C	43%
MSR	700-800°C	680-780°C	49-52%
SCWR	510-550°C	500°C	42%
VHTR	1000°C	800°C*	53%

Notes:

1. Nuclear News, Nov. 2002
2. * means limited by corrosion, and to a lesser extent by dissociation
3. IHX ΔT is 50°C for Gas/Gas, 20°C for Liquid/Gas
4. For net plant efficiency subtract approx. 4% for Gas/Gas and 2% for Liquid/Gas combinations

The S-CO_2 PCS is not limited to uses in advanced fission reactors. Recent studies conducted at MIT and in Japan have assessed the plausibility of coupling an S-CO_2 Brayton PCS to a fusion power reactor's breeding blanket via an intermediate heat exchanger (IHX) with a ΔT of 150°C [Driscoll, et. all, 2007]. This small differential temperature allows for the structural alloys to maintain their strength and corrosion resistance characteristics at modest core outlet temperatures (~600°C) without running the risk of fusion blanket liquid freeze-up.

Work on the S-CO_2 Brayton cycle is currently being conducted at MIT, under contract with Sandia National Laboratories (SNL) for larger indirect GEN-IV applications, with Lockheed-Martin for smaller applications [Hejzlar et al., 2007], and under the DOE through a Nuclear Energy Research Initiative (NERI) project grant for a direct cycle GFR [Handwerk, 2007]. In a March 6, 2007 MIT Symposium on Supercritical CO_2 Power Cycle for Next Generation Systems, participants reviewed the cycle's advantages, operation, transients, material selection, and turbomachinery and heat exchanger design considerations. However, most work to date has focused on the power cycle, with little attention paid to the required supporting systems.

1.2 Supercritical CO_2 Recompression cycle

The reference S-CO_2 recompression cycle currently being conducted at MIT, under contract with Sandia National Labs, is a 300 MW_e indirect cycle power conversion system (PCS). Figure 1.2.1 shows the basic layout for the direct or indirect S-CO_2 power conversion cycle. The design boundaries for this system are 650°C turbine inlet temperature (competitive down to 500°C), 32°C compressor inlet temperature, 20°C cooling water, ~7.7 MPa compressor inlet pressure, and 20 MPa compressor outlet pressure. [Hejzlar et al., 2007]

Also being considered are scaled versions ranging from 25 to 1200 MW_e (single-loop designs for 150 MW_e and smaller). This research presents a promising alternative to the prototypical helium-cooled GFR. More importantly, the S-CO_2 PCS can be adapted to *any* advanced reactor having a coolant outlet temperature of about 500°C.

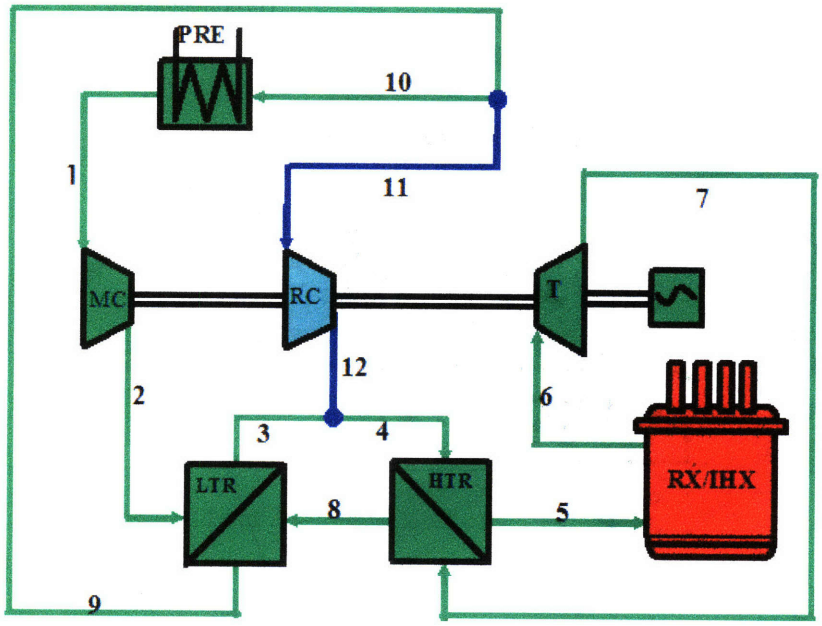

Figure 1.2.1 S-CO_2 Recompression Cycle Line Diagram [Dostal et al., 2004].

For the majority of the work presented in this thesis, this reference 300 MW_e indirect PCS is the primary focus for conceptual storage and make-up designs. However, one can assert that other ratings will use the same auxiliary systems scaled in capacity approximately proportional by power rating; except possibly for the small systems (< 50 MW_e) which will employ a direct current (DC) permanent magnet for electrical generation and an appropriate suite of other electrical systems. Additionally, direct cycle applications will be larger, with 42% more CO_2 inventory, since the primary loops are larger, and CO_2 also fills the core. According to Pope [2006], the 1200 MW_e (2400 MW_{th}) direct cycle will have about 330,000 kg CO_2 in the reactor vessel and primary loops. Using the estimate of 58,000 kg per 300 MW_e indirect loops, the 1200 MW_e indirect PCS would have about 232,000 kg.

Three-dimensional views of Pope's 1200 MW_e direct cycle are shown in Figures 1.2.2 and 1.2.3. These drawings were created using SOLID EDGE™ Version 17 [2005]. The direct cycle will also require additional chemistry control and purification due to CO_2 radiolysis and some inevitable leakage of fission products into the coolant.

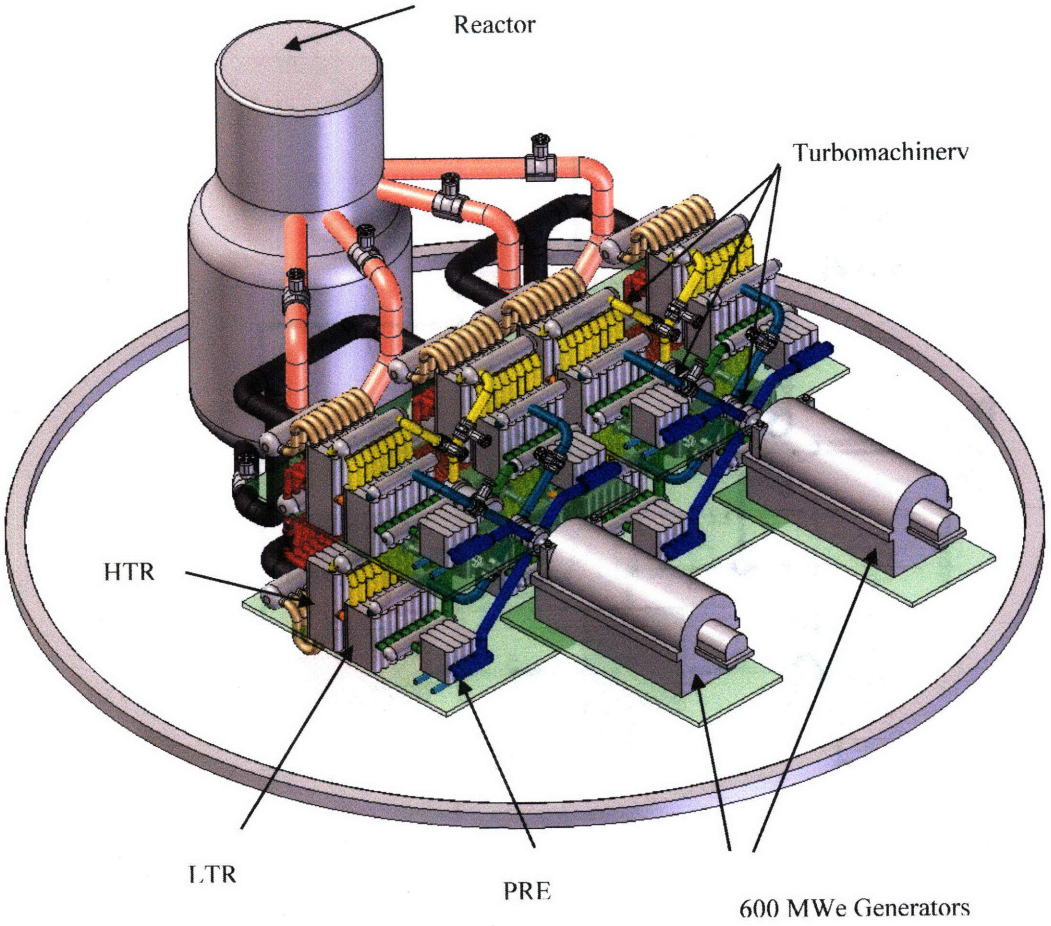

Figure 1.2.2 Isometric view of the 1200 MW_e direct S-CO_2 PCS. Four parallel 300 MW_e loops on two floors to achieve the total rated power [Gibbs, 2008].

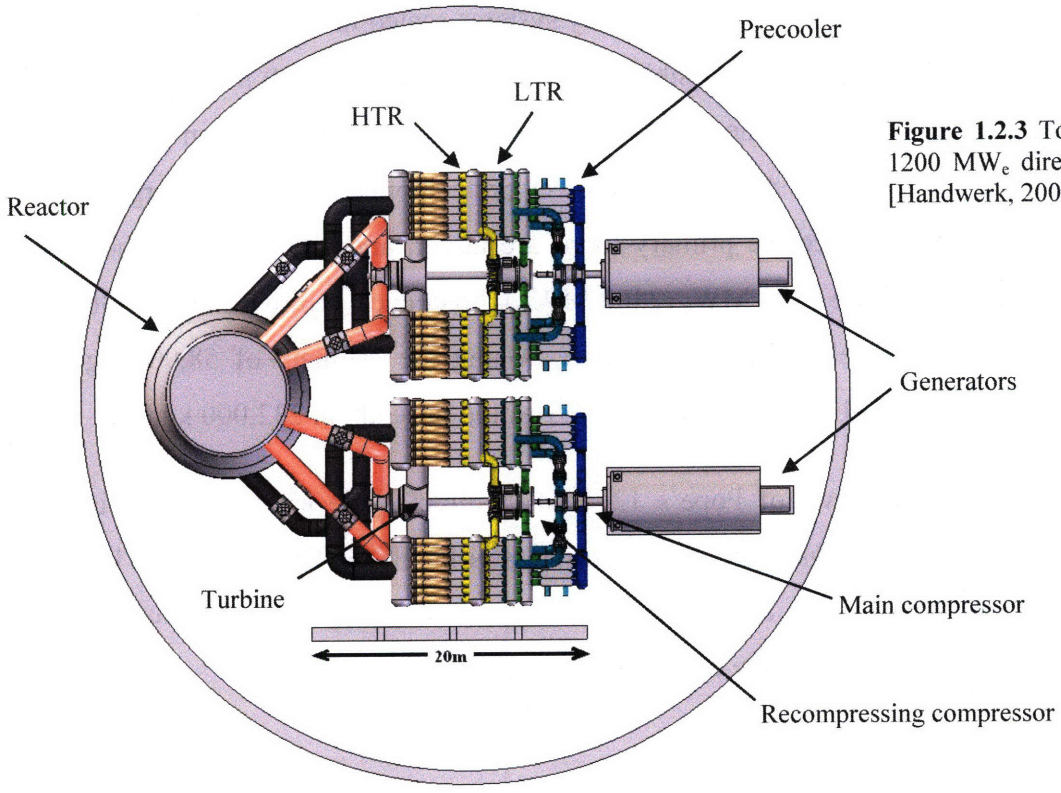

Figure 1.2.3 Top view of the 1200 MW_e direct S-CO_2 PCS [Handwerk, 2007].

1.3 Auxiliary System Requirements and Unique Features

Despite current progress on designing a Supercritical CO_2 Power Conversion System, little work has focused on the principal supporting systems required. Many of the required auxiliary systems are similar to those used in other nuclear or fossil-fired units; others have specialized requirements when CO_2 is used as the working fluid, and are therefore given attention in this thesis. Table 1.3.1 summarizes some of the principal auxiliary systems required [Harrington, 1992 and Hunt, 2002].

Table 1.3.1 Principal Auxiliary Systems Required for S-CO_2 PCS

Auxiliary System	Comments
Start-Up System	Tied into Plant Instrumentation and Control
Plant Instrumentation and Control System	Including pneumatic and hydraulic systems if non-electrical methods are preferred
Safety and Accident Mitigation System	Including autonomous control of instrumentation as well as operator response
Electrical Power Distribution System	From the Main Generator to component isolation breakers and fuses
Component Cooling System	Main Generator cooling in particular
Maintenance System	Including risk analysis, procedures and equipment
Inventory Control System	Can be integrated into the Make-up and Charging System
Coolant Make-Up and Charging System	Store, transfer, and possibly purify coolant
Coolant Purification System	Direct and Indirect cycles should be considered. Including a Waste Discharge System
Coolant Leak Detection System	Local, compartmental, and portable monitoring.

Generic Auxiliary Services Systems

Start-up System

As in any large scale plant, operations cannot commence without a start-up system. In some cases, the system consists of manual plant configuration changes by plant operators. In sensitive direct and indirect nuclear systems, however, a more robust, partially autonomous modern digital start-up system, with redundant safety features is required. This system will likely be tied into the plant instrumentation, control, safety, and accident mitigation system.

Plant Instrumentation, Control, Safety, and Accident Mitigation Systems

The plant control and protection systems should be designed with a high degree of automation; the need for operator intervention would need to be intentionally reduced. The Plant Control System and other distributed controls need to accommodate transients resulting from the loss of major plant components and to keep the plant operating with parallel equipment. The Reactor Protection System should be independent and designed to override the Plant Control System to maintain reactor safety. However, the operator should be able to assume manual control at any time, with some restrictions on his or her freedom of action as appropriate for safety. For example, the operator could not negate an automatic safety signal to shut down the reactor plant, or reactor trip.

Electrical Power Distribution System

The S-CO_2 power conversion unit will need to include the following main electrical systems to provide electrical power to other plant systems as required under all plant conditions:

1. Plant AC and DC Electrical Systems.
2. Plant Uninterruptible Power Supply System.
3. Lighting and Service Power System.
4. Grounding System.
5. Lightning Protection System.
6. Cathodic Protection System.
7. Heat Tracing System.
8. Standby Power Supply.

Component Cooling System

The component cooling train should provide cooling to the low temperature absorbers of the carbon dioxide purification train, analytical instruments in the Plant Instrumentation and Control and the Safety and Accident Mitigation Systems, and the Main Generator which will generate a significant amount of heat.

The component cooling train should normally operate on a continuous basis except when it must be shut down for maintenance, and includes separate trains to serve the individual systems. The major components of each train would likely be cooling fluid re-condensers, pumps, a phase separator storage tank, and interconnecting piping.

In the event that the component cooling systems serves the shaft seals and bearings, this would require the incorporation of a very important set of specific S-CO_2 requirements. If this becomes the case, future work beyond this thesis should ensue.

Maintenance System

The overall maintenance strategy is to provide the highest level of operability and availability of plant equipment consistent with safety, long-term cost, and production goals. This strategy requires some optimization since some preventive maintenance activities may preclude continuous plant operation. The strategy requires an iterative process in which operability, reliability, availability, maintainability, and safety goals are continually assessed during the design. Determinations of failure rates and equipment availability should be integrated into the program.

A list of items or components which are important to plant safety and availability is the starting point for a maintenance program assessment. The principal use of the list is to prioritize preventive maintenance actions. The time required for detecting, diagnosing, and repairing failures is first provided for the most essential items. When the essential components are identified, the principal failure modes that govern their likely failure rates, and repair times, are determined. These failure modes will usually be identified with the failure of a specific subcomponent part, or assembly, which in turn will require a sequence of tasks to verify, extract, and repair. A task analysis is then used to determine procedure

requirements, material, personnel, schedules and cost commitments associated with each maintenance job or task.

In support of the required maintenance tasks, proper equipment will need to be made available. Systems capable of safely moving heavy equipment, such as cranes and lifts, will be required. In addition to written step-by-step procedures, the maintenance personnel should have access to OSHA approved safety gear, warning signs/alarms, proper tools, and thorough standardized training.

Auxiliary Services Systems Specific to Using Carbon Dioxide

The CO_2-specific service systems consist of components and structures which make up the carbon dioxide storage and transfer trains, carbon dioxide purification trains and regeneration equipment, and local and compartment CO_2 leak monitoring systems.

Carbon Dioxide Make-Up and Charging System

The Coolant Make-Up and Charging System consists of one CO_2 storage and transfer train per loop. The storage system can be High Pressure Gas (HPG), Cryogenic, or a combination of the two.

Functions of the carbon dioxide make-up and charging train include

- transfer carbon dioxide to the power conversion system during pressurization and up-power operations,
- transfer and store coolant from the power conversion system during depressurization and down-power operations, and
- supply make-up carbon dioxide to the power conversion system to compensate for losses due to leakage, corrosion, radiolysis (direct cycle), and vented gases.

Carbon Dioxide Purification

The carbon dioxide purification trains consist of a specific sequence of gas processing components, plus related piping, valves, controls, and instrumentation designed to purify carbon dioxide for each loop during normal operation. The carbon dioxide purification trains are side-streams which run in parallel with the main PCS loop. Their purpose is to remove chemical impurities in order to maintain their concentration in the coolant within prescribed limits. They also remove the gas-borne radionuclides contained in the side-stream flow in direct cycles. The CPS is principally required for the removal of chemical impurities from the coolant, since elevated concentrations of these impurities could corrode or impinge system components. The purification system may also incorporate the addition of chemicals in small amounts to help control corrosion and suppress radiolysis. The system could also be used to purify carbon dioxide before it is transferred to storage during PCS depressurization or vice versa.

The Coolant Purification System (CPS) removes a small percentage of carbon dioxide from the PCS loop, processes it to remove impurities, and returns the purified carbon dioxide to the loop. Since only a portion of the CO_2 is redirected for purification in each cycle, it will take multiple passes to turn over one complete system volume. The side-stream flow rate required to purify 100% PCS inventory in a sufficient time period needs to be determined.

Coolant Leak Detection System

Similar to any system operating above atmospheric pressure, proper inventory control of the coolant is crucial. Since the PCS described relies on inventory control as a mechanism of power changes as well as cooling, strict monitoring for leaks must be a priority. Radiolysis (in a direct cycle) and corrosion will undoubtedly generate some carbon monoxide (CO) from the CO_2 [Rigual, 2004]. Due to the dangerous nature of CO_2 and CO to personnel, compartment monitoring will also be required. Therefore, the leak detection system will monitor for localized leaks as well as large scale compartment levels.

1.4 Objectives of the Present Work

The objective of this thesis is the evaluation of the requirements, and discussion of conceptual designs for the principal supporting systems required for both direct and indirect S-CO_2 cycles. Auxiliary systems analyzed are restricted to those specific to using CO_2 as the working fluid. These systems include the coolant make-up and storage system, coolant purification, and coolant leak detection systems. Systems will be discussed in terms of basic functionality, system requirements, desired features, basic safety and design concerns, and identification of issues to be resolved by future research.

1.5 Selected Previous Works at MIT

As mentioned earlier, much progress has been made on the S-CO_2 by previous contributors which deserve mention. In the last year alone, the S-CO_2 PCS has picked up more steam prompting significant contributions by the following individuals:

- Michael Pope's [2006] thermal hydraulic design of a 2400 MW_{th} direct supercritical CO_2-cooled fast reactor;
- Jon Gibbs' [2006, and 2008] applicability of supercritical CO_2 power conversion systems to GEN-IV reactors and Power Conversion System Design for Supercritical Carbon Dioxide Cooled Indirect Cycle Nuclear Reactors (forthcoming);
- Chris Handwerk's [2007] core design and performance assessment for a supercritical CO_2-cooled fast reactor;
- Nate Carstens' [2007] control strategies for supercritical carbon dioxide power conversion systems; and
- Pavel Hejzlar et al.'s [2007] power conversion system design for supercritical carbon dioxide-cooled indirect Brayton cycle for medium power applications.

1.6 Organization of this Thesis

Chapter 2 describes potential forms of coolant storage for power-change operations and make-up. Two methods of storage are discussed and compared; cryogenic and high pressure gas. Simple "back of the envelope" methods for determining the mass transfer capability of the high pressure gas system suitable for use by plant operators are developed and compared against RELAP5-3D [INL[(b)], 2005] simulations.

Chapter 3 discusses the potential contaminants in the coolant from impurities in make-up coolant, from general corrosion in the system components and piping, and from imperfect seals on system components. Options for the procurement of the CO_2 are discussed including available purities and cost. Purity considerations for the S-CO_2 system, and potential purification methods are also discussed. A brief review of special considerations in direct cycle applications is also presented, e.g. radiolysis and N-16 produced in CO_2 oxygen by (n,p) reactions.

Chapter 4 describes the various methods of coolant leak detection using both in-situ monitors and analyzers, and portable devices for maintenance personnel. This chapter will cover instrumentation sensitivity requirements for detecting small scale leaks into both the surrounding compartment's environment and into the primary loop via the Intermediate Heat Exchanger (IHX). Instrumentation for the monitoring of compartmental CO_2 concentrations to meet Occupational Safety and Health Administration (OSHA) standards and prevent asphyxiation or CO poisoning of maintenance personnel conducting routine or emergency operations is also discussed.

Chapter 5 summarizes the findings of this work and identifies several areas where future work is needed.

2 Coolant Make-up and Charging Systems

2.1 Introduction and Motivation

A gas storage complex is the major auxiliary system required in support of an S-CO_2 PCS. Sufficient CO_2 mass must be available on site for system fill, emptying, and leakage make-up. Free capacity is also necessary to accommodate PCS inventory control for power change operations.

A generic estimate of 58,000 kg of CO_2 in a 300 MW_e PCS will be assumed for design development purposes. In consideration of a required capability to completely discharge or fill the PCS, as well as maintain a 100 day's supply for leakage make-up (for a daily leak rate estimated to be 0.5% per day, or 290 kg/day per 300 MW_e loop), this thesis shows the estimated volumes of the prospective storage systems required to transfer and contain 150% of the PCS-full-power-mass, or 87,000 kg for a 300 MW_e PCS.

Two methods are employed in practice: high pressure canisters and cryogenic tanks. If the high pressure canisters were pressed up to 20 MPa with CO_2 and allowed to reach an ambient temperature of about 27°C (300K), the density of the CO_2 in the tanks would be about 905 kg/m^3. Thus to store 87,000 kg of CO_2, 96 m^3 of tank volume would be required. This thesis will show that without such compression, ~460 m^3 of high pressure gas (HPG) storage would be required depending on the tank sizes and desired equilibrium pressures during transfer.

The second possible storage method is liquid CO_2 (cryogenic) tanks operated typically at around -20°C. This, for example, is the approach taken at the MIT Research Reactor (where CO_2 is used to displace air from the graphite reflector). The CO_2 is supplied

by tanker trucks and stored in an insulated Dewar tank located outside the facility. Advantages of this method include the modest operating pressure (about 2 MPa at saturation) and high fluid density, about 1030 kg/m^3. Allowing for a 20% volume gas-space, the effective density is ~900 kg/m^3 – about the same as 20 MPa HPG storage. The designed cryogenic tank presented in this thesis has a volume of 116 m^3 in order to contain the required 150% PCS-full-power-mass.

It is likely that the final system design will include both types, based on the following considerations:

1. Compressed gas is more amenable to cycle inventory control. A cylinder at 15 MPa can receive gas from the 20 MPa main compressor outlet and return it to the pre-cooler inlet at 8 MPa using only control valves -- and no compressor. However, only part of the HPG can participate in the transfer (~30%).

2. Liquid (cryogenic) CO_2 can be sprayed into the pre-cooler inlet plenum by a compressor, and the full tank inventory is extractable.

3. Some CO_2 purification can be accomplished in either mode (or a combination) by condensing the cryogenic vapor or by membrane filtration of the HPG.

4. Larger capacity single tanks can be used for cryogenic storage while the HPG method will require a bank of smaller tanks.

With respect to HPG tank volumes, the largest commercial HPG canisters identified to date are 25 MPa vessels, 1 m ID, 36 m in length, for a volume of about 28 m^3 (manufactured by Europipe) [Gräf et al, 2003]. On the other hand, Shropshire [2004] reports use of 52 m^3 CO_2 liquid tanks at the UK's AGR installations.

2.2 High Pressure Gas (HPG) Storage Method

Discharging the PCS:

Based on Carstens' work [2007], about 20,000 kg (~1/3rd) of the CO_2 must be removed from the reference 300 MW_e S-CO_2 Power Conversion System (PCS) in order to decrease the plant power to 50% using inventory control. It would be desirable to accomplish this task without additional auxiliary compressors in a HPG storage system. Figure 2.2.1 shows the simple schematic of this HPG storage system with connections to the PCS and no auxiliary compressor. In Carstens' [2007] inventory control specifications, the 300 MW_e PCS CO_2 removal/addition flow rate does not exceed 10 kg/sec when using inventory control for power changes. The flow rate out of the main compressor at full power is about 1700 kg/sec [Carstens, 2007], therefore the flow diverted to storage will require throttling.

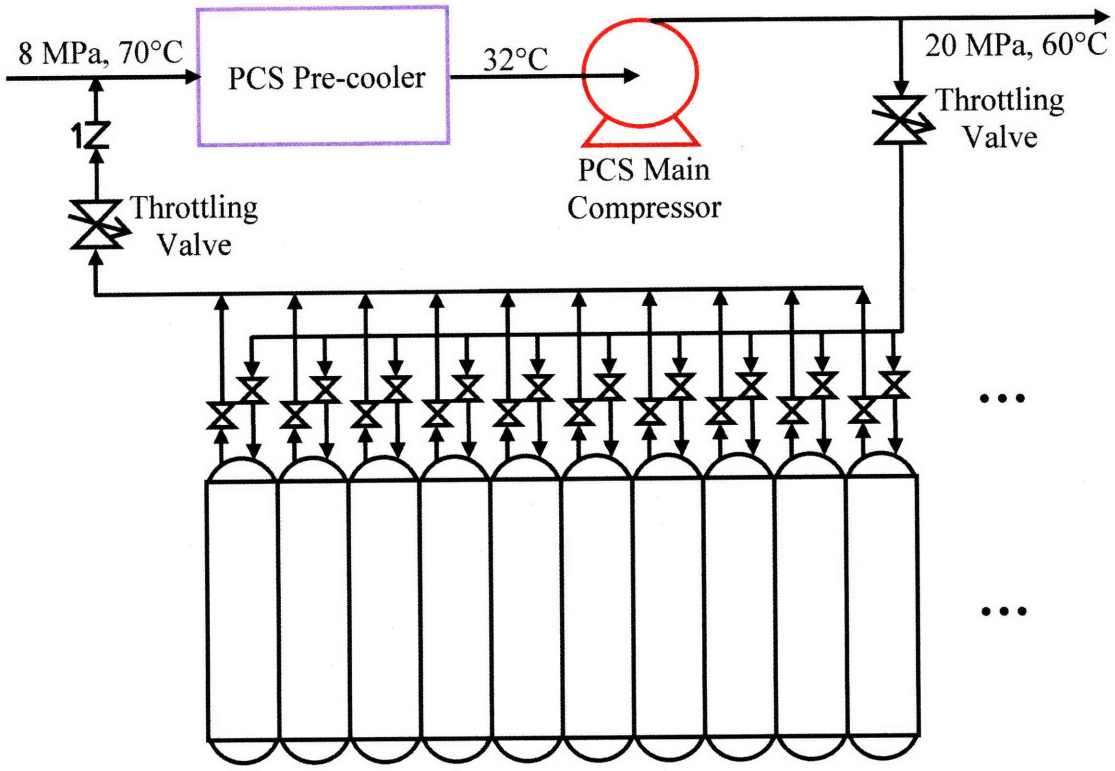

Figure 2.2.1 Proposed HPG storage system schematic for make-up and inventory control, without an additional compressor.

If the 20 MPa PCS is allowed to discharge into inventory control storage initially at 8 MPa, using the main compressor's outlet pressure as the driving force, an estimate of the amount of CO_2 that could be transferred is needed in order to determine the total tank volume required for such a power change.

Initial estimates were made doing a simple mass balance to obtain a ball-park value for the desired equilibrium pressure. All temperatures were assumed constant at the temperature of the main compressor outlet, which varies in Carstens' design from ~61°C to 74°C. For the purpose of simulation, an estimated temperature of ~60°C (or 333K) was used. Table 2.2.1 shows the mass balance results. From these results, one can see that an equilibrium pressure of approximately 12.5 MPa is estimated to transfer 20,000 kg. However, the assumption that the temperatures would remain constant is not accurate. Additionally, an equilibrium pressure of 12.5 MPa may not be high enough for recharging a sufficient amount of CO_2 into a pre-cooler at 8 MPa without an additional compressor. A more reliable method of determining the amount of mass transferred is needed. Also keep in mind that the actual volume of the PCS is not 80.14 m^3. The pressure and temperatures for the main compressor outlet were used along with the actual mass contained within the PCS at 100% power. These values yield an effective PCS volume for the purpose of simulation.

Table 2.2.1 Simple mass balance for emptying the PCS into a Storage Complex

PCS Mass (kg)	ρ @ 8MPa (kg/m^3)	ρ @ Equil Pressure (kg/m^3)	ρ @ 20MPa (kg/m^3)	eff. PCS Volume (m^3)	ICV Volume (m^3)	Δmass (kg)	Equil Press (MPa)
58000	191.67	357.98	723.81	80.14	176.26	29314.5	11
58000	191.67	434.67	723.81	80.14	95.35	**23169.2**	**12**
58000	191.67	505.61	723.81	80.14	55.69	**17484.7**	**13**
58000	191.67	561.6	723.81	80.14	35.14	12998.1	14
58000	191.67	604.29	723.81	80.14	23.21	9577.3	15
58000	191.67	637.68	723.81	80.14	15.47	6901.7	16
58000	191.67	664.75	723.81	80.14	10.00	4732.6	17
58000	191.67	687.39	723.81	80.14	5.89	2918.4	18
58000	191.67	706.82	723.81	80.14	2.64	1361.4	19

The second phase of ICV design was determining the effect of equilibrium pressure and CO_2 transferred when changes in temperature are considered. Using RELAP5-3D (described in appendix A), the mass transfer of the 300 MW_e PCS CO_2 into a 28 m^3 high pressure gas (HPG) Inventory Control Vessel (ICV) (similar to the tanks made by Europipe) was simulated. Figures 2.2.2 and 2.2.3 show the equilibrium pressure and mass transfer trends given by RELAP5.

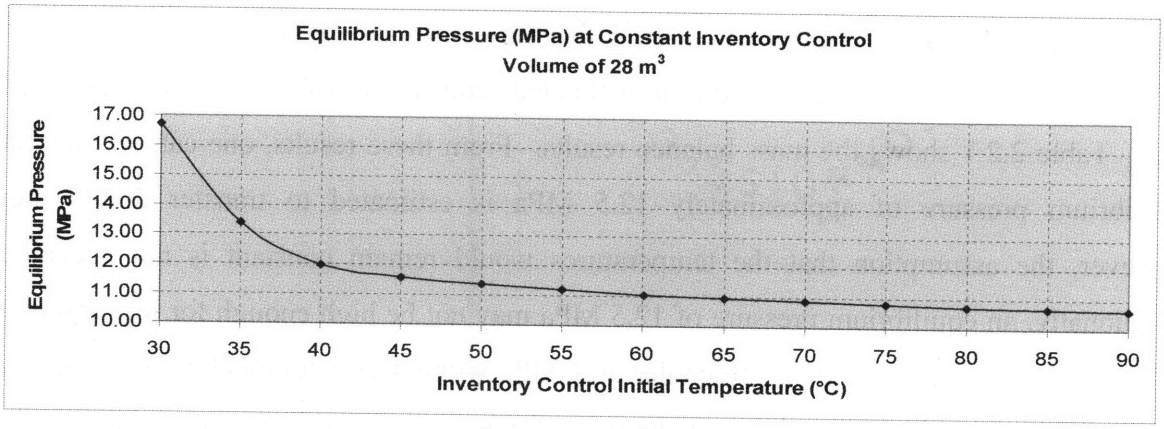

Figure 2.2.2 Effect on Equilibrium Pressure of Changing ICV Initial Temperature for emptying PCS

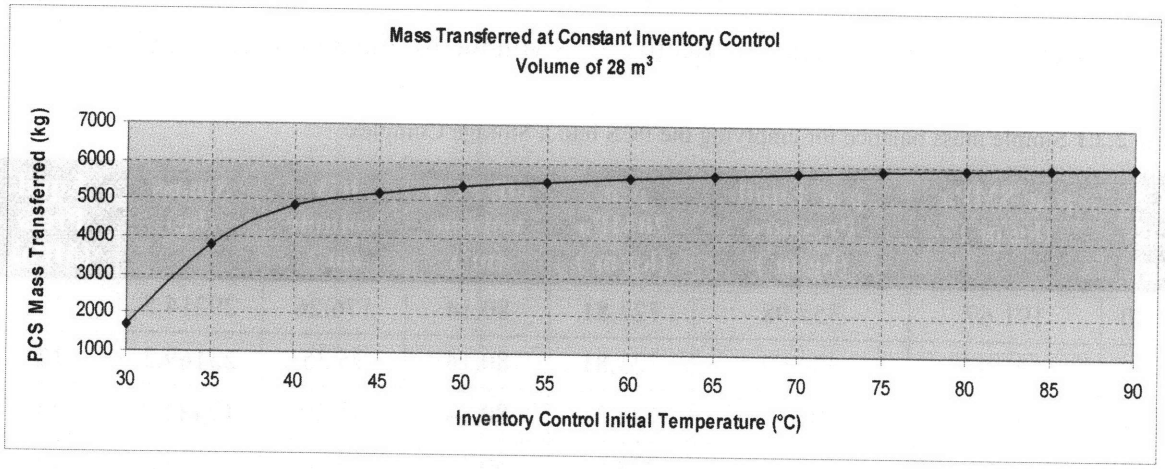

Figure 2.2.3 Effect on Mass Transferred of Changing ICV Initial Temperature for emptying PCS

Since both the PCS and ICV temperatures simulated by RELAP5 were allowed to vary as they would in a real working system, the results are closer to what could be expected. From the crude mass balance estimation, a 28 m^3 tank should accept the transfer of about 10,000 kg. However, one can see from figure 2.2.3 that the mass balance method of

determining the mass transfer capability was far too optimistic. As the initial ICV temperatures reach 90°C, the mass transferred levels off to a maximum of about 6000 kg. Additionally, the equilibrium pressure at these temperatures reaches as low as 10.5 MPa which would most likely not provide a large enough pressure head for re-injecting a significant amount of the CO_2 into the pre-cooler inlet (8 MPa) without a compressor.

With this in mind, it was decided that an equilibrium pressure of approximately 15 MPa would be the reference target value for charging the HPG ICV. From figure 2.2.2, this would require an initial temperature in the ICV of about 32.5°C. (This low initial temperature will become handy in a moment.) Hence, another simulation was run to determine the effect of varying the ICV volume. Figures 2.2.4 and 2.2.5 show the trends found using a consistent initial ICV temperature of about 70°C, the approximate temperature at which figures 2.2.2 and 2.2.3 seem to level off (so as to not influence the results).

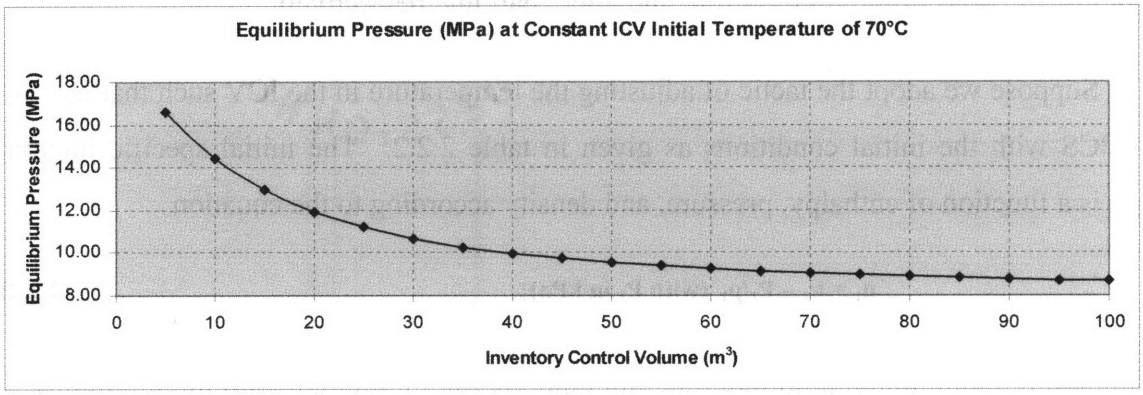

Figure 2.2.4 Effect on Equilibrium Pressure of Changing ICV Volume for emptying PCS

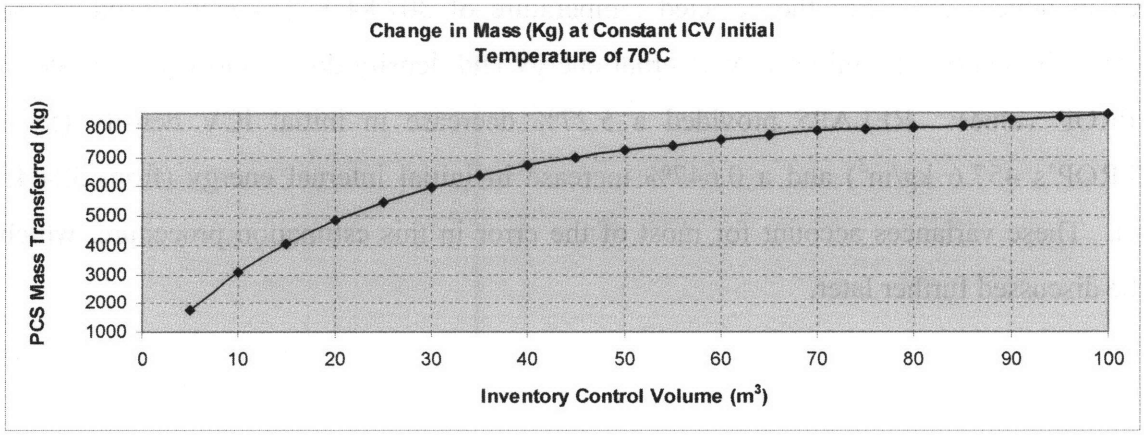

Figure 2.2.5 Effect on Mass Transferred of Changing ICV Volume for emptying PCS

From these preliminary RELAP5 results, one can see that a reduction in ICV volume or initial ICV temperature results in a higher equilibrium pressure to assist in the re-injection back into the pre-cooler. The trade off in doing so is a reduced mass transfer capability; therefore a balance must be achieved. For the RELAP5 simulation discussed next, a 10 m^3 ICV was used. Following the simulation results will be a comparison of the equilibrium pressures and mass transferred using 10, 15, 20, 25, and 28 m^3 vessels.

Many thermo-hydraulic text books treat filling of a vessel from a line using the following energy transfer equation:

$$h_{in}^* (m_2 - m_1) = m_2 u_2 - m_1 u_1 \qquad (2.2.1)$$

where h_{in} represents the enthalpy of the fluid entering the vessel, m_1 and m_2 are the masses of fluid in the vessel before and after charging, respectively, and u_1 and u_2 are the internal energies of the fluid in the vessel before and after charging, respectively.

Suppose we adopt the tactic of adjusting the temperature in the ICV such that $u_1 = h_{in}$ for a PCS with the initial conditions as given in table 2.2.2. The initial specific internal energy is a function of enthalpy, pressure, and density according to the equation

$$u_1 = h_1 - P_1/\rho_1 \text{ (with } P_1 \text{ in kPa)} \qquad (2.2.2)$$

and density is also a function of pressure and temperature. Using REFPROP an initial ICV temperature can easily be selected that will allow $u_1 \approx h_{in}$. The results using REFPROP are shown in table 2.2.3. For the selected temperature of 307.84°K (34.71°C) used in the RELAP5 simulation, the initial ICV internal energy and density do not closely correlate to REFPROP values: RELAP5 provided a 5.27% decrease in initial ICV density (from REFPROP's 457.6 kg/m^3) and a 0.647% increase in initial internal energy (from 324.45 kJ/kg). These variances account for most of the error in this estimation procedure, which will be discussed further later.

Table 2.2.2 State Points from RELAP5 Simulation for emptying the PCS into a Storage Complex

	ICV		PCS	
	Initial	Final	Initial	Final
Press (MPa)	8.00	16.68	20.00	16.68
Temp (K)	307.84	337.52	333.13	327.44
Density (kg/m^3)	433.50	619.24	722.83	701.58
Enthalpy (kJ/kg)			324.45	
Internal Energy (kJ/kg)	326.55	322.61		
Volume (m^3)	10.00		80.15	

Table 2.2.3 Determination of initial ICV Temperature using REFPROP for emptying PCS into Storage

T (K)	P (MPa)	ρ (kg/m^3)	u (kJ/kg)	h (kJ/kg)
333.13	20.000	723.81	296.82	324.45
307.84	8.0000	457.61	324.45	341.93

By selecting a temperature in this manner such that $u_1 \approx h_{in}$ one can see from equation 2.2.1 that $u_1 \approx u_2$, allowing us to treat the charging of the ICV as a constant specific internal energy process. From the data shown in figure 2.2.6, one can see that RELAP5 confirms this assumption. The overall change in ICV internal energy is 1.21%, which is essentially constant. With the assumption that the ICV's gas-specific internal energy is essentially unchanged, two NIST plots (figures 2.2.7 and 2.2.8) were generated for CO_2 in order to demonstrate a rather easy interpolation method to "pick off" points and estimate the amount of mass transferred.

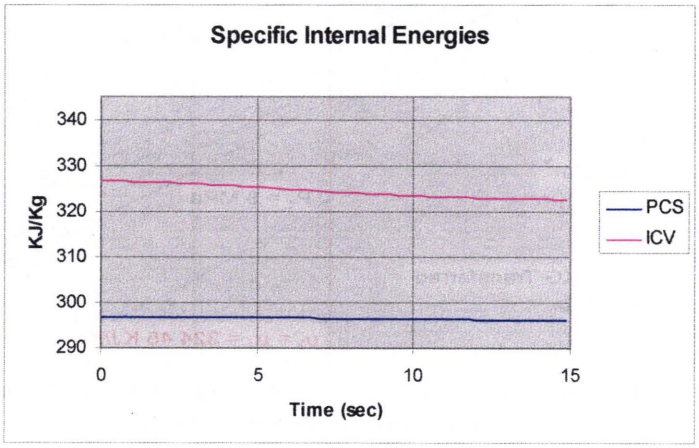

Figure 2.2.6 Internal Energy from the RELAP5 simulation for charging the ICV from the PCS. The process is essentially at constant internal energy $u_{ICV} \approx 325$ kJ/kg.

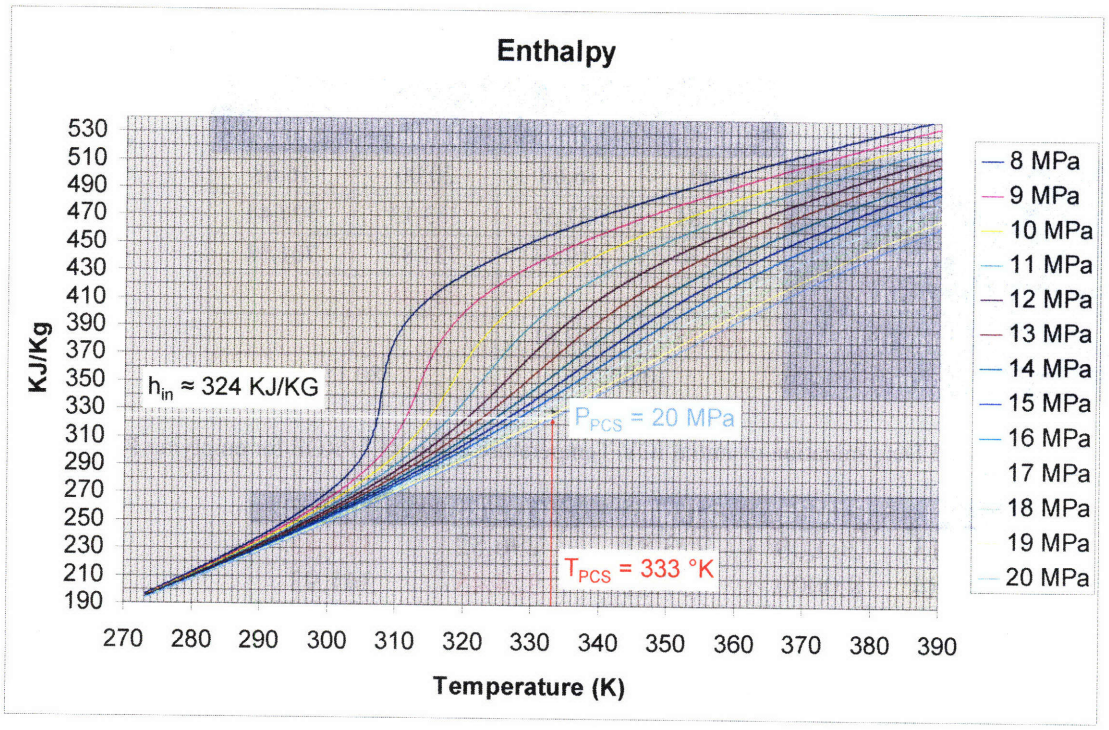

Figure 2.2.7 NIST h-T/P plot used in "pick-off" method for PCS Discharge. Enthalpy vs. Temperature at varying Pressures for CO_2.

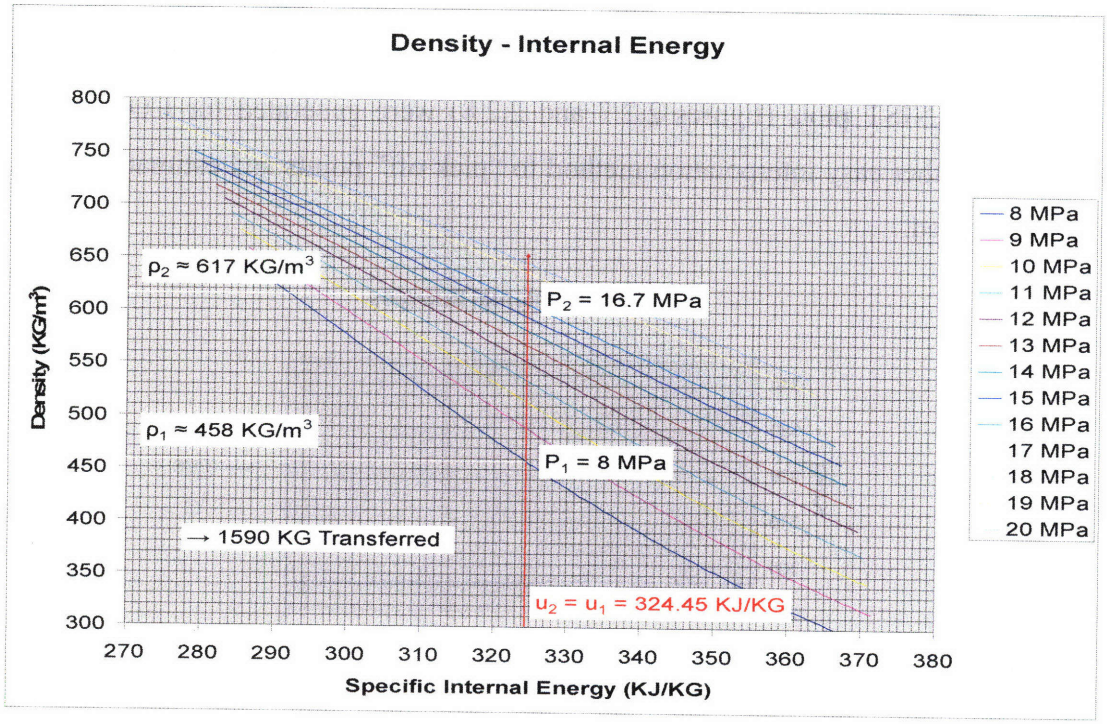

Figure 2.2.8 NIST ρ-u/P plot used in "pick-off" method for PCS Discharge. Density vs. Specific Internal Energies at varying Pressures for CO_2. Using the constant internal energy conditions for the ICV, the quantity of mass transferred is estimated to be 1590 kg for a 10 m^3 ICV.

Referring to figure 2.2.8, for a constant ICV internal energy of ~324 kJ/kg, the quantity of mass transferred is estimated to be 1590 ± 10 kg for a 10 m^3 ICV. Compare this to the $\Delta\rho$ found in RELAP5 of 170.27 kg/m^3 for a mass transferred of 1702.7 kg (approximately a 7% difference).

There are three types of errors introduced by using this method which may account for the 7% difference between the RELAP5 simulation and the subject interpolation method. As can be seen in the data presented in figure 2.2.6, the gas-specific internal energy begins at a value of 326.55 kJ/kg and decreases by as much as 1.21% to a value of 322.61 kJ/kg. The second error is introduced from the graph interpolation. Using a protractor for increased precision, one can extract values from figures 2.2.7 and 2.2.8 with the approximate accuracies listed below in table 2.2.4. The accuracy ranges of temperature, pressure, enthalpy, and internal energy lead to a variability of ± 10 kg/m^3 in density; a possibility for 0.6% error.

Table 2.2.4 Precision of PCS Discharge interpolation method

Variable	Accuracy Range using Protractor
Temperature	± 0.2 K
Pressure	± 0.2 MPa
Enthalpy	± 2 kJ/kg
Internal Energy	± 2 kJ/kg
Density	± 10 kg/m^3

In this particular simulation, it appears that the difference in RELAP5 computed initial ICV density may contribute the most to the error. As mentioned earlier, RELAP5 provided a significant 5.27% decrease in the expected initial ICV density. By careful inspection of figure 2.2.8 one can see that the NIST plot also gives excellent correlation to the REFPROP density at P_1. Two similar RELAP5 runs were conducted to test for possible causes of the large difference between RELAP5 and NIST/REFPROP initial densities. The first method was to allow a 100 second stabilization period before starting the CO_2 transfer to see if the initial density would stabilize closer to the values provided by both NIST and REFPROP. This test proved that the initial ICV density provided by RELAP5 was not transient, but possibly due to the variety of interpolation methods used by RELAP5 in determining property values. The second test run used an initial PCS temperature increased

by 10°C in order to push the initial ICV state slightly further above the "dome" (further above the critical point of T = 31°C, P = 7.29MPa; see the Mollier diagram in appendix B). When the new initial ICV temperature of 309.18°K (36.05°C) was applied to the RELAP5 run, a 5.05% *increase* from the NIST REFPROP initial ICV density was observed. It appears that the varied interpolation methods used by RELAP5 cause large fluctuations in density when operating close to the critical point. This fluctuation of RELAP5 densities thus needs further investigation. If the NIST REFPROP state points are assumed to be most reliable, these results indicate that our subject method may actually give more accurate results than the RELAP5 confirmation run.

For larger ICV volumes under the same procedure, the following equilibrium pressures and CO_2 kg transferred would be obtained (table 2.2.5). Blank NIST plots similar to those used here are included in appendix A and can be used for any ICV volume chosen.

Table 2.2.5 PCS Discharge - Equilibrium Pressures and CO_2 kg transferred for varied ICV Volumes

ICV Volume (m3)	Equilibrium Pressure (MPa)	Mass Transferred (kg) by RELAP5	Mass Transferred (kg) by subject method	Percent Difference (%)
10	16.68	1702.73	1590 ± 10	7.1
15	15.55	2327.99	2130 ± 10	9.3
20	14.65	2945.63	2600 ± 10	13.3
25	13.92	3462.05	3025 ± 10	14.4
28	13.55	3703.67	3220 ± 10	15.0

Charging the PCS:

It appears advisable to insulate and trace heat the HPG tank to maintain a high enough pressure to allow recharging via the pre-cooler inlet. The main compressor outlet operates at about 20 MPa, 60°C (333K). Isenthalpic throttling to about 15 MPa as demonstrated above gives a final ICV temperature of 60°C (333K). If the tanks were allowed to cool to room temperature (27°C or 300K), the pressure would drop. But the system needs to be able to inject the stored gas into the pre-cooler inlet which operates at 8 MPa. This throttling process, assuming no heat was lost, would inject ~35°C CO_2 into a pre-cooler inlet operating at 70°C. Note that these estimates are only at the start of each process, and charging or discharging the PCS will change the PCS pressure. Hence, a more sophisticated analysis is required.

Using RELAP5, the mass transfer of Carbon Dioxide from an Inventory Control Vessel (ICV) into the 300 MW_e S-CO_2 Power Conversion System (PCS) was simulated. Table 2.2.6 shows the simulation initial and final state points. Notice that the initial ICV temperature is about 69°C assuming that the tanks are well insulated and trace heated in an attempt to maintain the tank pressure at about 15 MPa. From the data shown in figure 2.2.9, one can see that RELAP5 confirms what most thermo-hydraulic textbooks assume: the process is essentially isentropic for emptying the ICV. With the assumption that the ICV's internal gas specific entropy is essentially unchanged, NIST plots (figures 2.2.10, 2.2.11) were generated for CO_2 in order to demonstrate a rather easy interpolation method to "pick off" points and estimate the amount of mass transferred.

The simulation discussed here treats the PCS as an infinite volume with unchanging pre-cooler inlet (the injection point) thermo-hydraulic parameters. As can be seen by the Gas-Pass simulation [Carstens, 2007] for charging the PCS, the control module maintains the pre-cooler inlet pressure at approximately 8 MPa for PCS power as low as 40%. Thus it can be assumed that the PCS pre-cooler inlet parameters are independent of the changes in the ICV during charging. Setting the PCS pre-cooler inlet pressure to 8 MPa in the RELAP5 simulation gives a conservative estimate of the CO_2 mass that can be transferred.

Table 2.2.6 State Points used in RELAP5 Simulation for filling PCS from Storage Complex

	ICV		PCS	
	Initial	Final	Initial	Final
Press (MPa)	14.47	8.00	8.00	8.00
Temp (K / °C)	342.09 / 69	309.51 / 36	343.13 / 70	343.13 / 70
Density (kg/m^3)	489.26	359.18	173.98	173.98
Volume (m^3)	10.00		infinite	

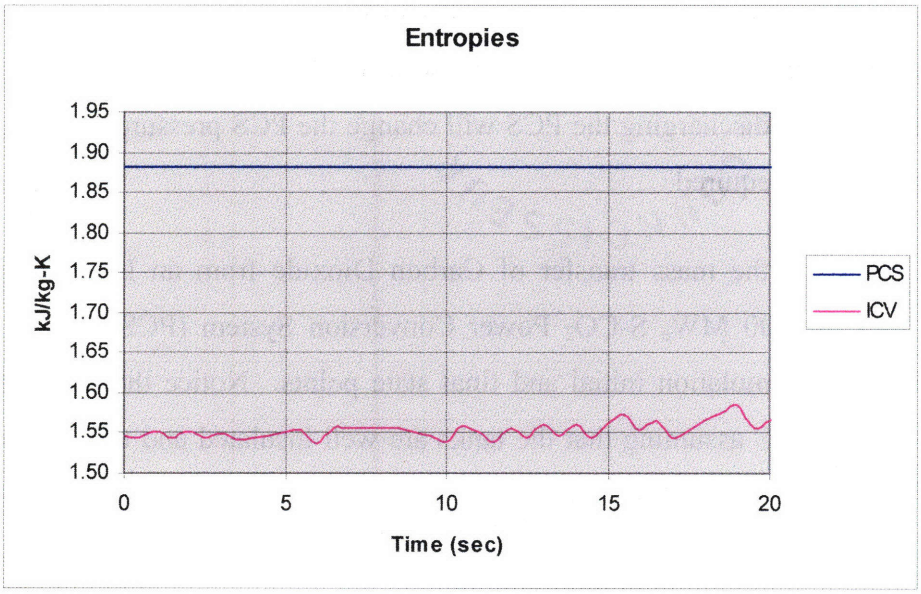

Figure 2.2.9 REFPROP Entropy from using the P/Ts in the RELAP5 simulation for filling the PCS. The process is essentially isentropic at $s_{ICV} \approx 1.55$ kJ/kg-K.

Referring to figure 2.2.10 for an initial ICV temperature/pressure of 342.09K/14.47 MPa, the specific entropy is 1.546 ± 0.010 kJ/kg-K. Using this value of s_{ICV} on figure 2.2.11, and the initial and final pressures, the change in density in the ICV $\Delta\rho = -125 \pm 5$ kg/m^3. This means (for a 10 m^3 ICV) that the amount of mass transferred to the PCS is about 1250 ± 50 kg. Compare this to the $\Delta\rho$ found in RELAP5 of 130.06 kg/m^3 for a mass transferred of 1300.6 kg (approximately a 4% difference).

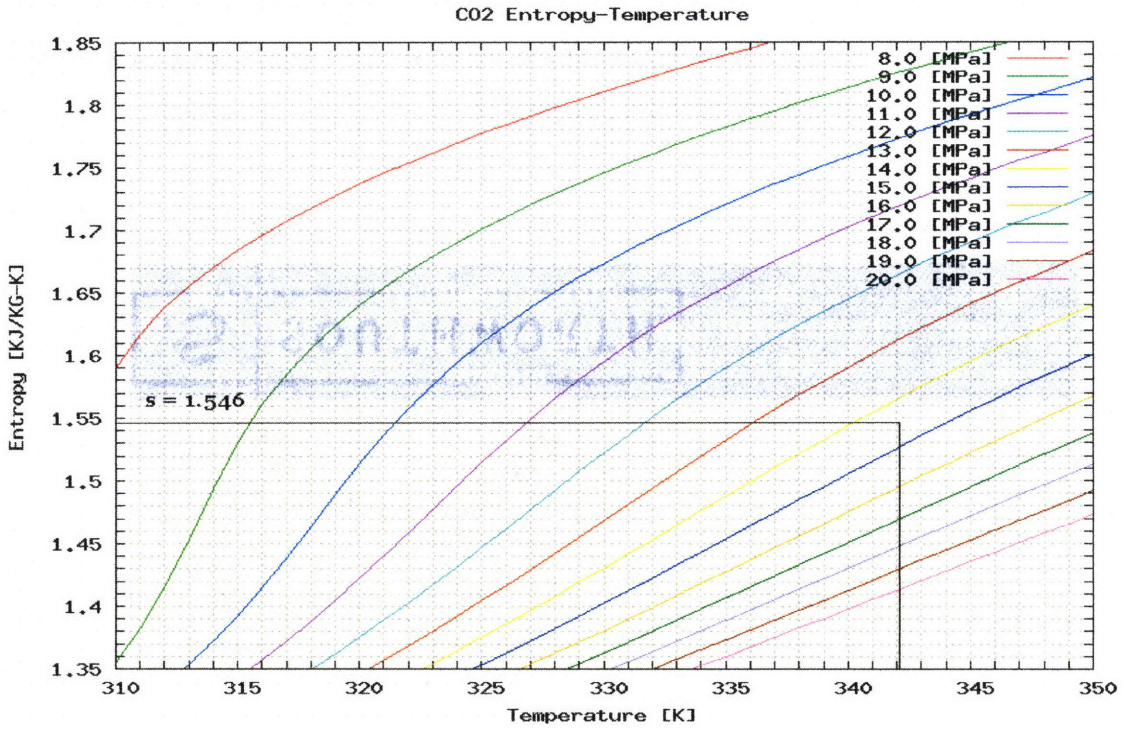

Figure 2.2.10 NIST s-T/P plot used in "pick-off" method for filling the PCS from Storage. Entropy vs. Temperature at varying Pressures for CO_2. Using the initial conditions for the ICV, the value of constant entropy is $s_{ICV} = 1.546 \pm 0.010$ kJ/kg-K.

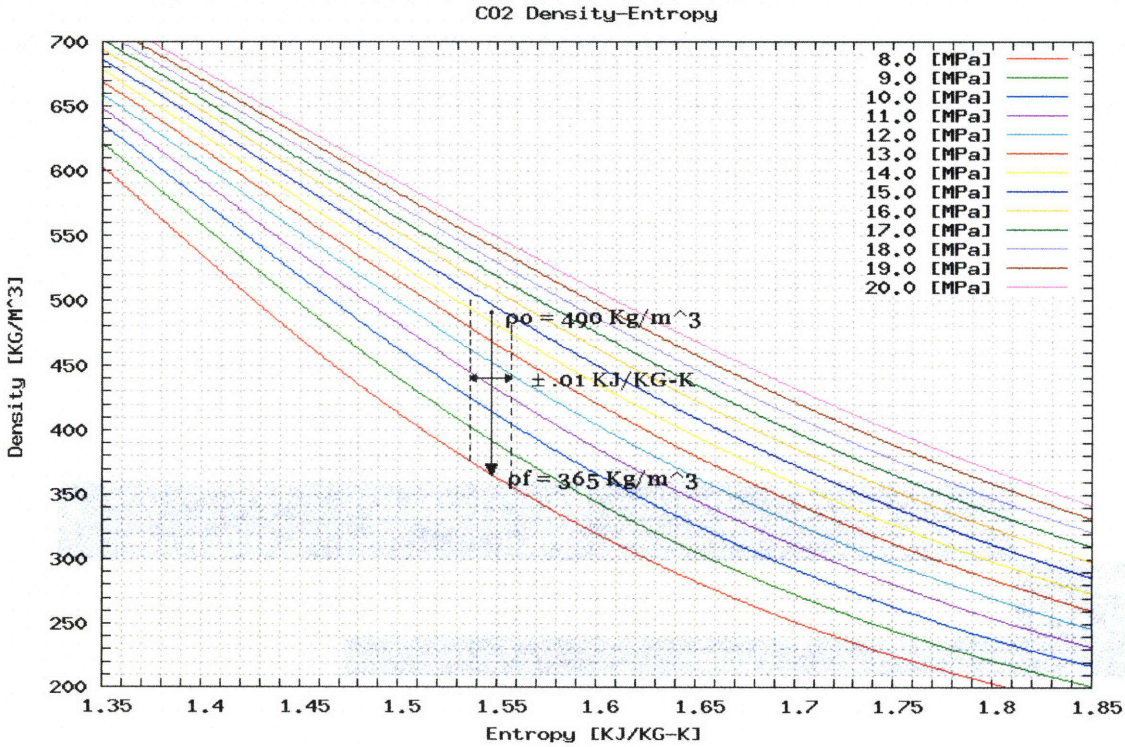

Figure 2.2.11 NIST ρ-s/P plot used in "pick-off" method for filling the PCS from Storage. Density vs. Entropy at varying Pressures for CO_2. Using the initial and final conditions for the ICV, and the entropy found from figure 2.2.10, the change in density $\Delta\rho = -125 \pm 5$ kg/m^3.

For larger ICV volumes under the same procedure, the following CO_2 kg transferred would be obtained (table 2.2.7). Blank NIST plots similar to those used here are included in appendix A and can be used for any ICV volume chosen.

Table 2.2.7 PCS Fill - Equilibrium Pressures and CO_2 kg transferred for varied ICV Volumes

ICV Volume (m^3)	Mass Transferred (kg) by RELAP5	Mass Transferred (kg) by subject method	Percent Difference (%)
10	1300.63	1250 ± 50	3.97
15	1952.31	1875 ± 50	3.96
20	2602.72	2500 ± 50	3.95
25	3253.18	3125 ± 50	3.94
28	3643.53	3500 ± 50	3.94

To appreciate the advantage of having CO_2 as a working fluid, from an inventory storage standpoint, the results can be compared to results from the ideal gas approximation. Using the ideal gas approximation shown in equation 2.2.3, one can see that the real gas properties of CO_2 increase the amount of mass transferred by as much as a factor of 1.5 (table 2.2.8).

$$\rho_{ideal} = 5293 \cdot \frac{P(MPa)}{T(K)} \left[\frac{kg}{m^3}\right] \qquad \textbf{(2.2.3)}$$

Table 2.2.8 Comparison of Ideal Gas and RELAP5 Real Gas Approximations for PCS fill

	Densities (Kg/m^3) in the ICV		
	Initial	Final	Difference
Ideal	223.87	136.81	87.06
RELAP5	489.26	359.18	130.08
Factor			1.494

It is also of interest to compare these results to a similar ideal gas analysis treating this process as the blow down of one vessel into another, as shown in figure 2.2.12. This model was obtained from a 2003 International Nuclear Energy Research Initiative (NERI) report for the development of Gen-IV GFR's, GFR-010. In this case, the analysis is simplified since both vessels contain only CO_2.

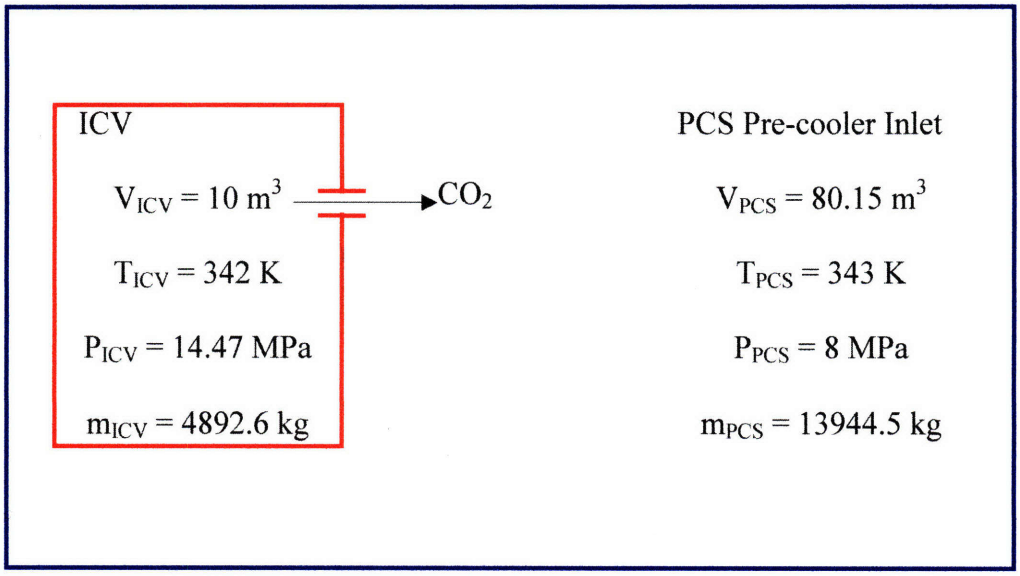

Figure 2.2.12 Simplified Model for discharging ICV into PCS Pre-cooler Inlet.
V = Volume, T = Temperature, P = Pressure, and m = mass.

The initial conditions are given in figure 2.2.12. After blow down, these values change according to:

Conservation of internal energy:

$$m_{ICV} \cdot T_{ICV} + m_{PCS} \cdot T_{PCS} = m'_{ICV} \cdot T'_{ICV} + \left(m_{ICV} - m'_{ICV}\right) \cdot T'_{PCS} + m_{PCS} \cdot T'_{PCS} \qquad \textbf{(2.2.4)}$$

Pressure equilibrium:

$$m'_{ICV} \cdot \frac{T'_{ICV}}{V_{ICV}} = \frac{\left(m_{ICV} - m'_{ICV}\right) \cdot T'_{PCS} + m_{PCS} \cdot T'_{PCS}}{V_{PCS}} \qquad \textbf{(2.2.5)}$$

Isentropic expansion in the ICV:

$$\frac{T'_{ICV}}{T_{ICV}} = \left(\frac{m'_{ICV}}{m_{ICV}}\right)^{\gamma-1}, \qquad \gamma = \text{heat capacity ratio} = c_P / c_V \qquad \textbf{(2.2.6)}$$

where a tick mark indicates final steady state conditions.

Rearranging equations 2.2.4 and 2.2.5, solving for the final PCS temperature, and substituting equation 2.2.6 gives,

$$T'_{PCS} = \frac{T_{ICV} \cdot \left(\frac{V_{PCS}}{V_{ICV}}\right) \cdot m'_{ICV} \left(\frac{m'_{ICV}}{m_{ICV}}\right)^{\gamma-1}}{\left(m_{ICV} - m'_{ICV}\right) + m_{PCS}} \tag{2.2.7}$$

$$m_{ICV} \cdot T_{ICV} + m_{PCS} \cdot T_{PCS} = m'_{ICV} \cdot T_{ICV} \left(\frac{m'_{ICV}}{m_{ICV}}\right)^{\gamma-1} + T_{ICV} \cdot \left(\frac{V_{PCS}}{V_{ICV}}\right) \cdot m'_{ICV} \left(\frac{m'_{ICV}}{m_{ICV}}\right)^{\gamma-1} \tag{2.2.8}$$

so that,

$$\frac{m_{ICV} \cdot T_{ICV} + m_{PCS} \cdot T_{PCS} - T_{ICV} \cdot \left(1 + \frac{V_{PCS}}{V_{ICV}}\right) \cdot m'_{ICV} \left(\frac{m'_{ICV}}{m_{ICV}}\right)^{\gamma-1}}{m_{ICV} \cdot T_{ICV}} = 0 \tag{2.2.9}$$

$$\Rightarrow 1 + \frac{T_{PCS}}{T_{ICV}} \cdot \frac{m_{PCS}}{m_{ICV}} - \left(\frac{m'_{ICV}}{m_{ICV}}\right)^{\gamma} \cdot \left(1 + \frac{V_{PCS}}{V_{ICV}}\right) = 0 \tag{2.2.10}$$

$$\Rightarrow f = \left(\frac{m'_{ICV}}{m_{ICV}}\right) = \left[\frac{1 + \frac{T_{PCS}}{T_{ICV}} \cdot \frac{m_{PCS}}{m_{ICV}}}{\left(1 + \frac{V_{PCS}}{V_{ICV}}\right)}\right]^{1/\gamma} \tag{2.2.11}$$

Equation 2.2.11 yields the fraction of ICV inventory that is injectable into the PCS, f, using this ideal gas analysis. In order for the PCS pressure to be maintained at 8 MPa, let $m_{PCS} >> m_{ICV}$, $V_{PCS} >> V_{ICV}$, and $T_{ICV} \approx T_{PCS}$. Then the equation reduces to

$$\Rightarrow f \approx \left[\frac{\left(\frac{m_{PCS}}{m_{ICV}}\right)}{\left(\frac{V_{PCS}}{V_{ICV}}\right)}\right]^{1/\gamma} = \left[\frac{\rho_{PCS}}{\rho_{ICV}}\right]^{1/\gamma} = \left[\frac{P_{PCS}}{P_{ICV}}\right]^{1/\gamma} \tag{2.2.12}$$

For CO_2, $\gamma \approx 1.3$. Plugging in the two initial pressures, $f \approx 63\%$. Therefore if CO_2 behaved like an ideal gas, 63% of the ICV initial mass would remain in the ICV and 37% would be transferred into the PCS. However, the RELAP5 simulation shows 26.6% of the ICV mass would actually be transferred.

The simulations here do not include the addition of a compressor for re-injection of CO_2 into the PCS pre-cooler inlet. Should an auxiliary compressor be added, the entire contents of the storage system could participate in transfers, leading to a required total of ten 10 m^3 tanks. Figure 2.2.13 shows the simple schematic of this HPG storage system with an auxiliary compressor and connections to the PCS. This diagram assumes that the main compressor is capable of pumping down the PCS to 0.1 MPa. Should this not be the case, an additional compressor would replace the throttle valve.

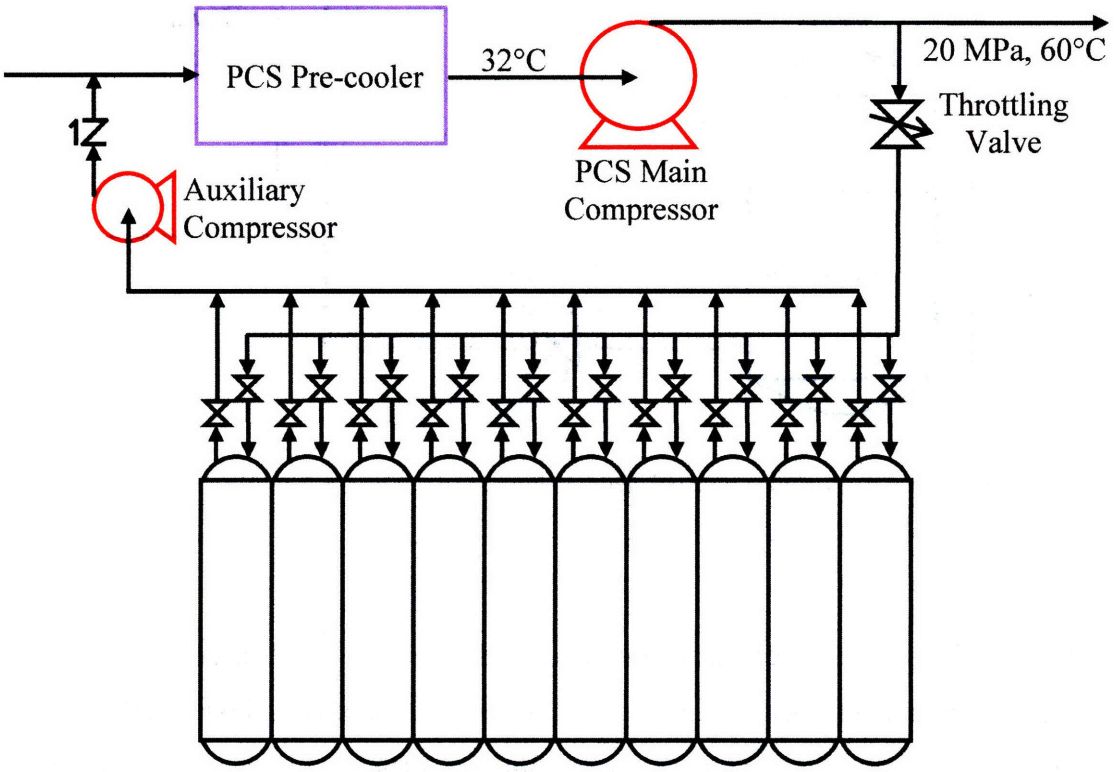

Figure 2.2.13 Proposed HPG storage system schematic for make-up and inventory control, with compression.

2.3 *Cryogenic Storage Method*

For cryogenic storage, the use of a simple Dewar tank system is appropriate. Figure 2.3.1 shows a Dewar tank schematic with a refrigeration loop for removing heat added by the surrounding environment.

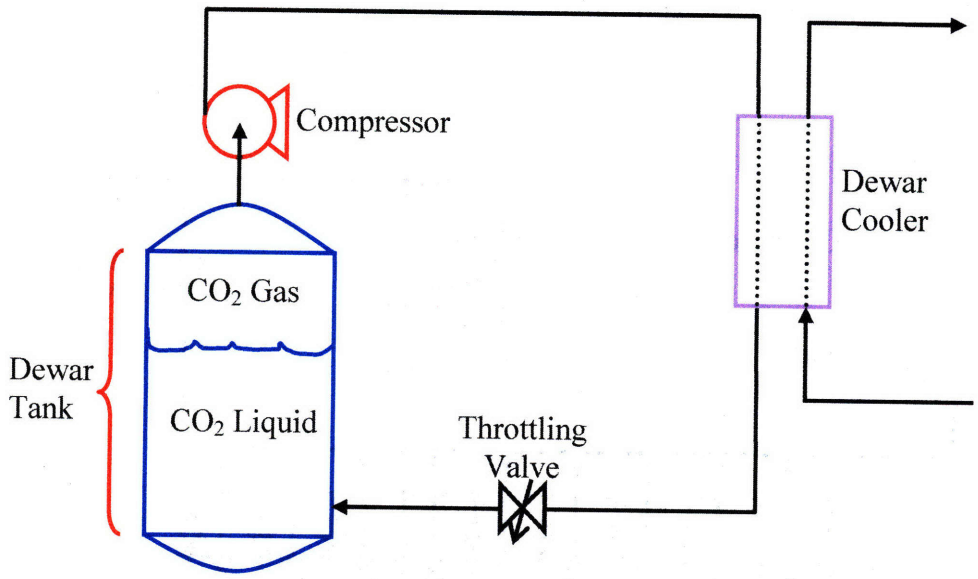

Figure 2.3.1 Dewar Tank with simple refrigeration loop

Additionally, since ambient heat should be small, the cooling requirement will not be large. Hence exceptional efficiency is not needed at the expense of complexity in the cooling loop; a small self-contained heat exchanger loop could be sufficient. One approach could be the use of a thermoelectric cooler (as described in the CRC Handbook by Rowe). EXAIR Corporation also provides an even simpler cooling solution. Their small (barely a hand's length) stainless steel Vortex Tube can provide ¼ ton (225 kg) of refrigeration, in a temperature range of -45°C to 121°C, with no moving parts to wear out. Traditional methods of cooling including using cooling water or refrigerant can also be implemented. In any approach, icing on the heat exchanger may be a problem.

Since a high pressure compressor is needed to add the CO_2 to the PCS, it may be possible to combine makeup, inventory control, and refrigeration as shown in figure 2.3.2. For this configuration, opening valve A would allow the withdrawal of coolant into storage similar to the HPG set-up. Once the tank is at desired capacity, closing valve A, opening valve B, and turning on the auxiliary compressor would redirect the flow through the auxiliary cooler to reach and maintain the desired storage conditions. When ready to charge the coolant back into the PCS, valve C would be opened and valve B closed. The auxiliary compressor would then inject the CO_2 into the PCS pre-cooler inlet.

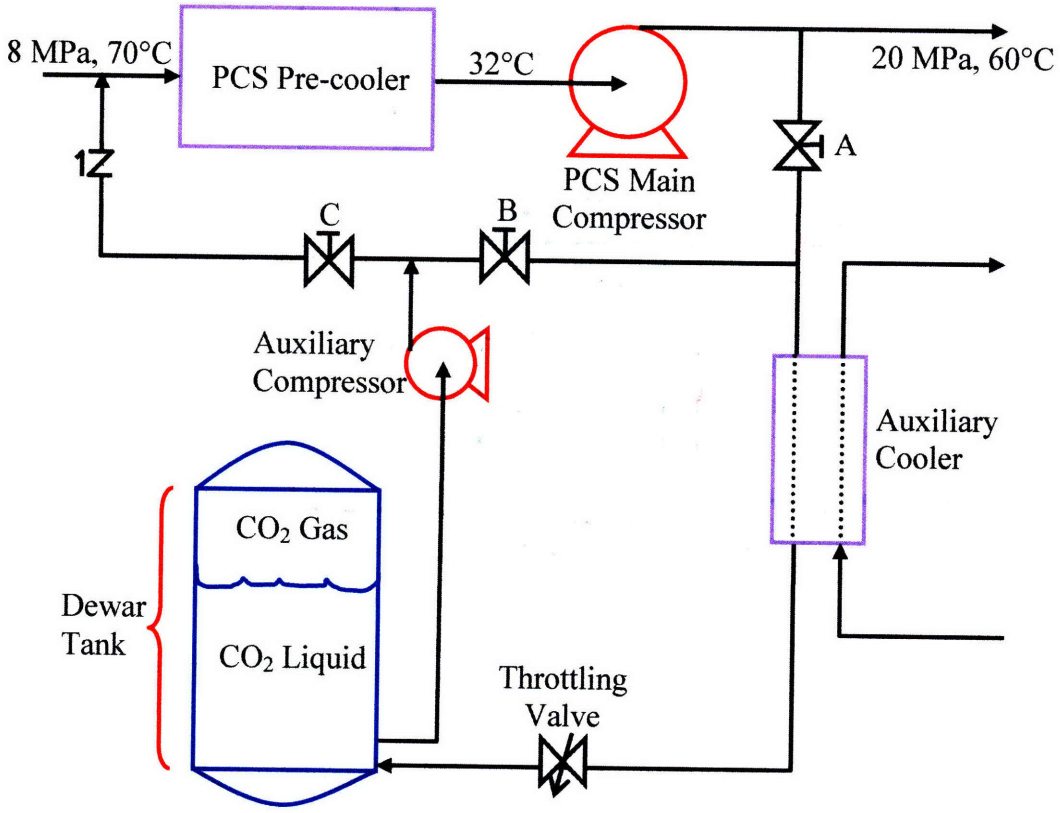

Figure 2.3.2 Possible way to combine make-up, inventory control, and refrigeration

However, one potential problem could arise in such a configuration; when throttling the CO_2 into the cryogenic tank, some of the CO_2 will flash to vapor potentially leading to vapor lock. To overcome this situation, a third configuration is proposed. Figure 2.3.3 shows the most likely connection configuration between the cryogenic tank and the PCS.

Unlike just described (and in the HPG storage system), the connections to a cryogenic tank from the PCS could be made across the pre-cooler. This would allow the use of the pre-cooler as a heat exchanger for recondensing the vented off gas during PCS draw-down into storage.

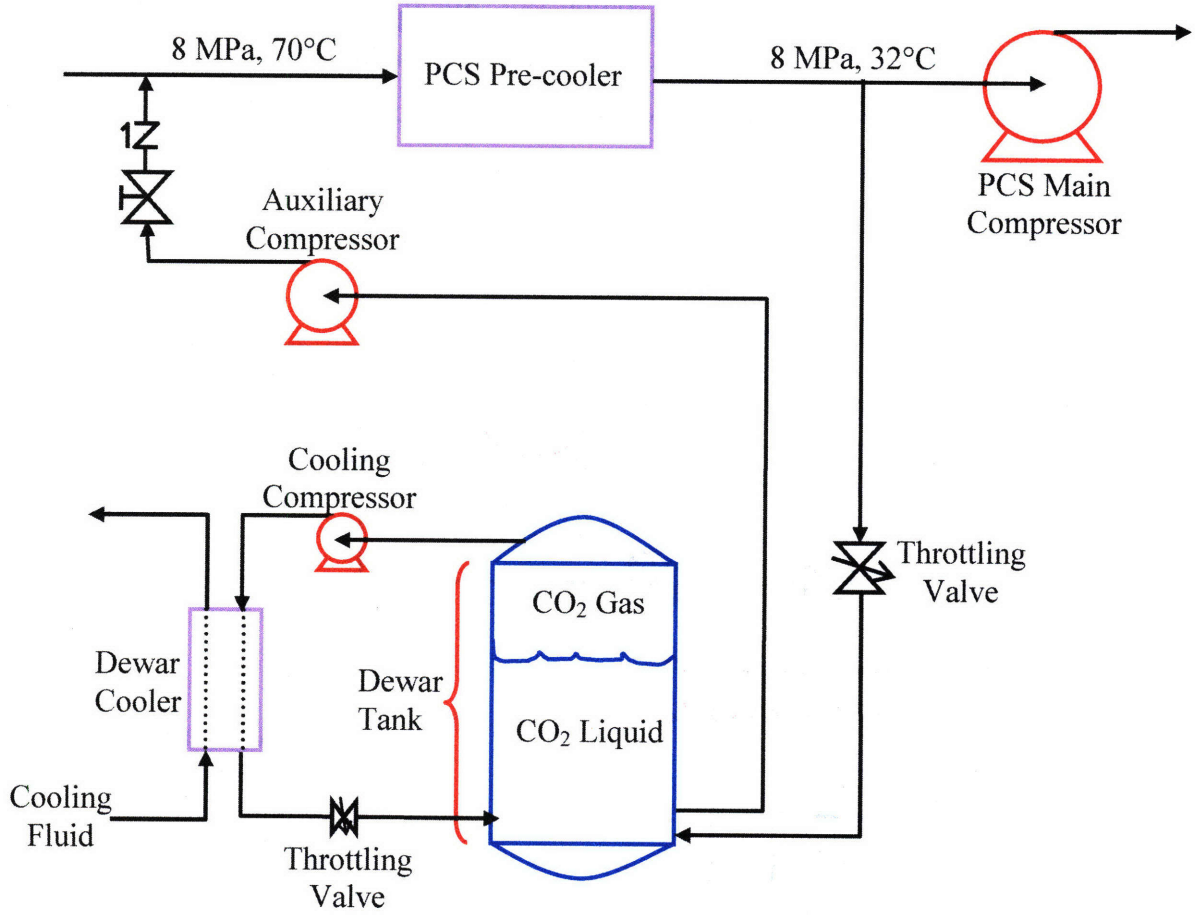

Figure 2.3.3 Proposed cryogenic system schematic for make-up, inventory control, and refrigeration

At 100% PCS power, in the 300 MW_e plant, the pre-cooler inlet and outlet conditions are as shown in table 2.3.1.

Table 2.3.1 Pre-cooler inlet and outlet conditions

	Pressure (MPa)	Temperature (K / °C)
Pre-cooler outlet	7.69	305 / 32
Pre-cooler inlet	7.72	341 / 68

If the pre-cooler outlet is throttled to liquefy part of the extracted fluid, the isenthalpic expansion (using equation 2.3.1) gives the values estimated in table 2.3.2. The vapor phase can then be re-compressed to ~8 MPa and re-injected into the pre-cooler inlet. This will also allow the pre-cooler to dampen any fluctuations.

$$isenthalpic \Rightarrow H_{out} = H_{in} = H_{out}^{\ell} + X_{out} \cdot \Delta H_{out}^{\ell\upsilon} = H_{out}^{\ell} + X_{out} \cdot (H_{out}^{\upsilon} - H_{out}^{\ell}) \qquad \textbf{(2.3.1)}$$

where superscripts ℓ and υ stand for liquid and vapor phase respectively

Table 2.3.2 Results of isenthalpic expansion from a throttled pre-cooler outlet

Final Pressure (MPa)	Temperature (K / °C)	%Liquid X_{out}	Liquid Density (kg/m3)
6	295 / +22	77	751
5	287 / +14	68	827
4	278 / +5	62	894
3	268 / -5	56	959
2	254 / -19	42	1029

However, there will be trade offs in selecting a configuration from table 2.3.2 as the inlet condition for the cryogenic storage tank. A higher storage pressure yields more liquid and lower vapor recompression work, but a more expensive cryogenic tank will be required to sustain the higher pressure and a lower liquid density will result in a larger storage tank. A benefit would result from the higher storage temperature (closer to ambient); less cooling would be required by the refrigeration loop, and the tank would require less insulation.

In this thesis, the cryogenic storage tanks are designed to operate at ~4 MPa to give a fair mid-range estimate of the tank requirements for one 300 MW_e loop. For up-scaling the plant in multiples of these loops, the same number of tanks is added.

Like the HPG method, this cryogenic tank design has the capacity to hold 87,000 kg: enough carbon dioxide for a complete discharge or press-up of a 300 MW_e PCS loop plus 100 days of leakage make-up at 290 kg/day (0.5%/day). For a pressure and temperature of ~4 MPa and 5°C, the liquid density is about 896 kg/m^3. Around 3,000 kg of the CO_2 in vapor form hovers over the liquid with a vapor quality of about 25% (25%(w) vapor, 75%(w) liquid), a density of close to 157 kg/m^3, and an occupied volume of 19.4 m^3 (20% of the tank

volume). The 87,000 kg of liquid CO_2 occupies the lower 97 m^3 giving a total tank volume of 116.5 m^3. By optimizing the cylindrical tank dimensions for a minimum surface area to reduce heat losses, the height will need to be about twice the radius. Thus the selected internal tank dimensions are a 2.65 m radius and 5.29 m height. The full tank liquid level is then 4.41 m leaving 0.88 m of vapor height above the liquid.

The main structural component of the tank is steel. For a 0.05 m thick steel wall under these pressure conditions, the steel will experience less than a 230 MPa hoop and 115 MPa longitudinal stresses. Also, to reduce heat losses, the CO_2 held inside the tank is surrounded by polished aluminum sheets, which serve as a reflector. This reflector is perforated which allows pressure to equalize across the plates to prevent overstressing the metal. An insulation layer of 0.15 m thick Polyisocyanurate foam surrounds the aluminum reflector. The approximate cylindrical tank dimensions are 5.7 m outer-diameter and 5.7 m height. Figure 2.3.4 shows a cross section and an isometric view of the cylindrical cryogenic tank.

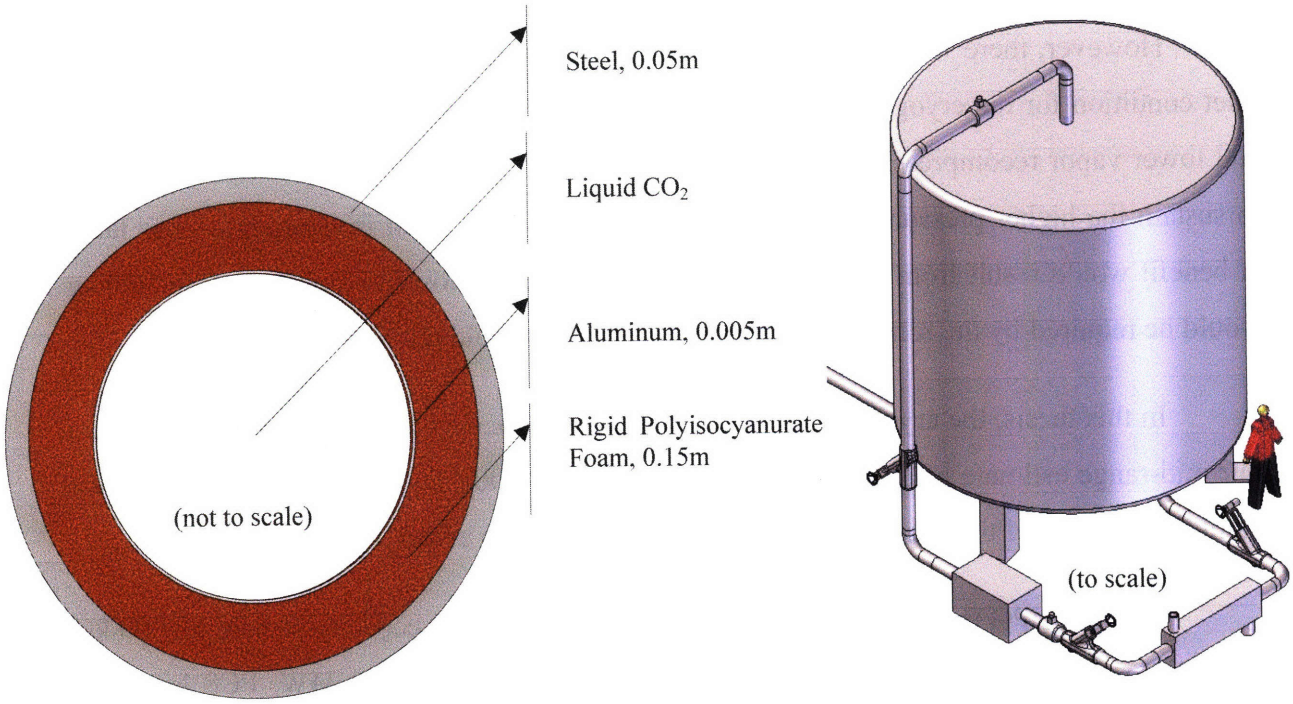

Figure 2.3.4 Cross section and an isometric view of cryogenic tank. Man is 6 ft tall.

For a tank designed in this manner and placed in a compartment at 0.1 MPa, 30°C ambient conditions, the total heat loss rate would be about 563 Watts. This ambient heat can

be removed using a simple refrigeration loop, as shown in figure 2.3.3, with a flow of about 3.7 g/sec. Assuming 80% efficiency, a 563 Watt compressor is required to compress the CO_2 to 7.72 MPa, 55°C. The CO_2 then passes through the cooling condenser where the outlet temperature drops to about 25°C, and is throttled back into the cryogenic tank.

The cooling fluid used in this estimate is R-134a; a very common, cheap, CFC free refrigerant. Also assuming 80% efficiency for the refrigerant loop compressor, rated at 367 W, the R-134a is compressed from 0.1 MPa, -26°C to 5 MPa, 129°C. The refrigerant is then fed into a condenser which removes heat collected in the Dewar cooler (or evaporator). Once the R-134a temperature is lowered to 25°C, it is throttled back to 0.1 MPa, -26°C as a 2-phase saturated liquid with quality of 32%. As the refrigerant re-enters the Dewar cooler, energy is absorbed increasing the quality to a 100% saturated vapor for entry into the compressor.

In Carstens' design [2007], the PCS CO_2 removal/addition flow rate does not exceed 10 kg/sec when using inventory control for power changes. For 58,000 kg in the reference 300 MW_e PCS, this allows the removal of less than 1% of the PCS inventory per minute. This flow rate was used to estimate the rating for an auxiliary compressor for re-injection into the pre-cooler inlet. An 80% efficient 427 kW auxiliary compressor is required to press up the CO_2 to the 7.72 MPa pressure at the pre-cooler inlet.

2.4 Comparison of Storage Methods

The use of cryogenic storage has its advantage in reduced storage volume, but presents a much slower transfer capability with a more complex system design. Using the HPG method, a rapid blow down or injection is attainable.

A volume comparison between cryogenic storage and HPG storage of the S-CO_2 Power Conversion System (PCS) Carbon Dioxide will be useful in plant design considerations, and is therefore described in this section. In consideration of a required capability to completely discharge or fill the PCS, as well as maintain a 100 day's supply for leakage make-up (for a daily leak rate estimated to be 0.5% per day, or 290 kg/day per 300 MW_e loop), this thesis shows the estimated volumes of the prospective storage systems

required to transfer and contain 150% of the PCS-full-power-mass, or 87,000 kg. Table 2.4.1 shows the values used to determine the percentages discussed, and table 2.4.2 shows a table of options for storage configurations.

The previous sections of this chapter have estimated the carbon dioxide storage and transfer capabilities of a 10 m^3 HPG Inventory Control Vessel (ICV) using RELAP5 simulations. The simulation for charging the HPG ICV from a 300 MW_e PCS demonstrated an estimated 2.7% PCS-full-power-mass transfer capability and a 10.6% PCS-full-power-mass storage capability once fully charged. For a 28 m^3 tank like the one made by Europipe, upwards of 6% of the PCS mass can be transferred and 28% of 58,000 kg could be stored. Therefore, for the capability of storing 150% of the PCS-full-power-mass using only high pressure CO_2 storage, a network of 14 smaller 10 m^3 tanks (140 m^3) or 6 larger 28 m^3 tanks (168 m^3) would be required per 300 MW_e loop.

However these simulation results are for a system using only differential pressure as the primary driving force, and these total tank volumes would not be sufficient for the complete discharge of the PCS S-CO_2 into storage. For a 100% PCS-full-power-mass transfer in this configuration at a rate of 2.7% per 10 m^3 tank, 37 smaller tanks would be required (totaling 370 m^3). The same could be done with 17 of the larger Europipe tanks (476 m^3). These estimates assume that the tanks are loaded sequentially (not in parallel), and that the main compressor can be used to provide an outlet pressure of 20 MPa at the beginning of each sequential tank fill. Should this assumption prove unfeasible, an additional compressor would be required to completely pump down the PCS into HPG storage. Should such a compressor be added, this system would also benefit from an increased transfer capability and a reduction in volume. Complete filling of the PCS to 20 MPa or pump-down to 0.1 MPa would meet the 150% mass storage requirement using 10 smaller tanks (100 m^3) or 4 larger Europipe tanks (112 m^3) pressed up to 20 MPa at room temperature. A decision would need to be made as to the size and type of compressor desired in this case. Use of a piston compressor, with design flow rate of ~10 kg/sec, is recommended due to the piston compressor's ability to handle large changes in inlet pressure.

Similarly, the RELAP5 simulation for venting a 10 m^3 ICV back into the 300 MW_e PCS using differential pressure as the driving force demonstrated a 2.2% PCS-full-power-mass transfer and a remaining 6.2% PCS-full-power-mass left in the tank. At a rate of 2.2% per tank, 46 smaller tanks (460 m^3) would be required for returning the 300 MW_e PCS from empty to 100% PCS-full-power-mass. Using the mass transferred in table 2.7 for a 28 m^3 Europipe tank, about 6.2% PCS-full-power-mass is transferred; therefore about 16 larger tanks (448 m^3) would be required for 100% PCS-full-power-mass.

By using the most conservative estimate of forty-six 10 m^3 tanks, both transfer and storage capability requirements are met when using only HPG storage. Figures C-1 through C-4 (in appendix C) show a relative size comparison of the required tank capacity for the 300 MW_e PCS (rounding to 50 tanks). The approximate tank dimensions for each 10 m^3 tank are 1 m inner-diameter and 4 m in height with hemispherical domes on the vertical ends. The tanks are banked 5x10 and spaced roughly 32 cm apart within the rack. Three-dimensional views of this bank of tanks are shown below in figure 2.4.1. For pumpable HPG storage, only 10 of these tanks per 300 MW_e loop would suffice. The large difference indicates that provision of the compressor is worthwhile.

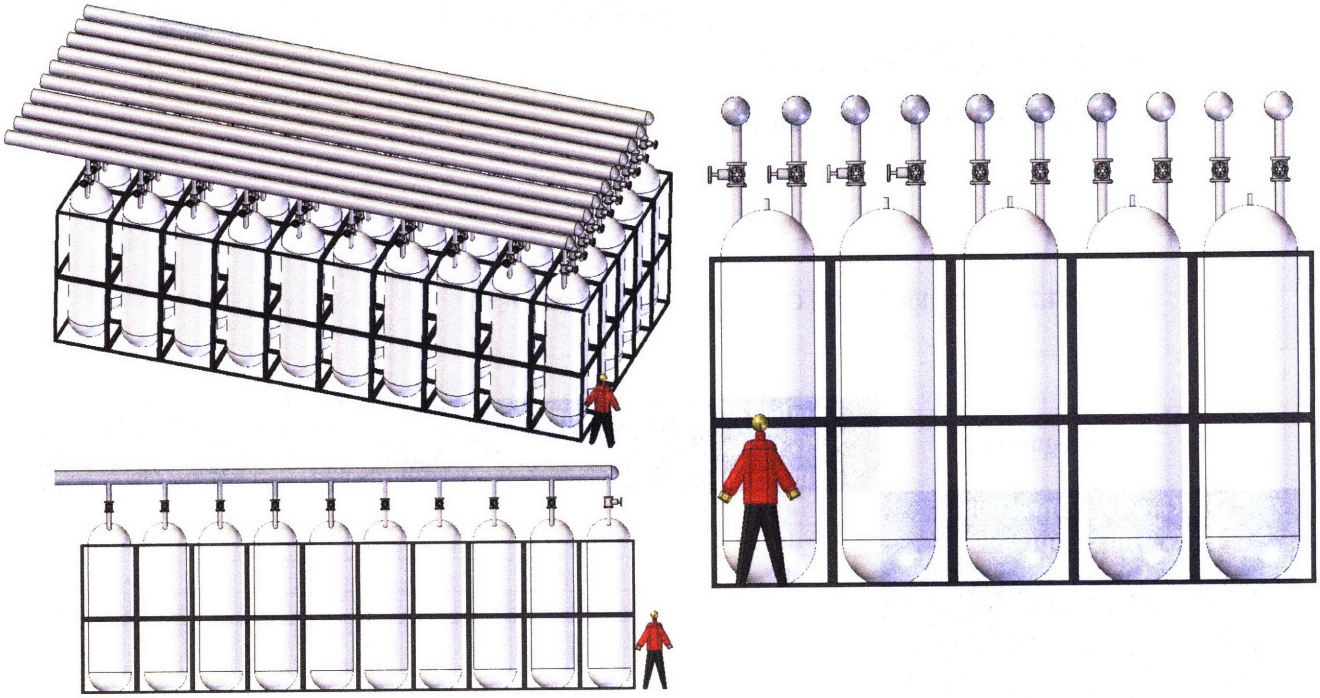

Figure 2.4.1 Isometric and side views of 5x10 bank of 10 m^3 HPG tanks. Man is 6 ft tall.

Preliminary cryogenic storage calculations would allow for the same 150% PCS-full-power-mass storage capability in a single 116 m^3 tank per 300MW_e loop. Figures C-5 through C-7 show a 300 MW_e PCS with the required cryogenic tank.

Table 2.4.1 Summary - Transfer and Storage Capabilities (300MW_e PCS)

Charging HPG ICV w/o Compressor	ICV (10 m^3)		PCS (80.15 m^3)	
	Initial	Final	Initial	Final
Density (kg/m^3)	458	617	722	701
Mass (kg)	4580	6170	57934	56231
Mass transferred into ICV (kg)	1590			
% ICV-mass participating in xfer	25.7			
% full-power-mass transferred	2.7			
Final % initial-PCS-mass in ICV	10.6			
Venting HPG ICV w/o Compressor	**ICV (10 m^3)**		**PCS**	
	Initial	Final	Initial	Final
Density (kg/m^3)	489	359	174	174
Mass (kg)	4890	3590	infinite	infinite
Mass transferred from ICV (kg)	1300			
% ICV-mass participating in xfer	26.6			
% full-power-mass transferred	2.2			
Final % initial-PCS-mass in ICV	6.2			
Cryogenic ICV	**ICV**		**PCS (80.15 m^3)**	
Density (kg/m^3)	748.2 (effective, incl void)		722 (full power)	
150% full-power-PCS-Mass (kg)	87000			
ICV required volume (m^3)	116.5			

Table 2.4.2 Options for Storage Configurations (300MW_e PCS)

Configuration	Number of HPG tanks (10 m^3 each)	HPG Storage Volume (m^3)	Cryogenic Storage Volume (m^3)	Total Storage Volume (m^3)
HPG w/o compression	46	460	0	460
HPG with compression	10	100	0	100
Cryogenic	0	0	116	116
Equal Split w/o HPG compression	23	230	58	288
100% PCS-mass in Cryo, 50% PCS-mass in HPG (w/o comp)	16	160	77	237
100% PCS-mass in Cryo, 50% PCS-mass in HPG (with comp)	3	30	77	107

Without exogenous compression in the high pressure gas storage system, the cryogenic system provides a large advantage in mass transfer capability. Either way, cryogenic storage has a superior storage capability due to the density ratio of 1.5 when compared to the final HPG ICV density after charging from the PCS (896/617). However, due to the simplicity and rapid response capability of the HPG storage design, a combination of the two storage methods may be advisable. It is assumed that a 0.5% PCS-mass daily CO_2 leak rate may occur. The simple HPG ICV design is adequately capable of providing the make-up from such a small loss on a daily basis (290 kg/day per 300 MW_e loop). This system will also be sufficient for small power level adjustments. However, for larger scale plant operations requiring large PCS-mass adjustments, the more complicated cryogenic storage tank system can be at the ready to discharge or load the PCS. It is for this reason that the last two options in table 2.4.2 were included; the cryogenic system would be capable of fully charging or discharging the PCS while the HPG storage would contain 50% PCS-full-power mass for smaller power changes and daily leakage make-up. Figures C-8 through C-10 show the 1200 MW_e PCS with a combined configuration without an auxiliary compressor in the HPG system. The piping connections are the same as shown in the 300 MW_e figures (C-1 to C-7). For the four cryogenic tanks in this configuration, the volume is reduced to approximately two-thirds and each dimension (height and diameter) are reduced to approximately 87% ($\sqrt[3]{2/3}$) when compared to the configuration using cryogenic storage only. Additionally, the number of 10 m^3 HPG tanks is reduced to about one-third, with each tank maintaining similar dimensions as described in the HPG-only storage method.

2.5 Summary

For the reference 300 MW_e PCS discussed, the amount of CO_2 in the closed loop at full power is approximately 58,000 kg. Inventory storage capacity for make-up and charging must be sufficient for a complete system blow down or charging, as well as maintaining loop inventory from CO_2 losses. The preliminary estimate for daily leakage is 0.5% (or ~290 kg/day, or 8,730 kg/month). Additional make-up will likely be required either due to the breakdown of the CO_2 by corrosion or radiolysis, or losses of CO_2 in the purification process. Estimates on this amount are still to be determined. The conceptual storage designs presented in this thesis are intended for storage of approximately 150% system volume, or 87,000 kg. A variety of storage methods are presented including a high pressure gas (HPG) storage system, a single cryogenic tank, and hybrid combination of the two.

For the HPG storage method, the system will be required to operate at a maximum pressure of 20 MPa. For atmospheric temperature at this pressure, and with the compressor to utilize full storage tank capacity, an estimate of ~100 m^3 total tank volume situated in a bank of ten 10 m^3 tanks or four 28 m^3 Europipe tanks is required. In the event that differential pressure is used as the primary driving force between the plant and storage, this volume increases by a factor of 4-5 (meaning at least forty-six 10 m^3 tanks, or sixteen Europipe tanks).

For the cryogenic storage method, the tank is designed to operate at approximately 4 MPa/5°C with a 20% vapor pocket above the liquid CO_2. This leads to a tank size of about 116 m^3.

In the hybrid configuration, the HPG storage is used to contain 50% while the cryogenic tank contains the remaining 100%. For such a system, only sixteen 10 m^3 HPG tanks, and a 77 m^3 cryogenic tank are required. Should a compressor be added to the HPG system, the number of HPG tanks can be reduced to 3.

Another design consideration revolves around delivery truck capabilities. Hoop stress is $\frac{P \cdot r}{t}$, and most liquid CO_2 delivery trucks have a fairly large r. Therefore delivery trucks are generally capable of a low maximum pump outlet pressure around 350 psi (2.4 MPa) [Jones, 2007]. This means that an intermediate storage system may be required, as a designated fill station, and connected to the Inventory Control System by a compressor capable of supplying the required tank pressures discussed.

Safety

All storage containers should be designed, constructed, and tested in accordance with the requirements of the ASME Boiler and Pressure Vessel Code (ASME Code), Section VIII, Division 1, current at the time the vessels are constructed [CGA, 2003]. Carbon Dioxide storage quantities greater than 4,536 kg (10,000 lbs) are covered in 40 CFR, Part 370, section 312 by the U.S. Environmental Protection Agency (EPA) Superfund Amendments and Reauthorization Act (SARA) Title III, Tier II Hazardous Chemical Inventory Report requirements. Appropriate government reports must be filed by March 1 of each calendar year; and Tier II reports are to be sent to the appropriate State Emergency Response Commission (SERC), the appropriate local emergency planning committee (LEPC), and the local fire department [CGA, 2003].

Keep in mind that when a delivery truck connects to recharge tanks, there has to be a "blow-off" vent line which can be very noisy, requiring hearing protection for nearby personnel. It may be best to locate the filling station outdoors. In fact, if possible, the placement of the tank outdoors is highly recommended by the Compressed Gas Association (CGA) for safety reasons. Placement of tanks indoors is discouraged, but can be done in a well-ventilated, non-corrosive compartment above ground level provided that the pressure relief devices' capacities meet standards set forth in CGA S-1.3 [CGA, 2003]. However, these relief devices should still be piped outdoors. As the CO_2 is vented off, it would otherwise fill a closed compartment and become an asphyxiation hazard. Tank filling connections, and level and pressure gauges should also be piped outdoors for ease of accessibility by the person delivering the CO_2. Another safety concern for the CO_2 filling

station -- outdoor tanks should be bolted securely to the ground to protect the tank from bumping during filling.

Also, as carbon dioxide expands, dry ice crystals tend to form by the depressurization and could cause a potential ice blockage. It will be necessary to always maintain the flowing CO_2 pressure above 416 kPa in order to prevent CO_2 ice formation and blockage of pipes, which could be detrimental to system piping due to the increased pressure buildup of the encapsulated gas. If it becomes necessary to reduce the pressure below 416 kPa, the ice blockage can be prevented using a cross-over line which maintains a vapor pressure above 1380 kPa to one end of the purge line while removing the liquid from the other end. The system pressure is then held above the triple point and the formation of ice is inhibited in the vapor. Once the desired amount of liquid is removed, the pressure can be reduced to below 416 kPa. For high flow demands, a pre-heater in the tanks may also be advisable. [CGA, 2003]

It is important to note that the tank capacities described here do not account for the tanks being overfilled by CGA standards. The CGA recommends that tanks are not liquid-filled beyond 68% to allow enough vapor room for thermal expansion of the liquid [CGA, 2004]. In a system where the liquid will be trace heated, as discussed in section 2.2 for charging the PCS, and in a cryogenic tank as discussed in section 2.3, this can be of particular concern. Provided that the liquid in each tank has a vapor space for expansion, the pressure rise is only 62 kPa per °C. As soon as the liquid no longer has a vapor bubble to collapse, the pressure rise jumps to 10.55 MPa per °C! Should tanks not be given adequate vapor space, they could become liquid-full and expand beyond the steel's stress capabilities. Even for the cryogenic system which will have a cooling loop to remove ambient heat, there is still the possibility of power loss. Should a 68% fill density be applied to the systems presented, the HPG total volume would increase to 141 m^3 (14 tanks) with auxiliary compression. Similarly, the cryogenic tank vapor space would have to be increased from 20% to 32% creating a new total volume of 137 m^3. In the hybrid configuration, five 10 m^3 HPG tanks (with compression), and a 91 m^3 cryogenic tank would be required.

Obviously, relief valves would be required for further protection of overpressure. The CGA requires that sizing be sufficient to maintain a safe pressure in the event of a major external heat input, such as a fire. Valve sizing standards can be found in CGA S-1.3, Pressure Relief Device Standards, Part 3: Stationary Storage Containers for Compressed Gases, and in the ASME Code for Size Requirements. Sizing methods specifically for supercritical fluids can also be found in Ouderkirk [2002].

A maximum liquid-fill of 68% is not set in stone. Should a tank need to be "overfilled" (i.e. above 68% liquid), provisions should be made to ensure the tank does not become filled above where it can become liquid-full before the design pressure relief setting. This will also ensure that the cycling of the pressure relief valve does not occur and the tank is not subjected to undue cycling stresses. General rule of thumb – lower storage temperatures require larger vapor space. Additional insulation around the tank can also help alleviate the problem for tanks that are not intentionally heated above ambient temperature. Table 2.5.1 shows the temperatures and pressures for a 68% liquid-filled tank deemed "correct" by the CGA. Incorrect, or overfilled, pressures and temperatures are also shown, up to 100% liquid-filled. This is also graphically represented in figure 2.5.1.

Table 2.5.1 Temperature-Pressure relationship of CO_2 at various filling densities [CGA, 2003]*

	Filling Density (% of cylinder capacity)						
	Correct	Overfilled					
	68	75	80	85	90	95	100
Temp (°C)	Pressure (MPa)						
15.6	5.047	5.047	5.047	6.929	10.894	17.755	28.856
21.1	5.771	5.771	7.205	9.860	14.514	22.340	
26.7	6.619	7.791	7.791	12.963	18.341		
32.2	8.205	9.963	12.273	16.065	22.202		
37.8	9.998	12.204	14.962	19.285			
43.3	11.790	14.445	17.651	26.270			
48.9	13.652	16.789	20.409				
54.4	15.514	19.134	23.236				
60	17.444	21.581					
65.6	19.375						

* Reproduced from CGA G-6 with the permission of the Compressed Gas Association. No further reproduction is permitted.

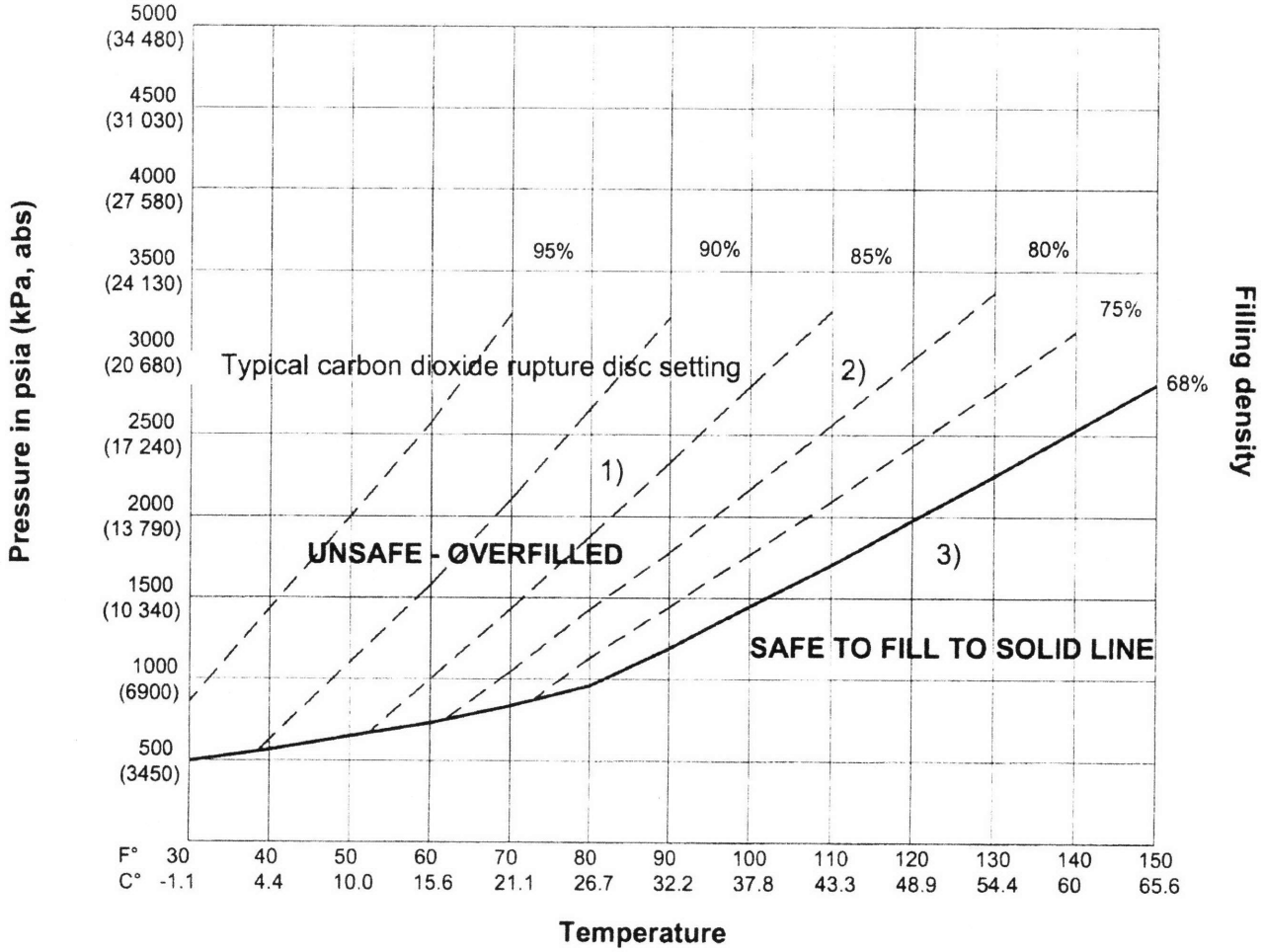

1) Dashed lines indicate temperature-pressure relationship when the cylinder is overfilled.

2) A correctly installed carbon dioxide cylinder rupture disk functions at 2800 psig to 3000 psia (19 310 kPa to 20 680 kPa) depending on design.

3) Maximum permitted filling capacity is 68%.

NOTE—This chart is based upon a cylinder filled to its correct maximum liquid carbon dioxide capacity of 68% of the total volume (water weight capacity). An overfilled cylinder obviously experiences enormous internal pressures from expansion of the liquid carbon dioxide as it warms to higher temperatures after filling.

Figure 2.5.1 Temperature-Pressure relationship of CO_2 at various filling densities [CGA, 2004]*

* Reproduced from CGA G-6.2 with the permission of the Compressed Gas Association. No further reproduction is permitted.

3 Coolant Purification

3.1 Introduction and Motivation

The intent of this chapter is to provide a summary of considerations for the required S-CO_2 coolant purity, options for the procurement of the CO_2, including available purities and cost, and suggested purification methods for S-CO_2. Principal materials under consideration for use in the S-CO_2 systems, the possible corrosion reactions and byproducts produced, the radiological effects in direct applications (e.g. radiolysis and N-16 produced in CO_2 oxygen by (n,p) reactions), and other sources of impurities such as imperfect seals and the make-up coolant system will be discussed in order to support the purification methods suggested.

3.2 Impurities from Corrosion in the S-CO_2 PCS

Since corrosion in any system cannot be completely prevented, appropriate material selection must play a major role in limiting the effects of corrosion. Other methods of corrosion prevention include plastic coated or cement lined tubing and valves, stainless steel wellheads and valves, inhibitors, and oxygen scavengers. A final consideration is maintenance of dry, reducing conditions inside the PCS to limit corrosion of its constituent metals. CO_2 tends to become acidic in the presence of water (forming carbonic acid, H_2CO_3), therefore dehydrating methods and materials resistant to this acid (pH $\approx$ 3.5) will have to be used: such as some stainless steels, Hastelloy metals, or Monel metals [CGA, 1990].

Experience with the British AGRs has shown that corrosion in CO_2 systems is significantly lower than in the conventional Rankine cycle; however, corrosion cannot be

considered insignificant to ignore. Note that AGR experience is not necessarily a valid guide to coolant chemistry control, due to the dominant effect of the presence of graphite and in-core radiation, and the higher pressure (20 vs. 4 MPa) in the PCS.

Additionally, subsystems can be included to purify the flowing coolant of the impurities it will collect as it passes through the system. One key to knowing what kind of purification system to incorporate is becoming familiar with the types of corrosion reactions that will occur between the coolant and plant materials, and the kinds of byproducts that will be produced.

Material selection for these S-CO_2 systems is still largely in the research and testing phase and the reaction processes under the design temperature and pressure conditions are still being determined. Research has been conducted recently at MIT and Idaho National Labs (INL) on the corrosion process for both the direct and indirect S-CO_2 PCS. Specifically,

(1) HSC Chemistry® 5.1 simulations of corrosion reactions for material in a 2400 MW_{th} direct S-CO_2 cooled GFR: designed by the Center for Advanced Nuclear Energy Systems (CANES) at MIT and sponsored by the DOE though NERI [Handwerk et al., 2007][Pope et al., 2006],

(2) S-CO_2 immersion testing for corrosion of various steels: designed and operated by the MIT CANES H. H. Uhlig Corrosion Laboratory and supported by Los Alamos National Laboratory [Ballinger, Lim, Eastwick, & McKrell, 2007], and

(3) One-pass flow S-CO_2 loop for corrosion testing of two steel alloys for a 600 MW_{th} indirect helium VHTR with S-CO_2 secondary loop: designed by INL [Oh et al., 2006].

There are many aspects of the S-CO_2 PCS that need to be examined in terms of corrosion mitigation and prevention. Key parameters that have an effect on the corrosion reactions and rates include material selection, temperature, pressure, humidity, pH of water vapor if present, coolant impurity concentration, etc. Once the corrosion reactions that may occur within the system are understood, the purification system can be designed to remove

byproducts as required to maintain coolant purity to specification. In order to determine the possible corrosion reactions, the materials under consideration that would make up the structural components, fuel, cladding, reflectors, and control assemblies must be discussed. In general, such products will be solid metal oxides, which can spall off surfaces and become entrained in the CO_2.

A summary of corrosion mechanisms, and recent testing and simulation results are included in appendix D. Useful readings of gas composition using a Residual Gas Analyzer (RGA) are included in the analysis from testing conducted at MIT's H. H. Uhlig Corrosion Laboratory. The RGA results for test 3 are shown on figure D-4 (in appendix D). From this test, a variance in the autoclave outlet can be seen at two different times since data acquisition began. At 14, 17, 18, 20, 32, and 40 amu, the 180 hour data show a significant increase in counts. The possible contaminants causing these peaks (shown in table D-1) include CH_2, OH, NH_3, H_2O, O_2, CH_3OH, C_3H_4, oil, and solvents. However, these results are largely inconclusive at present. The observed changes in the RGA spectra are an indication of possible system contamination and/or reactions of some species (CO_2, CO, H_2O, O_2, etc.) with one mo more of the alloys tested. Future tests will include improvements to the system that will reduce the chances of contamination from external sources. Additionally, it may be necessary to run some control tests to see if these compounds are still detected; for example, running the same test without the presence of test samples. Finally, once an alloy is selected for further investigation, a test will be run to determine the corrosion products carried by the CO_2 from that particular corrosion process.

HSC Chemistry® 5.1 simulations of corrosion reactions for material in a 2400 MW_{th} direct S-CO_2 cooled GFR were conducted by Handwerk [2007]. His simulations show that corrosion in a direct cycle could also lead to impurities entrained in the CO_2. For instance, titanium is proposed for use as an axial reflector. From the reaction equation shown in appendix D, there is a possibility for TiO_2 to form. TiO_2 is a fine white powder that could easily be picked up in the CO_2 flow. This reaction, and the corrosion reaction shown for boron carbide control assemblies also show the potential for generation of more CO.

3.3 Other Sources of Impurities

Impurities will inevitably be present upon delivery from any bulk supply method. Minimum purity levels and maximum concentrations for certain impurities are regulated in the United States by the Compressed Gas Association (CGA), and internationally by the International Organization for Standardization (ISO) 9001 2000. According to table 3.3.1, from the CGA standard publication G-6.2, there are at least 26 impurities that could be present depending on the CO_2 source used by the bulk distributor. Additional impurities not listed in this table include ammonia, nitric oxide, oxygen, non-volatile residues, oil/grease, and most importantly water.

Table 3.3.1 Possible trace level impurities by source type (excluding air gases and water). [CGA, 2004]*

Component	Com-bustion	Wells/ geothermal	Ferment ation	Hydrogen or ammonia	Phosphate rock	Coal gasi-fication	Ethylene oxide	Acid neutrali-zation
Aldehydes	X	X	X	X		X	X	
Amines	X			X				
Benzene	X	X	X	X		X	X	X
Carbon monoxide	X	X	X	X	X	X	X	X
Carbonyl sulfide		X	X	X	X	X		X
Cyclialiphatic hydrocarbons	X	X		X		X	X	
Dimethyl sulfide		X	X		X	X		X
Ethanol	X	X	X	X		X	X	
Ether		X	X	X		X	X	
Ethyl acetate		X	X			X	X	
Ethyl benzene		X		X		X	X	
Ethylene oxide						X	X	
Halocarbons	X					X	X	
Hydrogen cyanide	X					X		
Hydrogen sulfide	X	X	X	X	X	X	X	X
Ketones	X	X	X	X		X	X	
Mercaptans	X	X	X	X	X	X	X	
Mercury	X					X		
Nitrogen oxide	X		X	X		X	X	X
Phosphine					X			
Radon		X			X			X
Sulfur dioxide	X	X	X	X	X	X		X
Toluene		X	X	X		X	X	
Vinyl chloride	X					X	X	
Volatile hydrocarbons	X	X	X	X		X	X	
Xylene		X	X	X		X	X	

NOTE—The source types are generic sources, and there are variations in individual processes. Therefore, the supplier should assess whether or not all of the components listed are applicable to the actual plant.

* Reproduced from CGA G-6.2 with the permission of the Compressed Gas Association. No further reproduction is permitted.

Probably the most significant impurities to limit for maintaining the integrity of the PCS contain the elements O, H, or C; such as water, hydrocarbons, ammonia, oxygen gas, hydrogen gas, etc.

Other potential sources of impurities are inherent to a PCS system design. For direct cycles, radiological effects could introduce nitrogen (N-16) from (n,p) reactions with the carbon atoms in the coolant; or generate higher concentrations of CO, causing a subsequent buildup of O_2. Leakage of fission products into the coolant will also be inevitable. Impurities can also be introduced in low system pressure points due to leaky seals or bearings.

3.4 S-CO_2 Purity Requirements

As previously mentioned, and shown in table 3.3.1, there are several impurities that could be present depending on the CO_2 source used by the bulk distributor. However, the CGA only lists 18 impurities (table 3.4.1) that should be accounted for by distributors in order to meet various CGA grade specifications: acetaldehyde, ammonia, benzene, CO, carbonyl sulfide, hydrogen cyanide, hydrogen sulfide, methanol, nitric oxide, nitrogen dioxide, non-volatile residue, oil/grease, oxygen, phosphine, sulfur dioxide, total hydrocarbon (THC) as a methane equivalent, total sulfur, and water vapor. Also included is a test for odor and taste for all grades (not just food/beverage grade) of CO_2. THC covers aldehydes, benzene, ethanol, ether, ethyl acetate, ethyl benzene, ethylene oxide, mercaptains, toluene, xylene, and some ketones. The other impurities not covered in the minimum specification criteria are amines, halocarbons, mercury, forms of nitrogen oxide other than nitric oxide, radon, and vinyl chloride. If it is determined that any of these impurities would be of concern in the plant, it would be highly advisable to ask the distributor to specify/limit their concentrations.

Table 3.4.1 Directory of limiting characteristics to meet CGA QVLs. Units in ppm(v) unless otherwise stated. [CGA, 2004]*

Limiting characteristics	E	G	H	I	J
Carbon dioxide min. % (v/v)	99	99	99.5	99.9	
Acetaldehyde		0.5	0.5	0.2	
Ammonia	25			2.5	
Acidity				To pass JECFA test [1]	
Benzene				0.02	
Carbon monoxide	10 (vapor) [2]		10	10	
Carbonyl sulfide			0.5	[3]	
Hydrogen cyanide				None detected [4]	
Methanol				10	
Nitric oxide	2.5 (vapor) [2]		5 (total of NO + NO_2)	2.5	
Nitrogen dioxide	2.5			2.5	
Oxygen		50	50	30	
Phosphine [5]				0.3	
Sulfur dioxide	5		5	[3]	
Total sulfur		0.5	0.5	0.1 [3]	
Total hydrocarbon content (as methane)		50	50	50 max including 20 max of nonmethane hydrocarbons	
Hydrogen sulfide	1 (vapor) [2]		0.5 (vapor)	[2]	
Color					White opaque
Nonvolatile residues (wt/wt)		10	10	10	500
Oil/grease (wt/wt)				5	
Odor/taste	Free of foreign odor or taste				
Water	200	32	20	20	
Dew point °F	–33	–61	–68	–68	
°C	–36.1	–51.7	–55.6	–55.6	

NOTE—A blank indicates no maximum limiting characteristic.

[1] Due to lack of sensitivity, this test is not required if the assay results are acceptable.

[2] The use of vapor samples is required for USP. Also, the detection of impurities is determined based on the physical characteristics of the individual impurity and need to accurately represent the physical partitioning of impurities.

[3] If the total sulfur content exceeds 0.1 ppm (v/v) as sulfur, then the species shall be determined separately and the following limits apply:

Carbonyl sulfide	0.1 ppm (v/v) max
Hydrogen sulfide	0.1 ppm (v/v) max
Sulfur dioxide	1.0 ppm (v/v) max

[4] Applies only to carbon dioxide from coal gasification and combustion sources. Current detection level is 0.5 ppm.

[5] Applies only to carbon dioxide from phosphate rock sources.

* Reproduced from CGA G-6.2 with the permission of the Compressed Gas Association. No further reproduction is permitted.

There are several analytical procedures that can be conducted to verify the purity level of a given carbon dioxide sample: for example, volumetric absorption using an Orsat type gas analysis apparatus; individual and aggregate impurity concentration calculations using gas chromatography and/or mass spectrometry; and pressure differential with reference to a cylinder certified to be 99.9% pure CO_2. Table 3.4.2 lists potential test methods that can be performed to identify the presence of various impurities [CGA, 2004].

Table 3.4.2 Testing methods for CGA specified impurities, to test grade specifications

Impurity	Testing methods
Acetaldehyde	- color-reactive chemical in a detector tube - gas chromatograph
Ammonia	- color-reactive chemical in a detector tube - wet chemical analyzer - gas chromatograph - chemiluminescent nitrogen analyzer - infrared spectrophotometer (2.9 μm characteristic wavelength for ammonia absorption) - mass spectrometer
Benzene	- color-reactive chemical in a detector tube - gas chromatograph
Carbon Monoxide	- color-reactive chemical in a detector tube - infrared spectrophotometer (4.6 μm characteristic wavelength for CO absorption) - gas chromatograph
Carbonyl Sulfide	- color-reactive chemical in a detector tube - gas chromatograph
Hydrogen Cyanide	- color-reactive chemical in a detector tube - infrared spectrophotometer (4.1 μm characteristic wavelength for hydrogen cyanide absorption)
Hydrogen Sulfide	- color-reactive chemical in a detector tube - wet chemical analyzer - gas chromatograph - chemiluminescent analyzer - fuel cell analyzer
Methanol	- infrared spectrophotometer (3.5 μm characteristic wavelength for C-H stretching) - gas chromatograph
Nitric Oxide (not to be confused with Nitrogen Oxide)	- color-reactive chemical in a detector tube - wet chemical analyzer - chemiluminescent analyzer - mass spectrometer

Nitrogen Dioxide	- color-reactive chemical in a detector tube - wet chemical analyzer - chemiluminescent analyzer - infrared spectrophotometer (3.5 μm characteristic wavelength for nitrogen dioxide absorption – could be confused with C-H stretching) - mass spectrometer
Non-volatile Residues	- sublimation of a known sample size - passing of a known gas sample size through a small orifice - both methods follow with a residual-free solvent cleansing with gently heating to remove residual solvent/moisture
Odor/Taste	- NOT BY DIRECT INHALATION - bubbling through distilled water - expanding CO_2 as "snow" into a clean cloth and placing in distilled water - both methods require (after ~15 minutes) cautiously sniffing the air pocket above the liquid, or cautiously tasting the water
Oil/Grease	- gravimetrically - infrared analysis
Oxygen	- electro-chemical analyzer with aqueous electrolyte - gas chromatograph - mass spectrometer
Phosphine	- color-reactive chemical in a detector tube - gas chromatograph - infrared spectrophotometer (4.2 μm characteristic wavelength for phosphine absorption)
Sulfur Dioxide	- color-reactive chemical in a detector tube - wet chemical analyzer - gas chromatograph - chemiluminescent nitrogen analyzer - infrared spectrophotometer (7.3 μm characteristic wavelength for sulfur dioxide absorption) - mass spectrometer - fluorescent sulfur dioxide analyzer
Total Hydrocarbon (THC) (as methane)	- flame ionization - infrared spectrophotometer (3.5 μm characteristic wavelength for C-H stretching) - mass spectrometer capable of separating and detecting hydrocarbons from carbon dioxide
Total Sulfur (as sulfur)	- wet chemical analyzer - gas chromatograph - fuel-cell analyzer - fluorescent sulfur analyzer capable of detecting total sulfur
Water vapor/dew point	- color-reactive chemical in a detector tube - electrolytic hygrometer - dew point analyzer - piezoelectric oscillating quartz crystal hygrometer - metal oxide capacitor-equipped analyzer

From table 3.4.2, one can see there is no single test method that is recommended for all potential impurities. The best method would be to set up an array of analyzers in order to avoid a limited detection capability. For a fully capable laboratory, the following equipment are recommended: gas chromatograph, infrared spectrophotometer which can be calibrated from 2 to 8 μm, a mass spectrometer, and an electrolytic hygrometer. Detector tubes are generally more suitable for determining the presence of an impurity. They can be used to determine an approximate impurity concentration, but are not generally capable of higher degrees of accuracy provided from gas chromatography, mass spectrometry, or infrared spectrometry. However, for rapid indication of a specific impurity's presence, the laboratory should be equipped with detector tubes and a full selection of color reactive chemicals specific to acetaldehyde, ammonia, benzene, carbon monoxide, carbonyl sulfide, hydrogen cyanide, hydrogen sulfide, nitric oxide, nitrogen dioxide, phosphine, sulfur dioxide, and water.

3.5 Options for Procurement of CO_2

Appendix F covers some of the available purities made available from some distributors. Also included are their prices which currently vary from $0.50 to $40 per kilogram. Keep in mind that CO_2 prices shown are for delivery to the Cambridge area, and can vary dramatically for other intended destinations [Jones, 2007].

Some of the grades used at MIT's S-CO_2 testing facilities include 99.99% instrumentation grade CO_2 at $70 per 200 scf (standard cubic feet). The higher 99.9995% purity is $300 per 150 scf. A scf is the cubic feet a quantity of gas would occupy at STP; so using the density of CO_2 $\rho_{STP} = 0.052$ kg/ft^3, these values convert to $6.73/kg of 99.99% CO_2 and $38.46/kg of 99.9995% CO_2. However the MIT research reactor uses commercial grade CO_2 at $0.60/kg. With this vast price range, it is likely to be most cost efficient to purchase lower grade CO_2 in bulk from a distributor, and use a purification system on site to obtain the desired purity. Thus 150% of the plant inventory, or 87,000 kg per 300 MW_e, the cost for commercial grade CO_2 delivered to a facility near MIT would be approximately $52,200 (compared to the cost of using instrumentation grade at about $585,500). Also added to the

cost of CO_2 procurement are delivery charges (typically ~$45), hazmat charges (~$15), and yearly contracts with monthly equipment rental fees.

The purity specifications offered by a distributor are not the only ones available. It is possible to special order a specific composition of CO_2 and maximum impurities from their processing plant; however the price will obviously fluctuate. CO_2 prices are already quite volatile at present, and can vary dramatically based on intended destination from the distributor [Jones, 2007].

If purchasing CO_2 from a distributor, it is likely that the supply company will monitor tank levels via satellite link (~ twice daily). Once the tank reaches a specified low level they will schedule a delivery. It is the supplier's responsibility to ensure that deliverable CO_2 meets the minimum CGA/ISO standards; however it is recommended that the customer regularly review analytical records available from the supplier to ensure product qualification tests are regularly conducted. Additional quality tests can also be routinely performed in a laboratory as agreed upon by the supplier and customer.

Another high initial capital cost method of obtaining CO_2 is constructing a CO_2 recovery, purification and liquefaction plant which can recover various purities of CO_2 using amine, pressure swing adsorption (PSA), and/or membrane systems. Such equipment can be purchased and installed on a turn-key basis provided there is a nearby feed-stream such as an ammonia, ethanol, hydrogen, or fossil-fuel electricity generation plant. Other sources for CO_2 recovery include fermentation plants, limestone kiln gases, natural CO_2 wells, coke oven combustion gases, burning of natural gas or other various oils, and gas streams from chemical and petrochemical operations [Braker, 1971]. According to Universal Industrial Gases Inc. (UIG), a liquid CO_2 plant can recover of up to 250 tons per day of CO_2 off a corn-to-ethanol plant, or 100 metric tons per day off an ammonia plant. An estimate of the initial and long-term operational cost for such a project should be determined for comparison to the long term bulk CO_2 delivery cost over the plant's intended operational lifetime. Such a recovery plant design and cost analysis alone could cost over $25,000 [Hogan, 2007].

3.6 Suggested Purification Methods

The presence of water vapor in the CO_2 is the most significant concern. CO_2 and H_2O will react to form carbonic acid which will be highly corrosive. Therefore proper dehydration methods will be required to reduce acidity and hydrate formation in the system. One dehydration method involves flowing the CO_2 over a molecular sieve material, silica gel, or glycol. Additionally, the possible purification system could include an O_2/H_2O getter like heated titanium, or steel wool as a sacrificial material to scavenge O_2 and H_2O. Desiccants, like aluminum oxide spheres, can also be used for moisture absorption. H_2 and CH_4 will also lead to H_2O production, hence the need for their removal in a coolant purification system.

For the removal of gaseous/volatile impurities, a bypass loop can be added for distillation using cryogenic sequestration. Cryogenic distillation will help to remove H_2S and hydrocarbons from the CO_2. Other methods for accomplishing H_2S and hydrocarbon removal include amine scrubbing, molecular sieve material, or physical absorbent materials such as Selexol, Rectisol, and Sulfinol [Kuuskraa et al., 1981]. It is also possible that the cryogenic storage system would help to purify the CO_2 of volatile gases which could then be vented off periodically. However these methods would increase the system's daily leakage rate.

Also, a membrane filter can be used to separate CO_2 from moisture, solid, and gaseous impurities. Membranes are currently being developed for CO_2 sequestration for fossil plant service, and nitrogen purification systems. The byproducts often include the CO_2 in a stream of other contaminants; therefore the membranes would need to be specifically designed to separate the CO_2 from the waste stream.

Should a small side-stream be run in parallel with the PCS, purification could be accomplished continually during normal operation. The side-stream could be redirected from the main compressor outlet to the main compressor inlet with two identical parallel purification trains using some of the methods described. This would allow for one train to continue operation while the other is down for maintenance or filter media changeout. Since

some filter media may not be able to handle CO_2 in a supercritical state, it may be necessary to depressurize the coolant prior to entry into the CPS, and then repressurize for reinjection into the PCS.

3.7 Summary

Impurities in the CO_2 can come from a variety of sources. Contaminants can be present in the bulk delivered CO_2; or arise during PCS operation from corrosion, radiolysis, or leaks in the system. The carbon dioxide purification system (CPS) is principally required for the removal of such impurities from each loop during normal operation, since elevated concentrations of these impurities could corrode or impinge system components. The purification system may also incorporate the addition of chemicals in small amounts to help control corrosion and suppress radiolysis. Finally, the system could be used to purify carbon dioxide before it is transferred to storage during PCS depressurization or vice versa.

It is recommended that the CPS run in parallel to the PCS. In this configuration, it removes a small percentage of carbon dioxide from the PCS loop, processes it to remove impurities, and returns the purified carbon dioxide to the loop. Since only a portion of the CO_2 is redirected for purification in each cycle, it will take multiple passes to turn over one complete system volume. The side-stream flow rate required to purify 100% PCS inventory in a sufficient time period needs to be selected. For example, assuming a 100% PCS mass of 58,000 kg, and a flow rate of 1,700 kg/sec out of the Main Compressor outlet, the approximate times required to cycle the entire PCS are listed in table 3.7.1. If 1% of PCS flow was diverted to the CPS, the 300 MW_e PCS could be fully purified in about one hour.

Table 3.7.1 PCS inventory estimated cycle-time based on percent flow redirected to CPS

% flow redirected	Time to cycle 100% PCS CO_2	# cycles
1	57 minutes	100
2	28 minutes	50
3	19 minutes	33
4	14 minutes	25
5	11 minutes	20
6	10 minutes	17
7	8 minutes	14
8	7 minutes	13
9	6 minutes	11
10	6 minutes	10

Potential contaminants have been listed throughout this chapter, along with some suggested purification methods that can be incorporated into the CPS. Since corrosion testing is still in the preliminary phases, the exact composition of corrosion byproducts cannot be specified. However, impurities already present in the bulk CO_2 prior to use in the S-CO_2 PCS are generally well tabulated. Probably the most important impurities to limit for maintaining the integrity of the PCS contain the elements O, H, or C; such as water, hydrocarbons, ammonia, oxygen gas, hydrogen gas, etc. The presence of water vapor in the CO_2 is the most significant concern, due to the potential for carbonic acid buildup. H_2 and CH_4 will also lead to H_2O production and must be removed.

A comparative cost analysis should be performed evaluating the purchase of higher grade CO_2, lower grade CO_2 with additional purification on-site, or an in-situ CO_2 recovery plant designed to generate the purity required. Additional testing should be conducted once the decision of desired procurement method and purity has been made, and materials for use in the PCS have been selected. An appropriate purification system can be designed in detail once the contaminants generated from the selected materials and coolant purity grade, in the conditions that will be seen in the PCS, are better understood. The purification system could include an O_2/H_2O getter like heated titanium, or steel wool as a sacrificial material to scavenge O_2 and H_20; desiccant, like aluminum oxide spheres, for moisture absorption; a membrane filter; and/or distillation using cryogenic sequestration.

4 Coolant Leak Detection Systems

4.1 Introduction and Motivation

Similar to other higher-than-ambient pressure systems, attention must be paid to system leakage monitoring. The fact is, any system that uses gas will tend to leak. The concerning factor, however, is how fast a leak occurs. When the leak is large enough to become a potential hazard for the equipment or personnel, leak detectors are used to determine the amount leaked and the composition. For the S-CO_2 system, there are unique concerns that should be addressed regarding the leakage of coolant and the impurities it may contain.

It is likely that the PCS environments will have a larger than ambient level of CO_2. In confined spaces, the OSHA 8-hour exposure limit is 5000 ppm(v) CO_2 [OSHA, 2001 & OSHA[(b)]]. For less than a 24 hour exposure duration, the U.S. Navy Submarine Service limit is about 40,000 ppm(v) [Roberts, 2007].

Due to radiolysis (for a direct cycle), corrosion, and coolant dissociation, some carbon monoxide (CO) will undoubtedly be present [Rigual, 2004]. Its OSHA 8-hour limit is 50 ppm(v) [OSHA, 2005]. CO in high levels (12.5-74%) also poses a major flammability hazard [Braker, 1971]. The ratio of CO/CO_2 will be very small, hence control of CO_2 leaks will also minimize compartment CO levels. In any event, sensitive CO detectors are widely available and are required for in-home use by many municipalities.

Leaks can be found using electronic, chemical, and/or ultrasonic methods. Most leak detectors available on the market are hand-held battery-operated devices which are programmed to detect specific conditions. Having mobile leak detectors on-hand is

particularly important because of the tight and complex piping networks in the PCS. Local in-situ leak detectors can be used for general leak detection, while portable units can be used to pin-point a leak. Also, a "boot" can be placed over expected trouble spots, like welds and bends, with detector probes for localized monitoring. A similar detector probe can be used for detecting secondary-primary system leakage via the intermediate heat exchanger in an indirect system.

There are systems currently available which are capable of detecting CO_2, however it has been proposed that the addition of a small amount of helium to the CO_2 could greatly enhance detectability [Driscoll, 2007]. First of all, the ambient atmosphere contains about 380 ppm(v) CO_2, but only 5 ppm(v) He: hence He background is much lower. Secondly, helium is inert and lightweight. Furthermore, helium leak detection is much more sensitive and is a well-established commercial offering.

4.2 Compartment Monitoring

It is assumed that maintenance personnel with be required to enter the operating spaces for routine maintenance or to carry out emergency procedures. Due to the potential danger of asphyxiation or carbon monoxide (CO) poisoning, larger scale compartment monitoring of CO_2 and CO levels will be required. CO in high levels (12.5-74%) also poses a major flammability hazard [Braker, 1971].

There are a few methods available for larger scale compartment monitoring. The first is an "alarm only" leak detector. This type of system will set off an alarm when a gas is detected, but does not provide any specific information on gas composition/concentration, or leak rates.

The second, more common type is the residual gas analyzer (RGA). In the RGA, the gas sample is drawn and ionized. The ionized molecules then pass through a electromagnetic field which alters their projection. Depending on the trajectory, the mass of each molecule can be determined. This method is great for determining the composition of the air sampled, but cannot pinpoint a leak; therefore it is recommended for larger scale compartment monitoring when CO_2 and CO levels need to be determined. Additionally, the RGA data can

be interfaced with an alarm system for audible notification of exceeded CO_2 and/or CO levels. Stanford Research Systems has developed RGAs which offer mass ranges to 300 amu with six orders of magnitude dynamic range in a single scan. Their real-time data acquisition, analysis, and control software is windows based and their RGA's range in prices from $3,750 to $6,000.

The final detector uses ultrasonic-sensitive equipment. Since gas leaks tend to be very noisy, especially at high pressures, these detectors convert the very high frequency "hissing" to a lower audible range which can be heard through a set of headphones or speakers. Ultrasonic leak detectors are better suited for large scale leaks, but with the high PCS pressures, it may also be possible to detect smaller leaks before rupture.

Compartment Levels and Limits

According to the Handbook of Tables for Applied Engineering Science (2nd ed.), the average composition of air remains essentially constant at altitudes below 50,000 ft (15,240 m). The normal air composition is shown in table 4.2.1.

Table 4.2.1 Average Composition of Dry Atmospheric Air

Gas	Molecular Weight	%		ppm	
		By volume	By weight*	By volume	By weight*
Nitrogen	N_2 = 28.016	78.084	75.513	780,840	755,126
Oxygen	O_2 = 32.000	20.946	7	209,460	231,368
Argon	Ar = 39.944	0.934	1.288	9,340	12,878
Carbon Dioxide	CO_2 = 44.010	0.0383	0.0588	383	582
Neon	Ne = 20.183	18.18×10^{-3}	0.013	18.18	12.67
Helium	He = 4.003	5.24×10^{-4}	7.24×10^{-5}	5.24	0.72
Methane	CH_4 = 16.04	1.745×10^{-4}	9.66×10^{-5}	1.745	0.97
Krypton	Kr = 83.8	1.14×10^{-4}	3.30×10^{-4}	1.14	3.30
Hydrogen	H_2 = 2.0160	5.5×10^{-5}	3.83×10^{-6}	0.55	0.04
Nitrous Oxide	N_2O = 44.01	5×10^{-5}	7.60×10^{-5}	0.5	0.76
Xenon	Xe = 131.3	9×10^{-6}	4.08×10^{-5}	0.09	0.41
Ozone	O_3 = 48.000	$0 - 7 \times 10^{-5}$	$<1.16 \times 10^{-4}$	0 - 0.7	0 - 1.16
Radon	Rn = 222	6×10^{-18}	4.60×10^{-7}	6×10^{-14}	4.60×10^{-13}
Average Water Vapor content in air for non-dry atmospheres (region dependent)					
Water Vapor	H_2O = 18.016	~1	~0.622	~9,330	~5,802

*using a mean molar mass of air = 28.97 g/mol.

As can be seen in table 4.2.1, the average dry-air concentration of CO_2 is 383 ppm(v). According to the Occupational Safety and Health Administration (OSHA) standards, the maximum tolerable CO_2 concentration for an 8-hour total weight average (TWA) permissible exposure limit (PEL) is 5000 ppm(v) or 9000 mg/m^3 at 25°C and 760 torr (0.1 MPa) [OSHA, 2001 & OSHA[(b)]], which is a factor of 13 higher than background. These limits are based on an 8 hour work-day/40 hour work-week. According to the Naval Safety Center, the exposure limits imposed on submarine personnel in confined spaces are 3.8 torr $ppCO_2$ for a 90 day exposure and 30 torr $ppCO_2$ for an exposure time of 24 hours or less [Roberts, 2007]. Assuming the compartment's total pressure is at 760 torr, the conversion yields a 5000 ppm(v) limit for a 90 day exposure, and ~40,000 ppm(v) limit for 24 hours or less exposure time. Similarly, the American Conference for Governmental Industrial Hygienists (ACGIH) and the National Institute for Occupational Safety and Health (NIOSH) have threshold limit values (TLV) or recommended exposure limits (REL) of 5000 ppm(v), 9000 mg/m^3 for TWA; and 30,000 ppm(v), 54,000 mg/m^3 for short-term exposure (STEL), averaged over 15 minutes [OSHA, 2001].

The ACGIH TLV for CO is 25 ppm(v), 29 mg/m^3 TWA; and the NIOSH REL for CO is 35 ppm(v), 40 mg/m^3 TWA or 200 ppm(v), 229 mg/m^3 ceiling for a five minute sample [OSHA, 2005]. In the past, the OSHA carbon monoxide limit changed from a "transitional" limit of 50 ppm(v) or 55 mg/m^3 for the 8-hour TWA PEL at standard temperature/pressure (STP) conditions, to a "final rule" limit of 35 ppm(v), with an inclusion of a 200 ppm(v) ceiling limit (matching NIOSH) and a 1,500 ppm(v) instantaneous limit (also called the Immediately Dangerous to Life and Health (IDLH) limit) [OSHA, 1993]. Most recent OSHA publications however, have reverted back to stating the original limit of 50 ppm(v) or 55 mg/m^3 for the 8-hour TWA PEL at STP, with no ceiling or IDLH limits [OSHA, 2005 & OSHA[(b)]].

According to OSHA, 1000 ppm CO_2, and 9 ppm (8 hour) or 35 ppm (1 hour) CO are considered determinants of ventilation system performance and overall indoor air quality [OSHA, 1990 & 1993]. As a reference, MIT monitors office space CO_2 as a general indicator of air quality to keep levels $\leq$ 1000 ppm(v) [Hallock, 2007].

Health Hazards

CO_2 displaces O_2 and poses an asphyxiation hazard. Symptoms of CO_2 overexposure are headaches, dizziness, restlessness, parethesis; dyspnea; sweating; malaise; increased heart rate, elevated blood pressure, pulse pressure; coma; asphyxia; or convulsions [OSHA, 2001].

Due to the carbon monoxide's affinity for hemoglobin (greater than 200 times that of oxygen), the CO makes the hemoglobin incapable of carrying the necessary oxygen to the tissues thereby primarily attacking the cardiovascular system (CVS), lungs, blood, and the central nervous system (CNS) [OSHA, 1991 & 1993]. Symptoms of CO poisoning are headaches; tachypnea; nausea; weakness, dizziness, confusion, hallucinations; cyanosis; depression of the ST segment of electrocardiogram; angina; or syncope [OSHA, 2005]. Survivors of CO poisoning generally sustain damages to the CNS, while those whose exposure proves fatal most likely die from myocardial ischemia [OSHA, 1991 & 1993]. The best treatment for CO poisoning is pure oxygen inhalation, but simply removing the victim to a CO-free atmosphere can remove about half of the CO within one hour [OSHA, 1991 & 1993]. Table 4.2.2 shows the symptoms that can be expected from varying concentrations of CO (extracted from OSHA's toxicology report on CO in workplace atmospheres).

Table 4.2.2 Observed clinical effects at varying CO concentrations in air [OSHA, 1991 & 1993]

Atmospheric CO (ppm(v))	COHb in Blood (%)	Symptoms
70	10	Shortness of breath upon vigorous exertion; possible tightness across the forehead.
120	20	Shortness of breath with moderate exertion; occasional headache with throbbing in the temples.
220	30	Decided headache; irritability; easy fatigability; disturbed judgment; possible dizziness; dimness of vision.
350-520	40-50	Headache; confusion; collapse; fainting upon exertion.
800-1220	60-70	Unconsciousness; intermittent convulsions; respiratory failure; death if exposure is prolonged.
1950	80	Rapidly fatal.

Compartment Monitoring Specifics and OSHA recommendations

Due to the 1.5 greater density ratio of CO_2 to air, higher CO_2 concentrations will be found at lower elevations [CGA, 2003]. Therefore any CO_2 monitoring devices should be located at lower elevations in the compartment for maximized readings. Also, ventilation systems should be designed to exhaust near the floor and draw from near the ceiling [CGA, 2003].

OSHA has recommended specific methods for monitoring long-term industrial environment CO_2 and CO levels [OSHA, 2001 & 2005]; air samples are drawn by a sampling pump, fed through a gas sampling valve, and collected in a five-layer (5-L) aluminized sampling bag (6 liter capacity) to be analyzed electrochemically, by infrared spectrophotometry, or by gas chromatography (GC) [OSHA 1993]. The flow rate is adjusted based on the desired sample time and sample purpose. If using GC, the chromatograph is fitted with the gas sampling loop and a detector -- thermal conductivity detector (TCD) for CO_2 [OSHA, 1990 & 2001], or helium glow discharge ionizing detector (DID) or flame ionization detector (FID) for CO [OSHA, 1991 & 1993].

GC for CO_2 [OSHA, 1990]**:** If testing for a STEL, the flow rate should be set to ~0.3 L/min, taking 13-20 minutes to collect 4-6 liters. If only monitoring for a TWA, the flow rate can be set between 0.01 and 0.05 L/min. However, it is generally set to between 0.020 L/min and 0.025 L/min for a 4 hour sample time. CO_2 sensitivity of the GC-TCD gives a linear working range from around 200 to 30,000 ppm when using a Hewlett-Packard (HP) 5730A GC and 3385A Automation System. (The TCD upper linear limit may actually be larger.) Other configurations can be used but will have different specifications and ranges. The lower quantitative detection limit in this configuration is 500 ppm, while a qualitative analysis for a 1 mL sample can be achieved to as low as 200 ppm. A lower detection limit can be achieved with a larger sampling loop; however with typical ambient CO_2 concentrations of 338 ppm, this is likely to never become necessary. One advantage of the GC-TCD method is that the samples are not destroyed during analysis allowing for the analysis for other potentially hazardous gases in the same sample.

GC for CO [OSHA, 1991 & 1993]: If testing for a ceiling limit, the flow rate should be set to ~1 L/min for 5 minutes. However if only monitoring for a TWA, the flow rate is generally set to between 0.020 L/min and 0.025 L/min for a 4 hour sample. For FID, the CO is combined with a hydrogen (H_2) carrier gas and converted to methane (CH_4) by a nickel catalytic methanizer. However, the sensitivity using GC-FID is very low for CO, therefore OSHA primarily recommends GC-DID. With GC-DID, helium (research grade, $\leq$ 1 ppm impurities) is often used as a sample "carrier" gas and as the ionized species. The gas passes through a high-energy photon beam and is ionized for electron collection by an electrometer. CO sensitivity of the GC-DID gives a linear working range from 1.70 to 63.6 ppm when using a Tracor 540 GC, Tracor Model No. 706 DID, and HP 3557 Laboratory Automation System, rev 2540. Other configurations can be used but will have different specifications and ranges. The OSHA validated range for CO measurement of the GC-DID in this configuration is 17.2 to 63.6 ppm with an error of ±10.8%. The lower quantitative limit for CO is 0.40 ppm, while a qualitative analysis can be reached as low as 0.12 ppm for a 1 mL sample. A lower detection limit can be achieved with a larger sampling loop. Another OSHA tested CO monitor instrument using the GC-DID method is the Dräger Model 190 CO Datalogger with a 4.1 – 999 ppm range and 9.6% uncertainty. (With this limited range, the Dräger Datalogger is not capable of monitoring for the 1,500 ppm instantaneous limit.) The lower quantitative limit for this datalogger is 4.1 ppm, while a qualitative analysis can be reached as low as 1.2 ppm for a 1 mL sample.

An advantage to using the gas bag method of sample collection is that personal sample bags can be attached to the torso of maintenance personnel for close proximity testing within the work zone [OSHA, 1990]. Also, once a sample is collected, mass spectrometry can also be used for additional verification if desired [OSHA, 1990]. The disadvantage is that the samples have to be analyzed in a lab, and must be completed within 2 weeks of collection before the sample becomes too degraded (>10%) [OSHA, 1990, 1991 & 1993]. Therefore, on-site rapid sampling should also be available.

Short-term detector tubes can be used as a secondary CO_2 and CO sampling technique for spot checks on the environment. OSHA recognizes three different Safety Equipment Institute (SEI) certified detector tubes for CO_2 monitoring which are shown in table 4.2.3 below [OSHA, 2001]. Also shown are two OSHA approved infrared spectrophotometers (ISP) that can be used [OSHA, 2001]. As the sample contents are flooded with IR light from the ISP, the molecules will absorb some of the energy into the molecular bonds and emit their own distinct frequency as they de-excite. These emitted frequency pulses are counted and displayed with the ranges shown in the table. If opting to use the MIRAN 1A or 1B models, it is recommended that the newer 1B2 or 1BX models (parts are interchangeable with 1B) be purchased since they are specifically calibrated for CO_2 and CO, however the 1BX sells for about $1000 more. The prices shown do not include replacement filters (~$750 ea.) and annual recertification costs.

Table 4.2.3 OSHA approved CO_2 detector tubes and ISPs for short-term testing

Manufacturer	Part #	Range	Price
Gastec	2L	0.13 – 0.6 %(v), or 1300 – 6000 ppm(v)	$56.00
Matheson/Kitagawa	8014-126SA	0.1 – 2.6 %(v), or 1000 – 26,000 ppm(v)	
Dräger	CH 23501	0.5 – 6 %(v), or 5000 – 60,000 ppm(v)	$60.00
ISP	MIRAN 1A & 1B	0.4 ppm @ 4.3 μm	~$8,000
ISP	MIRAN 103	2% @ 4.45 μm	~$8,000

4.3 Local Monitoring

The previous section discussed monitoring specifically for CO_2 and CO for health reasons, as well as flammability of the compartment air. This section focuses more on detecting leaks and determining leakage flow rates for equipment and plant safety. These methods of detection are not limited to equipment designed to sniff for CO_2 and CO.

Once it has been determined that a leak has developed in the system, the leak must then be localized and assessed. A couple of methods are available for pinpointing the source of a leak. The first involves a colorimetric developer. In the vicinity of a leak, a color change will occur in the developer due to a chemical reaction with the high concentration of a specific gas. It must be "reset" by changing out the developer once a leak has been detected and secured. This test is sufficient for small leaks, but obviously must be performed manually or inspected routinely if permanently posted in key locations. It also cannot be

incorporated into an audible alarm system, unless the detectors use chemicals with fast, reversible reactions allowing for continuous operation.

Permanently mounted and portable gas analyzers are also available, which generally use mass spectrometry on a tracer gas such as hydrogen or helium. Since hydrogen poses a significant problem for water formation and corrosion in a S-CO_2 PCS, helium would be preferred. These detectors start at around $9000 (Varian 5.7 lb 2 ppm Portable Helium Detector PHD-4), and decrease in price as the minimum level detectable increases (i.e. $7000 for a Varian 12 lb 10 ppm PHD). These leak detectors can also measure the leak rate, displaying concentrations and rates numerically and graphically on a digital display in automatic, semi-automatic, or manual modes. This method would be particularly useful for detecting leaks through a heat exchanger using a detector probe on the low pressure side's effluent. Also, a "boot" can be placed over expected trouble spots, like welds and bends, with detector probes for continual monitoring.

For additional verification of a suspected leak, a maintenance person can cover the area with a thin film of a soapy solution, or hold a squeeze bottle containing aqueous ammonia in the vicinity of the suspected leak. Leaks will be indicated by the bubble formation in the soapy layer, or the formation of a white ammonium carbonate cloud in the bottle due to the reaction with CO_2 [Braker, 1971].

4.4 Helium Addition

Leak detectors generally use mass spectrometry. Since very few compounds ionize down to a mass of 2, this inert gas is commonly used for leak detection. For example, helium is currently being added as a tracer to greatly increase the safety, accuracy, and speed of leak detection in underground nitrogen pipelines, steam turbines, condensers, chemical and plastic production plants, and heat exchangers. Due to the well-established commercial market for He leak detectors, it has been proposed that He gas be added to the coolant. It will make leak detection easier due to the faster diffusion and effusion of the helium atoms, and less ambiguous due to the lower average background levels of He.

Helium leak detectors have been designed with an ability to detect He levels from as low as 2 ppm to roughly 300 ppm. Since background levels are generally about 5 ppm, an estimate of 25-50 ppm detectability should be sufficient. For a helium leak detector capable of sensing 25 ppm(v) He, one can calculate that less than 0.5 %(v) is more than sufficient to detect one day's worth of 0.5% leakage or more. This calculation is described in detail in appendix G. More research would need to be conducted on the coolant's potential property changes should this or larger amounts of helium gas be added.

For compartment CO monitors such as the 5-L aluminized sampling with GC-DID, helium (research grade, ≤ 1 ppm impurities) is often used as a sample "carrier" gas and as the ionized species. The gas passes through a high-energy photon beam and is ionized for electron collection by an electrometer. Thus, although adding He to the coolant will benefit local leak detection systems (in-situ and portable gas analyzers), it would not be useful for compartment CO monitoring.

If gas analyzers using trace helium are to be used for compartment CO_2 monitoring, it is suggested that the sampling locations be placed in higher altitudes due to light-weight helium's tendency to rise. This is in direct contrast with systems designed to detect CO_2 directly.

4.5 Summary

Rising levels of CO_2 could be a sign of a leak from a crack somewhere in the system; or it can also indicate a failure in the cryogenic tank refrigeration loop which can lead to a gradual loss of CO_2 through the pressure relief system. In either case, the effects can be dangerous to both the equipment and personnel. All systems that use gas will leak, so an estimated daily leak rate of 0.5% has been assumed acceptable. Leaks above this rate will require prompt action for locating and securing the leak. Also, due to the dangerous nature of CO_2 and CO for personnel, the risen compartment levels will require increased ventilation until levels have been reduced below the OSHA limits given in this chapter.

In-situ monitors will need to be strategically placed within the compartment for obtaining representative air samples, and ease of access as needed for maintenance and data

collection. For direct CO_2 and CO monitoring, these detectors should be placed at lower elevations, while detectors intended to pick up a helium tracer should sample from higher elevations. For system components expected to be trouble spots for leakage, detector probes can be situated in boots or effluent locations for virtually instantaneous notification.

Due to the complexity of the tight PCS piping networks, and the need to pinpoint a leak detected by other methods, portable detectors will have to be readily available to maintenance personnel. Additionally, in the event of routine maintenance, maintenance personnel should fasten a personal gas sampling bag to each of their torsos. This will help to ensure that CO_2 and CO levels are monitored while the personnel are in the work zone.

5 Summary, Conclusions and Recommendations

5.1 Summary of Findings

Despite current progress on designing a Supercritical CO_2 Power Conversion System, little work has focused on the principal supporting systems required. A compilation of the required supporting systems [Harrington, 1992 and Hunt, 2002] that need to be developed includes:

- Start-Up System,
- Plant Instrumentation and Control System,
- Safety and Accident Mitigation System,
- Electrical Power Distribution System,
- Component Cooling System,
- Maintenance System,
- Inventory Control System,
- Coolant Make-Up and Charging System,
- Coolant Purification System, and
- Coolant Leak Detection System.

Many of these required auxiliary systems will be similar in design to those used in other nuclear or fossil-fired units; however, the last three have specialized requirements when CO_2 is used as the working fluid. This thesis analyzes these three systems in detail and meets the following goals for:

- Coolant Storage for Make-up and Charging
  - Weighing potential forms of coolant storage: cryogenic and HPG,

- ❖ Finding "back of the envelope" methods for estimating the coolant transferred, and
- ❖ Developing a detailed conceptual design.

- Coolant Purification
  - ❖ Listing possible coolant contaminants and their sources,
  - ❖ Discussing options for the procurement of the CO_2 from potential distributors,
  - ❖ Specifying significant CO_2 purity concerns for the S-CO_2 system, and
  - ❖ Suggesting various purification methods to be incorporated into a future detailed design.
- Coolant Leak Detection
  - ❖ Describing various methods of coolant leak detection using both in-situ analyzers and portable devices,
  - ❖ Discussing the possibility of adding helium as a tracer gas for coolant leak detection, and
  - ❖ Providing required methods for monitoring of compartmental CO_2 and CO concentrations to meet OSHA limits.

Coolant Make-up and Charging System

Chapter 2 describes the potential coolant storage system for make-up and charging CO_2 to and from the PCS. For the reference 300 MW_e PCS discussed, the amount of CO_2 in the closed loop at full power is approximately 58,000 kg. Inventory storage capacity for make-up and charging must be sufficient for a complete system blow down or charging, as well as maintaining loop inventory from CO_2 losses. The preliminary estimate for daily leakage is 0.5% (or ~290 kg/day, or 8,730 kg/month). Additional make-up will likely be required either due to the breakdown of the CO_2 by corrosion or radiolysis, or losses of CO_2 in the purification process. Estimates on this amount are still to be determined. The conceptual storage designs presented in this thesis are intended for storage of approximately 150% system volume, or 87,000 kg. A variety of storage methods are presented including a high pressure gas (HPG) storage system, a single cryogenic tank, and a hybrid combination of the two. Three-dimensional drawings of these system configurations are included in appendix C.

For the HPG storage method, the system will be required to operate at a maximum pressure of 20 MPa. For atmospheric temperature at this pressure, and with the compressor to utilize full storage tank capacity, an estimate of ~100 m^3 total tank volume situated in a bank of ten 10 m^3 tanks or four 28 m^3 Europipe tanks is required. In the event that differential pressure is used as the primary driving force between the plant and storage, this volume increases by a factor of 4-5 (meaning at least forty-six 10 m^3 tanks, or sixteen Europipe tanks).

For the cryogenic storage method, the tank is designed to operate at approximately 4 MPa/5°C with a 20% vapor pocket above the liquid CO_2. This leads to a tank size of about 116 m^3.

In the hybrid configuration, the HPG storage is used to contain 50% while the cryogenic tank contains the remaining 100%. For such a system, only sixteen 10 m^3 HPG tanks, and a 77 m^3 cryogenic tank are required. Should a compressor be added to the HPG system, the number of HPG tanks can be reduced to 3.

Coolant Purification

Chapter 3 lists potential impurities that could be introduced into the CO_2 from sources in and outside of the PCS. Water Vapor is the most significant concern, since CO_2 and H_2O react to form H_2CO_3 (pH $\approx$ 3.5) which is highly corrosive. H_2 and CH_4 will also lead to H_2O production and must be removed. Dehydration methods which can be used include flowing the CO_2 over a molecular sieve material, silica gel, or glycol; using an O_2/H_2O getter like heated titanium, placing a sacrificial material like steel wool in the system to scavenge O_2 and H_2O; or flushing the coolant through desiccants, like aluminum oxide particles which absorb moisture.

Gaseous/Volatile Impurities can easily be removed using a bypass loop for distillation using cryogenic sequestration. Cryogenic distillation will also help to remove H_2S and hydrocarbons from the CO_2. An additional benefit to using a cryogenic storage system would be the removal of volatile gases from the CO_2 which could then be vented off periodically.

Membranes can also be used in a purification loop for the separation of CO_2 from moisture, solids, and gaseous impurities.

It is recommended that the CPS loop be run in parallel to PCS so that purification could be accomplished continually during normal operation. The coolant would be redirected from the main compressor outlet to the main compressor inlet and draw a small percentage of the 1,700 kg/sec flowing from the main compressor. It takes approximately 34 seconds for the CO_2 to cycle once through the PCS. If 1% of the PCS inventory is redirected to the CPS, it would take about an hour to purify the entire inventory. Increasing the percentage to 10% would allow the entire PCS volume to be purified 10 times in a single hour. If two identical parallel purification trains are added per loop, this cycle time could be cut in half. It would also allow for one train to continue operation while the other is down for maintenance or filter media change out.

Coolant Leak Detection Systems

If compartment CO and CO_2 levels begin to rise, it could be an indication of a leak from a crack in the system, or a failure in the cryogenic tank refrigeration loop which would cause a gradual loss of CO_2 via pressure relief system. This can be dangerous to both equipment and personnel. Since no gas system is impervious to leakage, an estimated daily leak rate of 0.5% has been assumed acceptable.

In-situ monitors should be strategically placed within the compartment for obtaining representative air samples, and ease of access as needed for maintenance and data collection. For direct CO_2 and CO monitoring, these detectors should be placed at lower elevations. Detectors sniffing for helium tracer should sample from higher elevations. Helium addition as a tracer gas has proven effective in underground nitrogen pipelines, steam turbines, condensers, chemical and plastic production plants, and heat exchangers. There is wide commercial availability for sensors with 2 ppm to roughly 300 ppm detectability. Since background He levels are approximately 5 ppm, an estimate of 25-50 ppm detectability should be appropriate. For a helium leak detector capable of sensing 25 ppm(v) He, less than a 0.5 %(v) He added to the CO_2 is needed to detect one day's worth of 0.5% leakage or more.

For system components expected to be trouble spots for leakage, detector probes can be situated in boots or effluent locations for virtually instantaneous notification.

Portable battery operated detectors will also be required due to the complexity of the tight PCS piping networks, and the need to pinpoint a leak detected by other methods. These should be readily available to maintenance personnel. Additionally, for routine maintenance, a maintenance person should fasten a personal gas sampling bag to his/her torso.

5.2 Issues to be Resolved by Future Work

Some additional key items for future work include:

- Designing seals and bearings for minimum leakage and coolant contamination,
- Testing of coolant property changes by adding He for leak detection,
- Evaluating emergency power requirements and methods of provision (diesel, battery back-up, alternate power-grid, etc.),
- Detailing start-up procedures and identifying special support features,
- Detailing an evacuating system to remove PCS air during initial start-up or following major maintenance,
- Designing filter cartridges capable of operating in both vapor and liquid phases of S-CO_2,
- Detailing purification system design and operation, including laboratory demonstration, and
- Measurements of distribution coefficients between vapor and liquid phases for impurities.

Designing a system to work with CO_2 requires certain safety considerations due to the nature of the fluid. Further design criteria should include the following requirements.

Allowances should be allowed for piping contraction as temperature is reduced. For example, if using copper piping, the pipes will shrink ~2.5 cm per 30.5 m length of tubing for every 55.6°C reduction in temperature [CGA, 2003].

Additionally, pressure relief valves should be placed anywhere in a CO_2 system where liquid CO_2 could become trapped. Should liquid CO_2 become trapped in between two points of isolation, the pressure will begin to rise as the liquid warms to ambient temperature. Provided that the liquid has a vapor space for expansion, the pressure rise is only 62 kPa per °C. As soon as the liquid no longer has a vapor bubble to collapse, the pressure rise jumps to 10.55 MPa per °C! Pressure relief valves (vented to a well-ventilated area) will alleviate the pressure before it rises above the system's design limits. This is of particular concern in ball and gate valves which should be designed such that liquid CO_2 cannot become trapped within a closed valve at all. Valve sizing methods can be found in Ouderkirk, 2002.

Neoprene, nylon, ethylene-propylene diene monomer (EPDM), and polytetrafluoroethylene (PTFE) are commonly used in both CO_2 regulators and cylinder valves. Materials that absorb carbon dioxide and swell or deform (i.e. certain formulations of Buena-N and natural rubber) should be avoided. When deciding on construction materials for CO_2 systems and piping, cast iron pipes and malleable iron and steel pipes should not be used to avoid fracture upon impact due their brittle nature under cold conditions.[CGA, 2003]

One of the auxiliary systems listed in the introduction included a component cooling system. In all likelihood, this system will not vary significantly from other nuclear or fossil fuel systems. However, in the event that the component cooling systems serve the shaft seals and bearings, this would require the incorporation of a very important set of specific S-CO_2 requirements. If this becomes the case, future work beyond this thesis should ensue.

References

Ballinger, R. G., J. Lim, G. Eastwick, and T. McKrell, *Corrosion of Materials in Supercritical CO_2 Environments*, TM-INES2, July 23 (2007).

Braker, W., A. L. Mossman, *Matheson Gas Data Book*, Fifth Edition, Matheson Gas Products, September (1971).

Carstens, N., M. J. Driscoll, and P. Hejzlar, "Dynamic Response and Safety Implications for Supercritical CO_2 Brayton Cycles Coupled to Gen-IV Reactors," MIT-ANP-TR-114, July (2007)

Compressed Gas Association, Inc., *Handbook of Compressed Gases*, Third Edition, Van Nostrand Reinhold Press, (1990).

Compressed Gas Association, Inc., *Carbon Dioxide*, Sixth Edition, CGA G-6, (2003).

Compressed Gas Association, Inc., *Commodity Specification for Carbon Dioxide*, Fifth Edition, CGA G-6.2, (2004).

DOE, GNEP website http://www.**gnep**.energy.gov (2007)

Dostal, V., M.J. Driscoll, and P. Hejzlar, "A Supercritical Carbon Dioxide Cycle for Next Generation Nuclear Reactors," MIT-ANP-TR-100, March (2004).

Dostal, V., P. Hejzlar and M.J. Driscoll, "High-Performance Supercritical Carbon Dioxide Cycle for Next-Generation Nuclear Reactors," *Nuclear Technology*, **154**, No. 3, June (2006).

Dostal[(b)], V., P. Hejzlar and M.J. Driscoll, "The Supercritical Carbon Dioxide Cycle: Comparison to Other Advanced Power Cycles," *Nuclear Technology*, **154**, No. 3, June (2006).

Driscoll, M. J., MIT Department of Nuclear Science and Engineering, Personal Communication, June 29, (2007).

Driscoll, M. J., and A. A. Hajj-Ahman, "Supercritical CO_2 Power Conversion Systems for Fusion Reactors," *Transactions of the American Nuclear Society*, **96**, June (2007).

Fishkin, L.B., "Prestressed Cast Iron Vessel (PCIV) Use for Gen-IV GFR Applications," MIT-GFR-006, April (2004).

Fernandez, S. S., A. A. Hajj-Ahmad, E. Bolukbasi and M.J. Driscoll, "Extended-Scope Applications of the Supercritical CO_2 Power Conversion System," MIT-GFR-039, August 15 (2006).

Gibbs, J. P., P. Hejzlar and M.J. Driscoll, "Applicability of Supercritical CO_2 Power Conversion Systems to GEN IV Reactors," MIT-GFR-037, September 15 (2006).

Gibbs, J., "Power Conversion System Design for Supercritical Carbon Dioxide Cooled Indirect Cycle Nuclear Reactors," to be published February (2008).

GIF, Generation IV International Forum website, http://www.gen-4.org/, (2007)

GIF[(b)], Generation IV International Forum website, http://www.gen-4.org/Technology/systems/index.htm, (2007)

Gilbreath, J.R. and O.C. Simpson, "The Effect of Reactor Irradiation on the Physical Properties of Beryllium Oxide," *2nd U.N. International Conference on the Peaceful Uses of Atomic Energy*, P/621 (1958).

Gräf, M. K., H. G. Hillenbrand, C. J. Heckman and K. A. Niederhoff, "High-Strength Large-Diameter Pipe for Long-Distance High Pressure Gas Pipelines," ISOPE, Honolulu, May 26-30 (2003).

Hallock, M., IHP Officer, MIT Office of Environment, Health & Safety, Personal Communication, July 30, (2007).

Handwerk, C.S., M.J. Driscoll, P. Hejzlar, P. Yarsky, and M.A. Pope, "Power Shaping of a Long-Lived GFR Core Using Diluents," *Transactions of the American Nuclear Society*, **93**, Nov. 13-17 (2005).

Handwerk, C.S., M.J. Driscoll, P. Hejzlar, "Use of Beryllium Oxide to Shape Power and Reduce Void Reactivity in Gas Cooled Fast Reactors," *Proceedings of PHYSOR '06*, Sept. 10-14 (2006).

Handwerk, C.S., M.J. Driscoll, P. Hejzlar, "Core Design and Performance Assessment for a Supercritical CO_2-Cooled Fast Reactor," MIT-ANP-TR-113, May (2007).

Harrington, R. L., Newport News Ship Building, *Marine Engineering*, The Society of Naval Architects and Marine Engineers Press, (1992).

Hejzlar, P., MIT Department of Nuclear Science and Engineering, Personal Communication, March 16, (2005).

Hejzlar, P., V. Dostal and M.J. Driscoll, "A Supercritical CO_2 Cycle- a Promising Power Conversion System for Generation IV Reactors," *Proceedings of ICAPP '06*, Paper #6307, Reno, NV, June 4-8 (2006).

Hejzlar, P., M.J. Driscoll, J. Gibbs, Yifang Gong, and S.P. Kao, "Supercritical CO_2 Brayton Cycle for Medium Power Applications," MIT-ANP-PR-117, July (2007)

Hogan, John F., Universal Industrial Gases Inc., Personal Communication, August 16, (2007).

Hunt, E. C., J. A. Harbach, A. L. Rowen, et al., *Modern Marine Engineer's Manual*, Third Edition, Volumes I and II, Cornell Maritime Press, (2002).

INL, Idaho National Laboratory website, *www.inl.gov/gen4/gfr.shtml*, (2006).

INL (b), Idaho National Laboratory, "RELAP5-3D© Code Manual," INEEL-EXT-98-00834, Rev. 2.3, April (2005).

Jones, Horace, Airgas Supply Company, Personal Communication, August 6, (2007).

Kuuskraa, V. A., E. C. Hammershaimb, D. E. Wicks, "EOR Major Equipment and Its Projected Demand," *Oil and Gas Petrochem. Equip.*, September (1981).

Oh, C. H. et al., *Development of a Supercritical Carbon Dioxide Brayton Cycle: Improving VHTR Efficiency and Testing Material Compatibility, Final Report*, Idaho National Labs, INL/EXT-06-01271, March (2006).

OSHA, U.S. DOL, "Carbon Dioxide in Workplace Atmospheres," Method No. ID-172, Last revised June (1990).

OSHA, U.S. DOL, "Carbon Monoxide in Workplace Atmospheres," Method No. ID-210, March (1991).

OSHA, U.S. DOL, "Carbon Monoxide in Workplace Atmospheres (Direct-Reading Monitor)," Method No. ID-209, March (1993).

OSHA, U.S. DOL, "Carbon Dioxide," Last revised September 12, (2001).

OSHA, U.S. DOL, "Chemical Sampling Information: Carbon Monoxide," Last revised March 20, (2005).

OSHA[(b)], U.S. DOL, "29 CFR 1910.1000 Z-1 Table."

Ouderkirk, R., Fluor Corp, "Rigorously Size Relief Valves for Supercritical Fluids." CEP Magazine, August (2002).

Pope, M.A., M.J. Driscoll, P. Hejzlar, "Reactor Physics Design of Supercritical CO_2-Cooled Fast Reactors," MIT-ANP-TR-104, September (2004).

Pope, M.A., "Thermal Hydraulics of a 2400 MWth Direct Supercritical CO_2-Direct Cycle GFR," MIT-ANP-TR-112, September (2006).

Rigual, D. et al., "Interim Report on Task 2: Loops for Corrosion Tests in Supercritical CO2 in the Presence of Radiolysis," MIT-GFR-010, March, (2004).

Shropshire, D., 2004, "Lessons Learned From Gen I Carbon Dioxide Cooled Reactors," *ICONE-12, Crystal City, VA, ICONE12-49380, INEEL/CON-04-01526*, April (2004).

SOLID EDGE™ Version 17.00.02.04 © 2005 UGS

Roberts, Senior Chief of Naval Safety Center, Submarine Division, Personal Communication, July 30, (2007).

U.S. DOE, "A Technology Roadmap for Generation IV Nuclear Energy Systems: Ten Nations Preparing Today for Tomorrow's Energy Needs," U.S. DOE Nuclear Research Advisory Committee (NERAC) and the Generation IV International Forum, GIF-002-00, December (2002).

Wang, Y., G. Guenette Jr., P. Hejzlar and M.J. Driscoll, "Supercritical CO_2 Turbine and Compressor Design," MIT-GFR-015, June (2004).

Yildiz, B., K.J. Hohnholt and M.S. Kazimi, "Hydrogen Production Using High-Temperature Steam Electrolysis Supported by Advanced Gas Reactors with Supercritical CO_2 Cycle," *Nuclear Technology*, **155**, July (2005).

Appendix A

Contained herein are the codes used in RELAP5-3D [INL[(b)], 2005] for simulations of the high pressure gas (HPG) storage method described in section 2.2 of this thesis. Selected RELAP5 output data were plotted in excel and included following each code fragment. Blank NIST plots like those used in the simple "pick-off" estimation methods described are also included.

The first simulation was the emptying of the power conversion system (PCS) into a reference 10 m^3 HPG inventory control vessel (ICV).

Discharging the PCS into HPG ICV (case discussed in section 2.2)

RELAP5 Code:

```
= Inventory Control Test (with time dependence)
*
* Prepared in Mar. 2007
* Rosemary Freas
*
*******************************************************************************
0000001      11 *modifies the coding for supercritical pressure conditions
*------------------------------------------------------------------------------
0000100                 newath               transnt
*------------------------------------------------------------------------------
0000101                 run
*------------------------------------------------------------------------------
*                    si units used in this system
0000102              si                 si
*------------------------------------------------------------------------------
0000120   101010000  0.0     co2   primary
*------------------------------------------------------------------------------
*      runtime minstep maxstep option mineditfreq majeditfreq  restartfreq
0000201  25.   1.0e-6  0.005   0003   100         100          1000
*------------------------------------------------------------------------------
*Trip number definitions
20600000        expanded
*------------------------------------------------------------------------------
**Initialize valve position at time 0 to closed and open at rate specified
20600010      p   101010000       ge   p   105010000       0.0      1
**close at equil press
20600020      p   101010000       lt   p   105010000       0.0      1
*==============================================================================$
*hydro           component name     component type
1010000          primary            snglvol
```

```
*---------------------------------------------------------------------$
*hydro          area                length              volume
1010101         0.01                0.0                 80.14592085
*
*hydro          horz angle          vert angle          delta z
1010102         0.0                 0.0                 0.0
*
*hydro          roughness           hyd diam            fe
1010103         0.0                 0.0                 10
*
*hydro          ebt                 pressure            tempe
1010200         003                 20000000.0          333.13
*=====================================================================$
*=====================================================================$
*hydro          component name      component type
1040000         mtrvlv              valve
*---------------------------------------------------------------------$
*hydro       from          to           area       f loss     r loss      vcas
1040101      101010000     105000000    0.01       40.0       40.0        00100
*
*hydro          vel/flw       f flowrate    g flowrate    j flowrate
1040201         1             0.0           0.0           0.0
*
*hydro          type
1040300         mtrvlv
*
*hydro          open trip number  close trip number  rate   init pos table
1040301         0001              0002               100.   0.0      0.0
*=====================================================================$
*=====================================================================$
*hydro          component name      component type
1050000         invent              snglvol
*---------------------------------------------------------------------$
*hydro          area                length              volume
1050101         0.1                 0.0                 10.0
*
*hydro          horz angle          vert angle          delta z
1050102         0.0                 0.0                 0.0
*
*hydro          roughness           hyd diam            fe
1050103         0.0                 0.0                 10
*
*hydro          ebt                 pressure            tempe
1050200         003                 8000000.0           307.84
*=====================================================================$
.
```

RELAP5 Output Data:

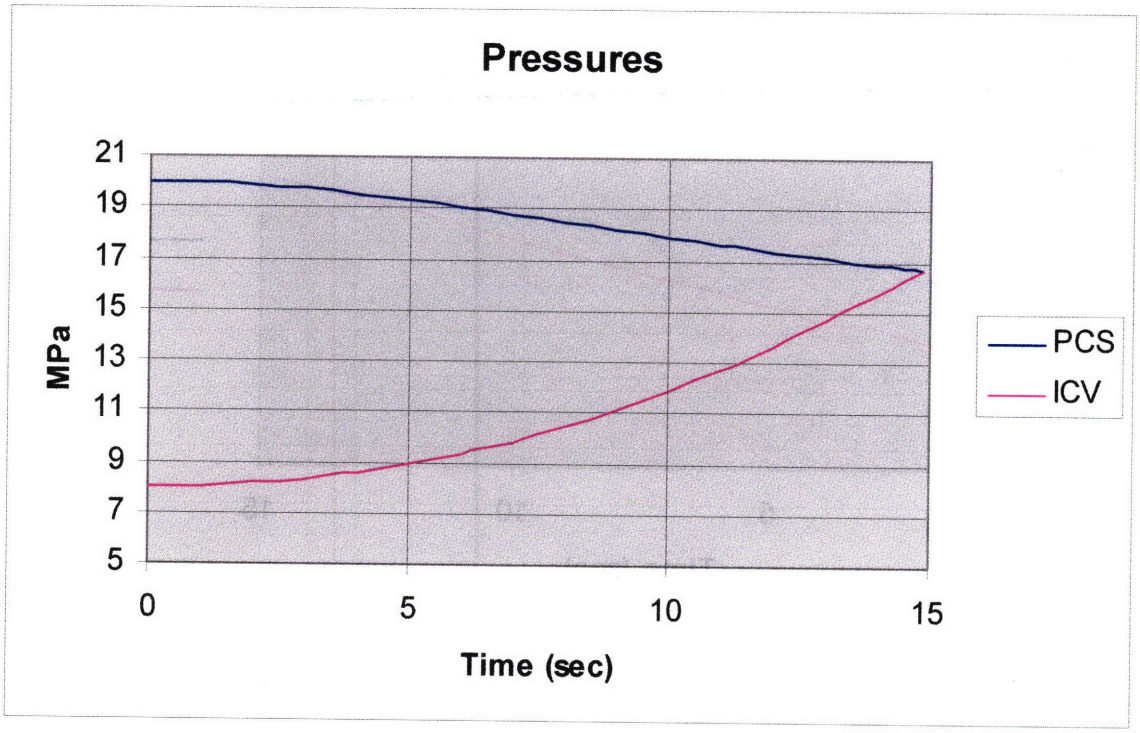

Figure A - 1 RELAP5 Pressure Data for PCS Discharge Simulation

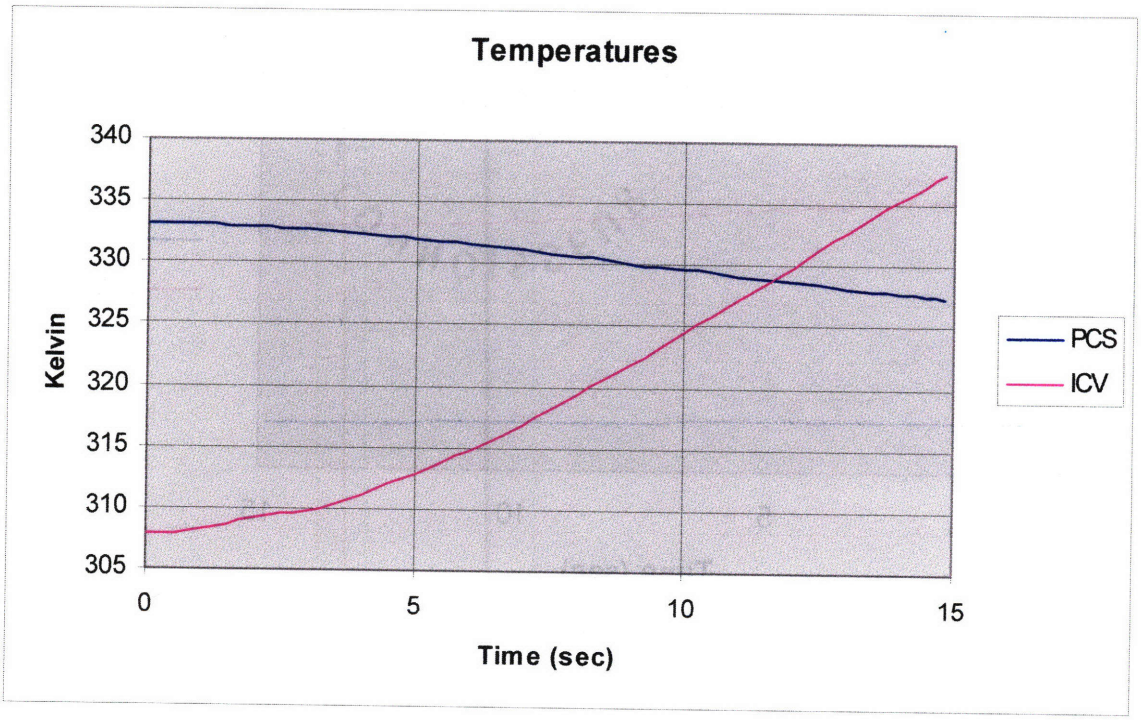

Figure A - 2 RELAP5 Temperature Data for PCS Discharge Simulation

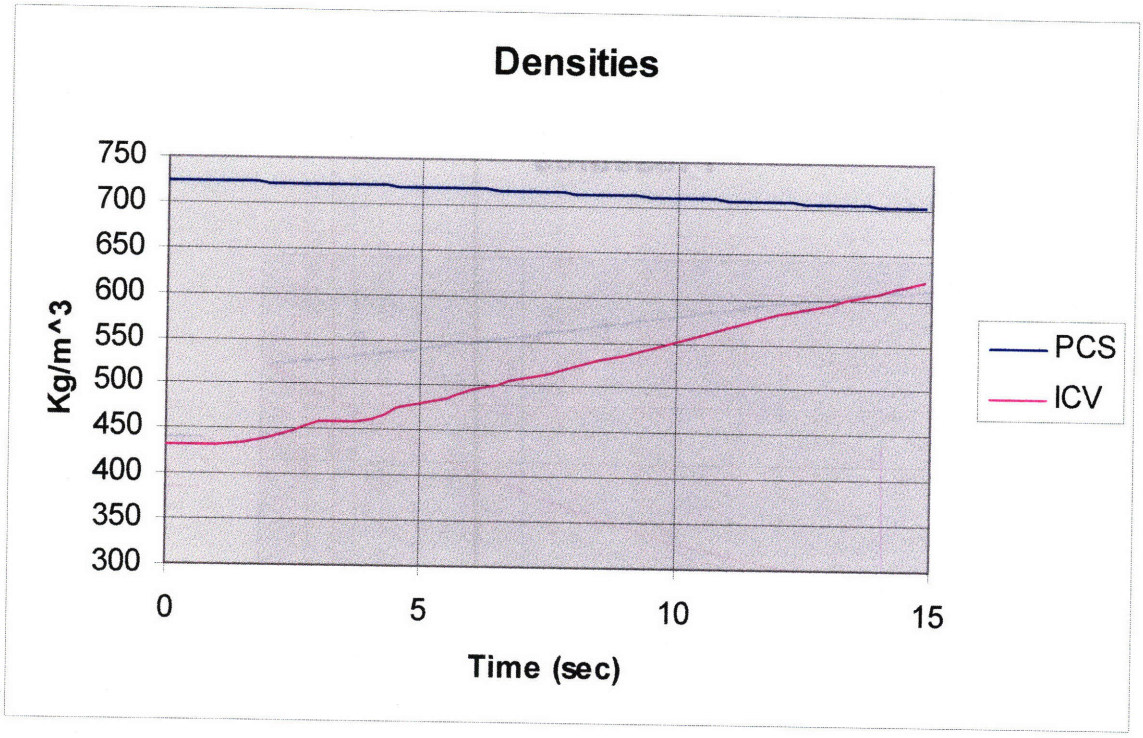

Figure A - 3 RELAP5 Density Data for PCS Discharge Simulation

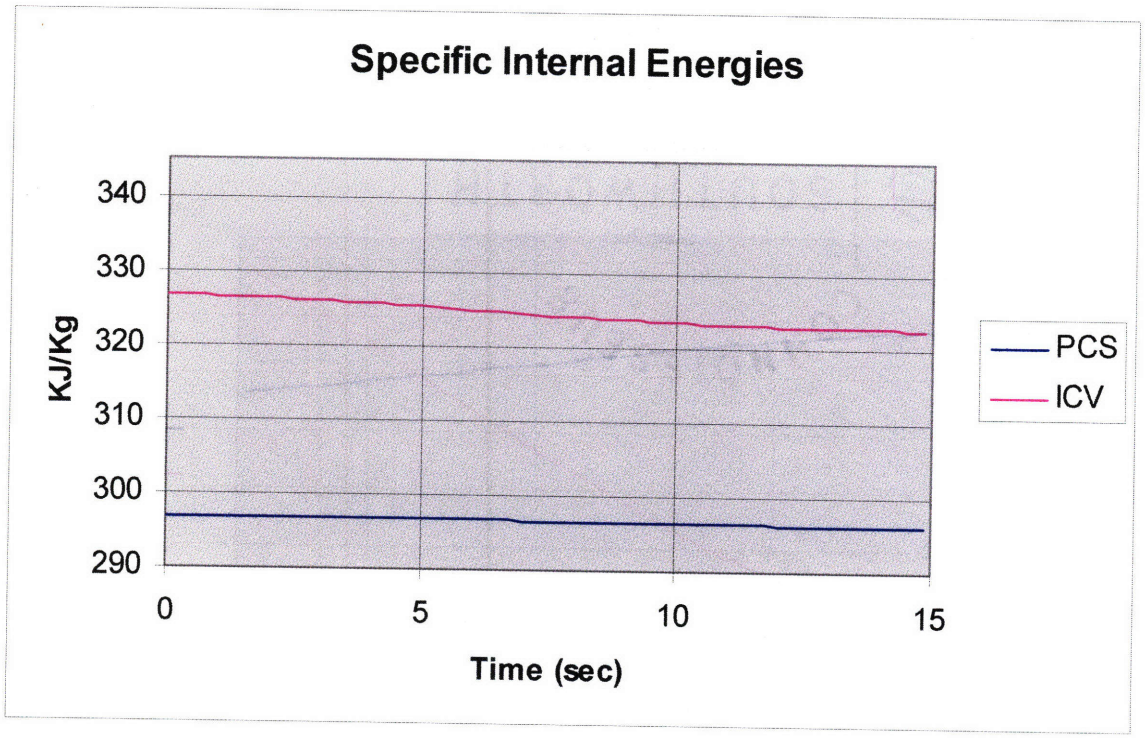

Figure A - 4 RELAP5 Specific Internal Energy Data for PCS Discharge Simulation

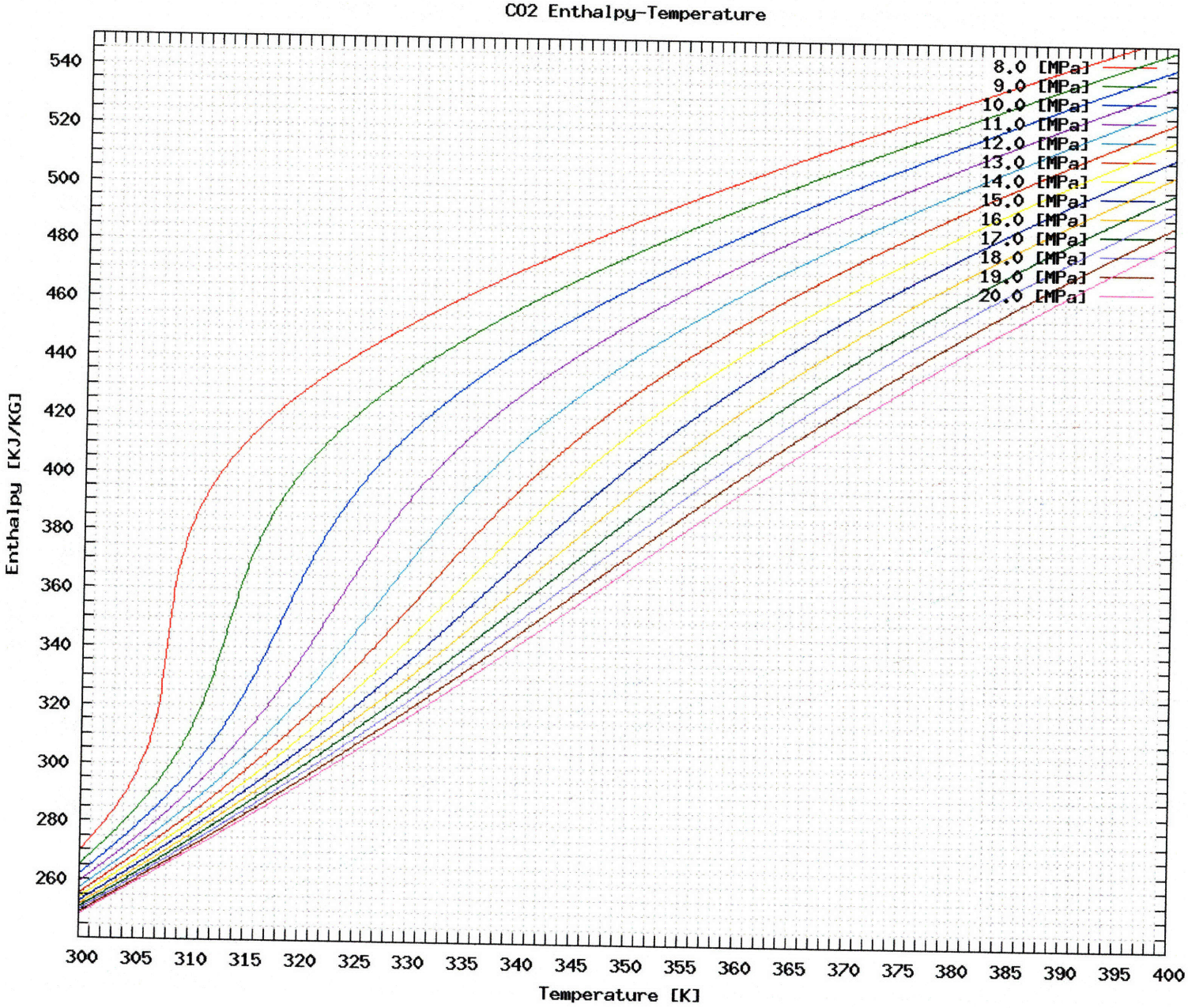

Figure A - 5 Enthalpy vs. Temperature at varying Pressures for CO_2

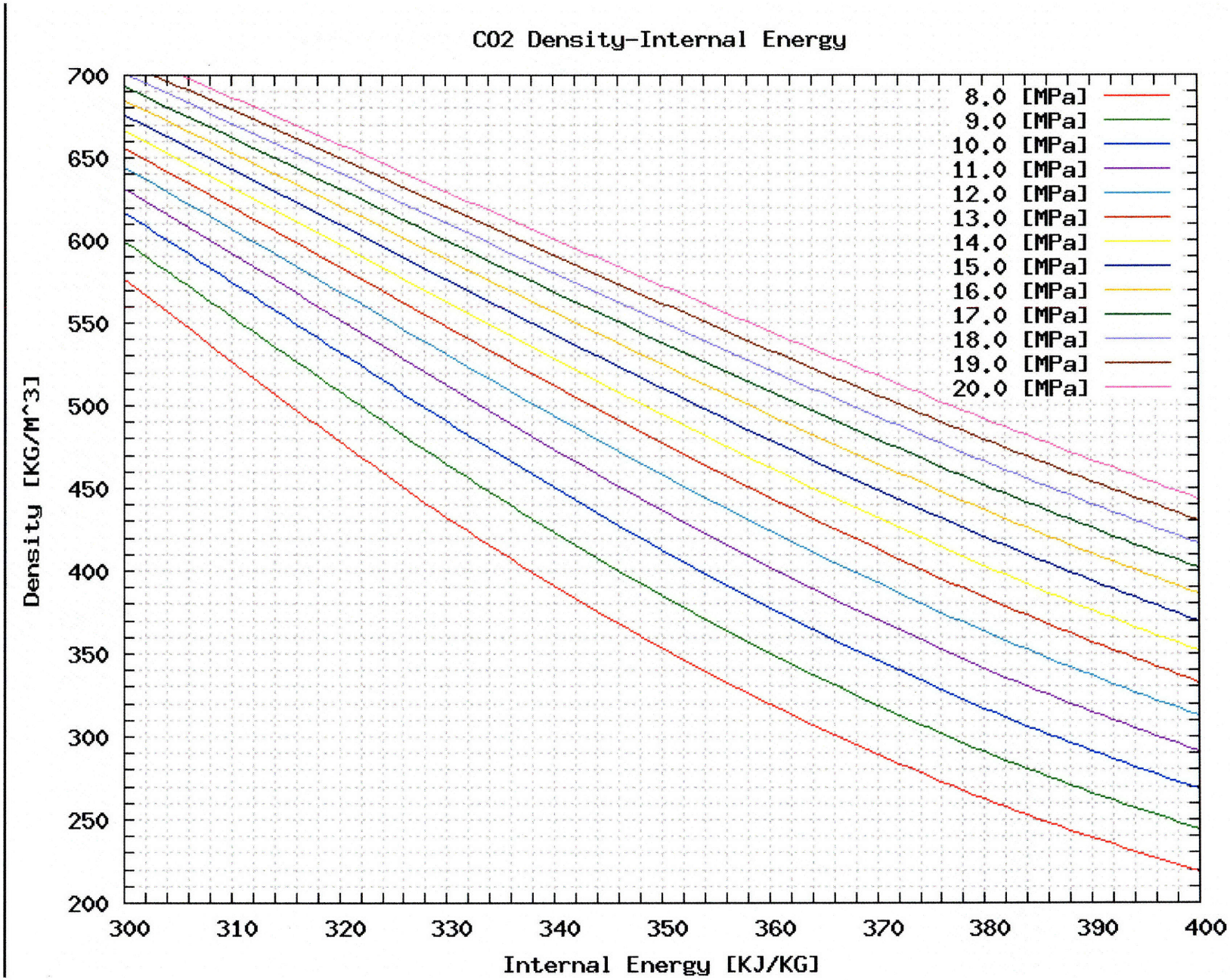

Figure A - 6 Density vs. Specific Internal Energies at varying Pressures for CO_2.

The second simulation was the returning carbon dioxide to the power conversion system (PCS) from a reference 10 m^3 HPG inventory control vessel (ICV).

Charging the PCS from HPG ICV (case discussed in section 2.2)

RELAP5 Code:

```
= Inventory Control Test (with time dependence)
*
* Prepared in Mar. 2007
* Rosemary Freas
*
*******************************************************************************
0000001      11 *modifies the coding for supercritical pressure conditions
*------------------------------------------------------------------------------
0000100                 newath                transnt
*------------------------------------------------------------------------------
0000101                 run
*------------------------------------------------------------------------------
*                    si units used in this system
0000102              si                 si
*------------------------------------------------------------------------------
0000120   101010000  0.0      co2   primary
*------------------------------------------------------------------------------
*       runtime minstep maxstep option mineditfreq majeditfreq restartfreq
0000201   25.   1.0e-6  0.005   0003   100         100         1000
*------------------------------------------------------------------------------
*Trip number definitions
20600000        expanded
*------------------------------------------------------------------------------
***********Initialize valve position at time 0 to closed and slowly open
20600010      time      0         ge   null   0            0.0      1
***********leave valve open
20600020      time      0         ge   null   0            1e6      1
*==============================================================================$
*hydro          component name     component type
1010000         invent             snglvol
*------------------------------------------------------------------------------$
*hydro          area               length             volume
1010101         0.1                0.0                10.0
*
*hydro          horz angle         vert angle         delta z
1010102         0.0                0.0                0.0
*
*hydro          roughness          hyd diam           fe
1010103         0.0                0.0                10
*
*hydro          ebt                pressure           tempe
1010200         003                14469000.0         342.087
*==============================================================================$
*==============================================================================$
```

```
*hydro          component name     component type
1040000         mtrvlv             valve
*-------------------------------------------------------------------$
*hydro      from          to           area      f loss    r loss    vcas
1040101     101010000     105000000    0.01      40.0      40.0      00100
*
*hydro          vel/flw       f flowrate   g flowrate    j flowrate
1040201         1             0.0          0.0           0.0
*
*hydro          type
1040300         mtrvlv
*
*hydro          open trip number  close trip number  rate    init pos
table
1040301         0001              0002               10000.  0.0       0.0
*===================================================================$
*===================================================================$
*hydro          component name     component type
1050000         primary            tmdpvol
*-------------------------------------------------------------------$
*hydro          area               length             volume
1050101         0.01               0.0                200
*
*hydro          horz angle         vert angle         delta z
1050102         0.0                0.0                0.0
*
*hydro          roughness          hyd diam           fe
1050103         0.0                0.0                10
*
*hydro          ebt                trip
1050200         003                0
*
*hydro                             pressure           tempe
1050201         0.0                8000000.0          343.13
*===================================================================$
.
```

RELAP5 Output Data:

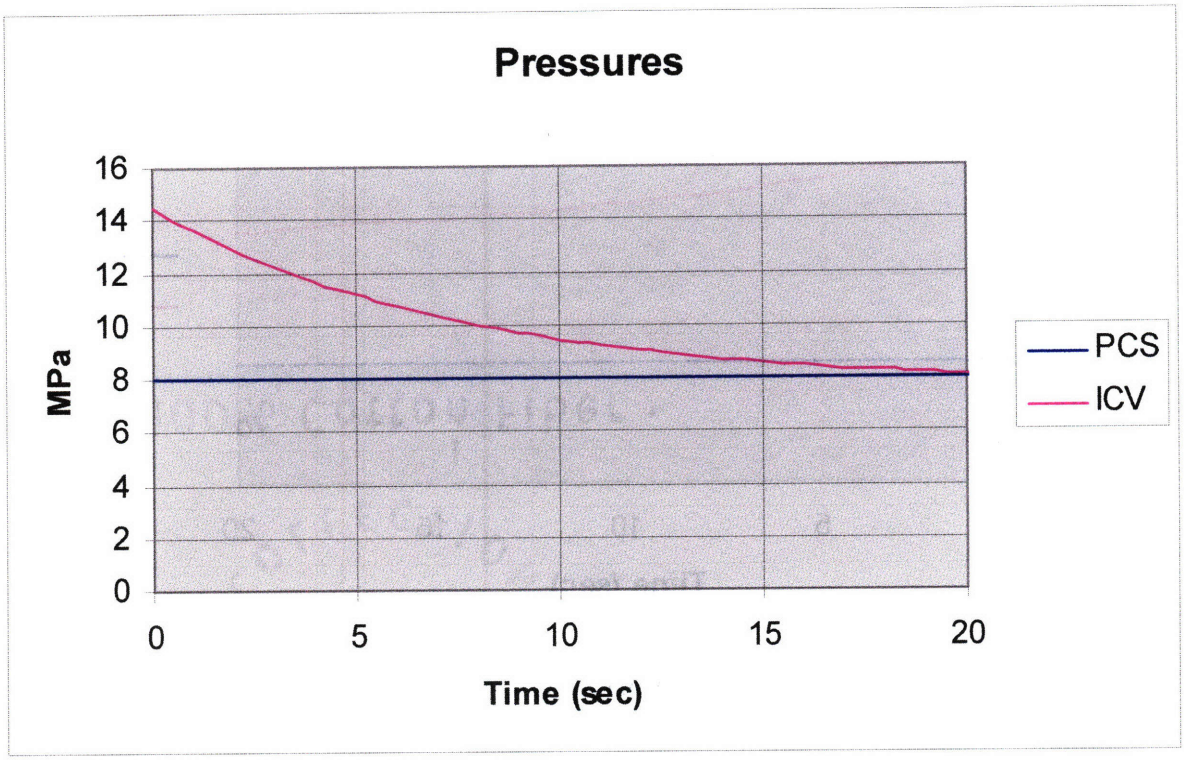

Figure A - 7 RELAP5 Pressure Data for PCS Fill Simulation

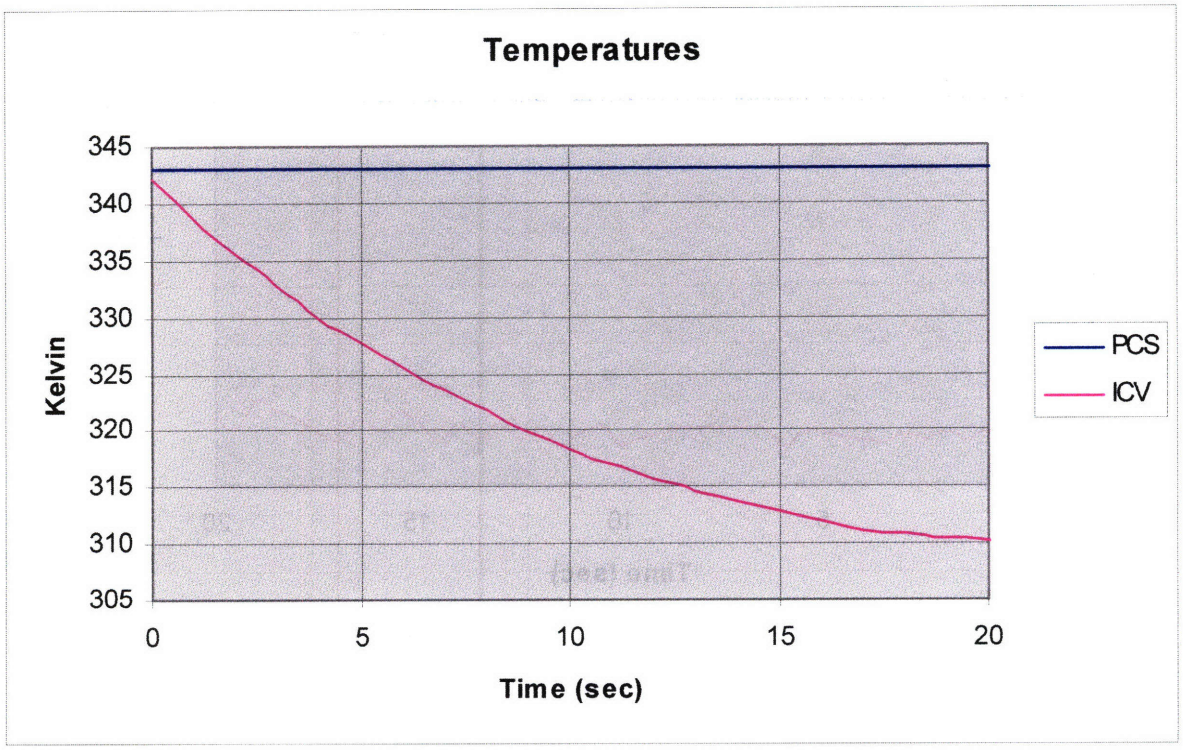

Figure A - 8 RELAP5 Temperature Data for PCS Fill Simulation

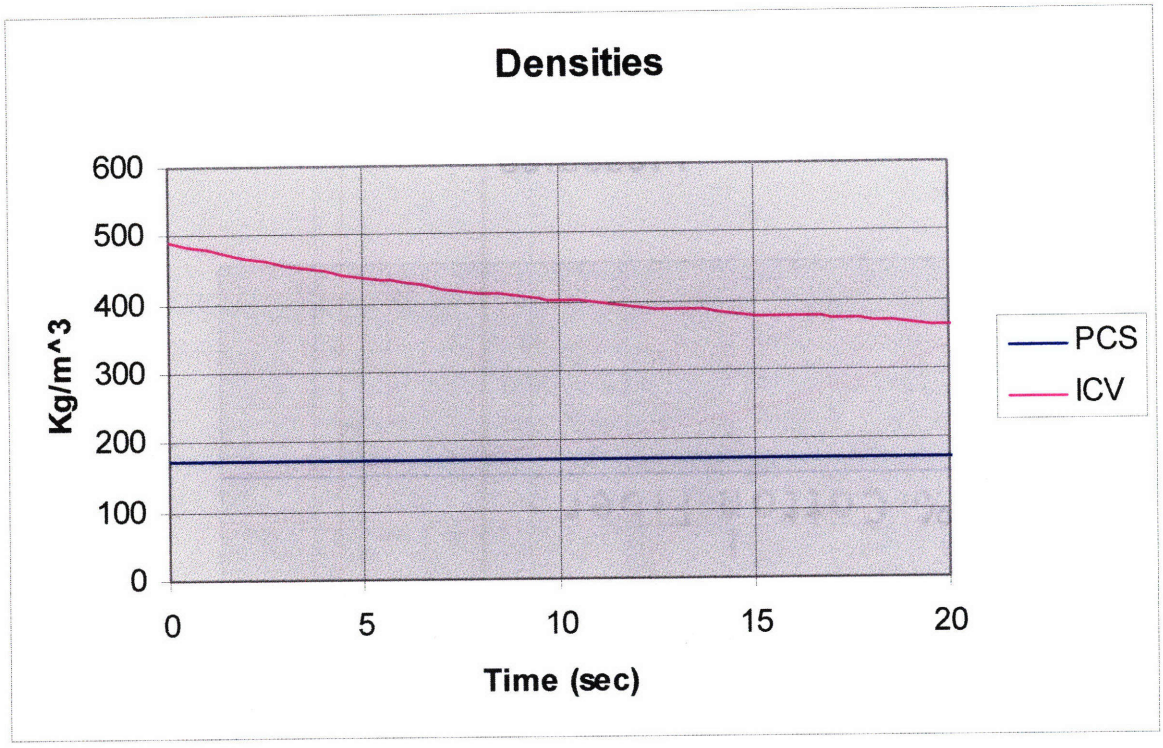

Figure A - 9 RELAP5 Density Data for PCS Fill Simulation

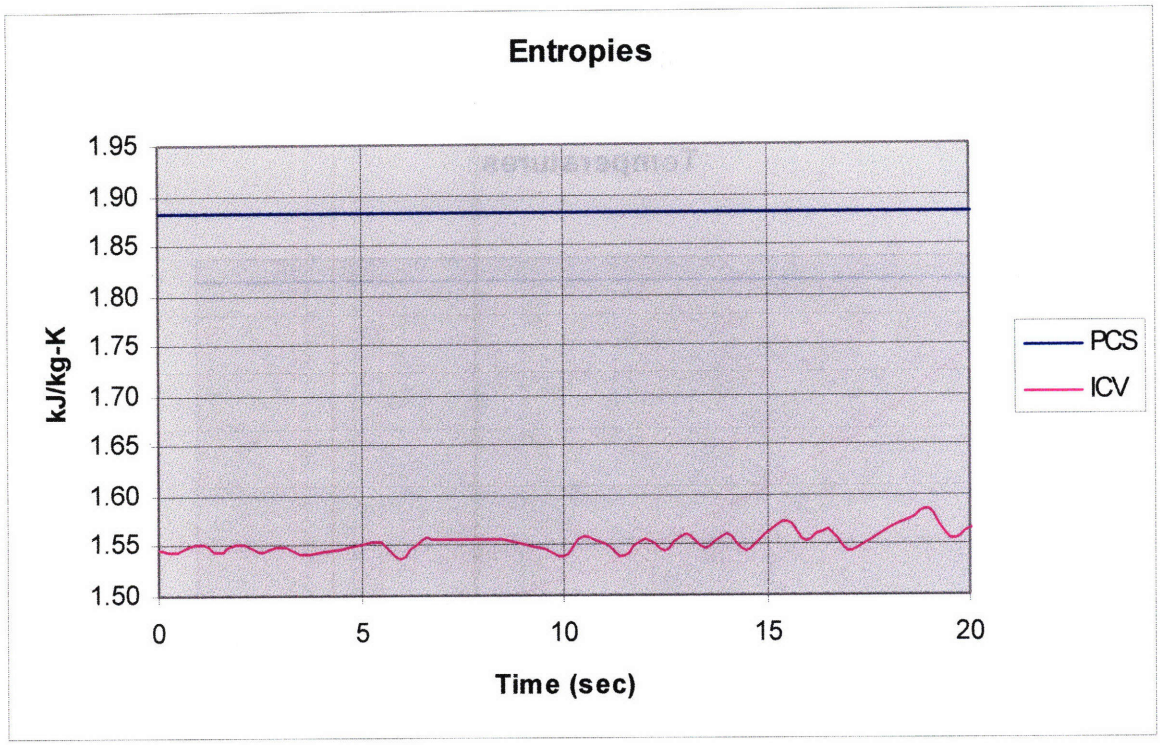

Figure A - 10 RELAP5 Specific Entropy Data for PCS Fill Simulation

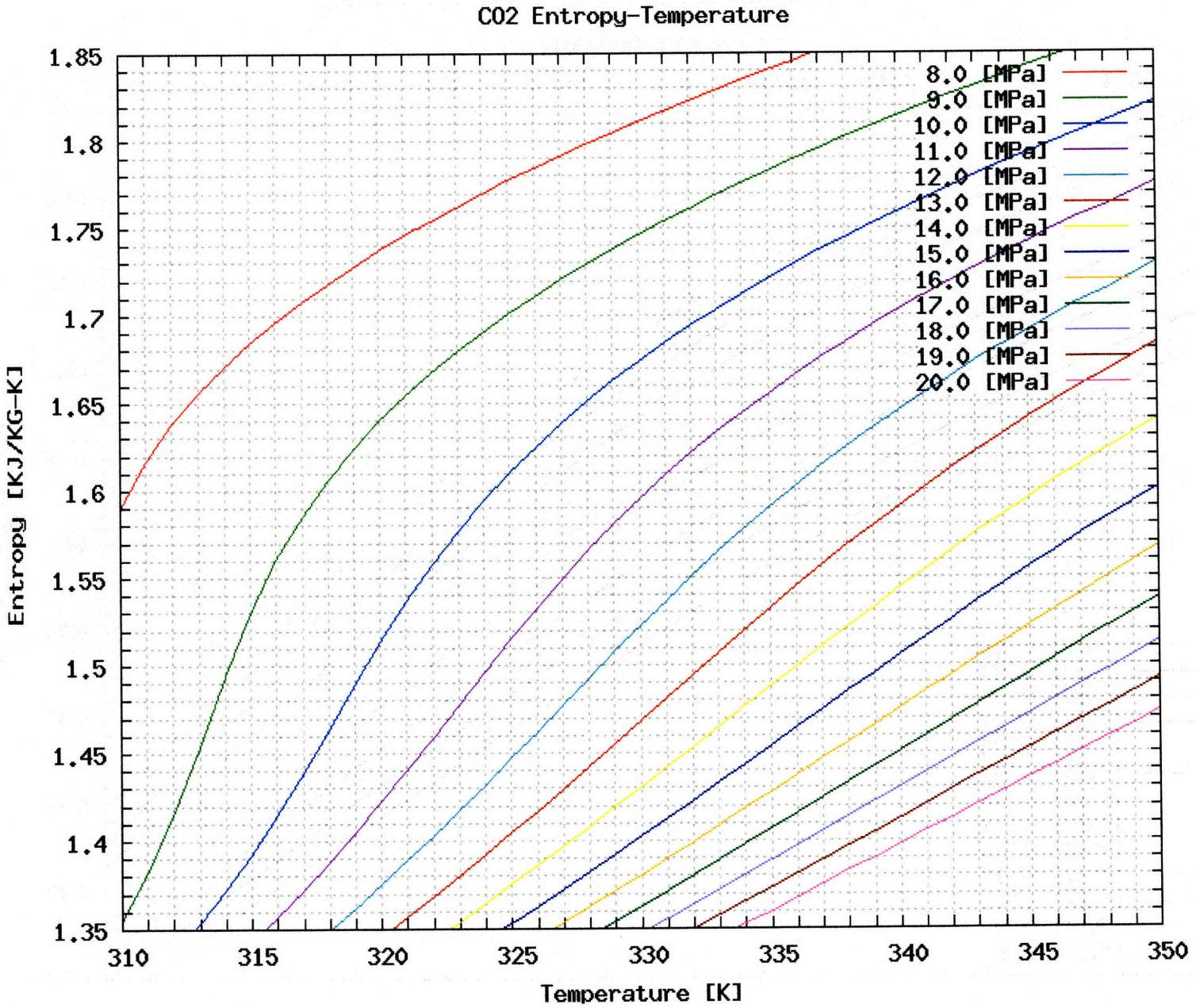

Figure A - 11 Entropy vs. Temperature at varying Pressures for CO_2.

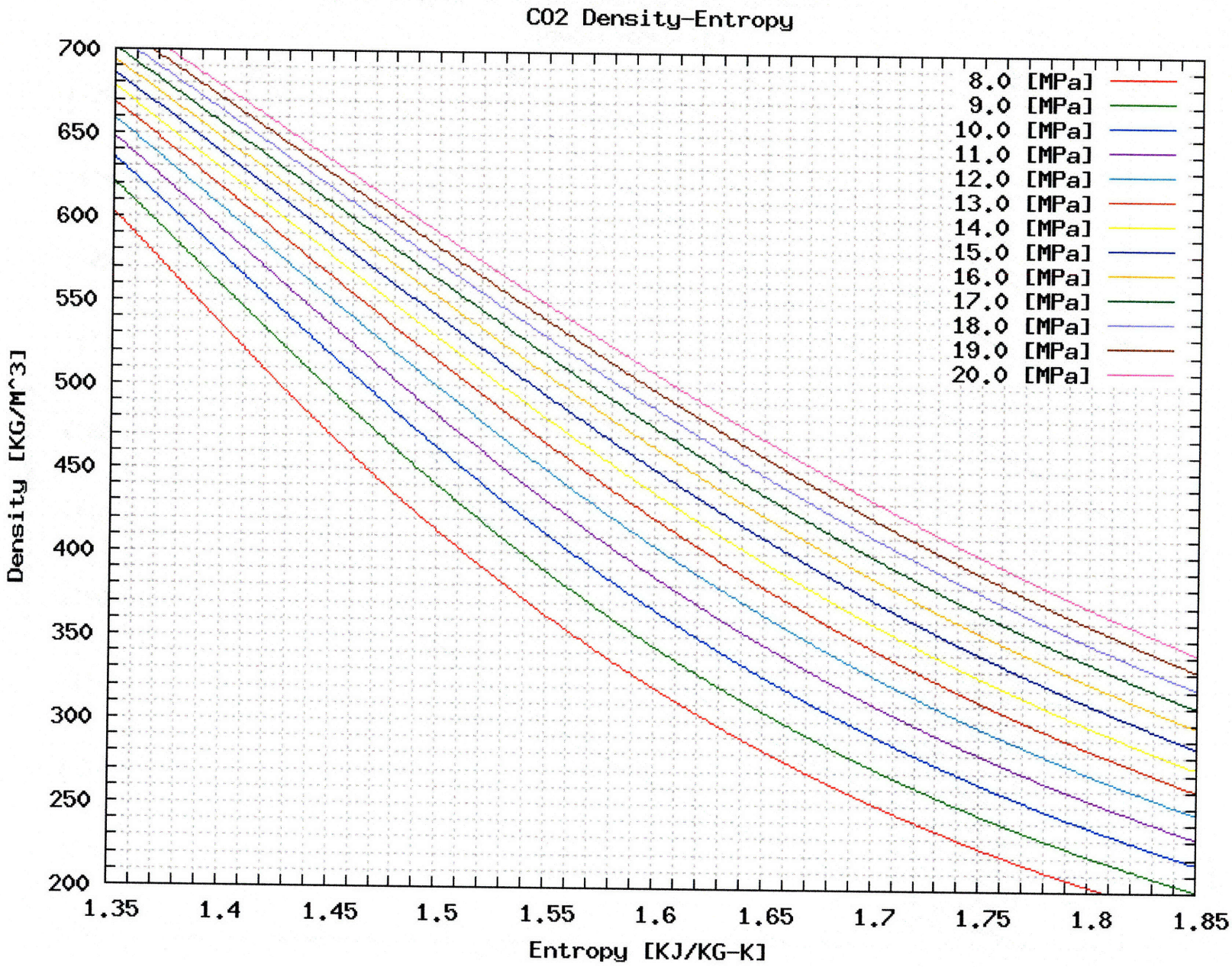

Figure A - 12 Density vs. Entropy at varying Pressures for CO_2.

Appendix B

The Mollier diagram provided here is useful in determining property changes for a variety of operations on CO_2. For example; isenthalpic throttling, isentropic expansion such as emptying of a vessel, or isobaric/isothermal changes in a 2-phase mixture's quality can readily be estimated on this handy diagram. Many of these processes are discussed throughout this thesis, particularly in chapter 2.

Another topic discussed is the rapid rise in density of CO_2 near the critical point (T_C = 31°C, P_C = 7.29MPa). For this reason, recent attention has been drawn to the viability of using supercritical carbon dioxide (S-CO_2) as a working fluid in modern reactor designs. The critical point, also called the "dome" is clearly visible on figure B-1, the Mollier diagram for CO_2. The rise in density above this point allows a significant reduction in the compressor work of a closed Brayton Cycle. Therefore a high efficiency (> 45%) can be achieved at much more moderate temperatures (550°C) than is optimal for the helium Brayton cycles (≥850°C) [Handwerk, 2007].

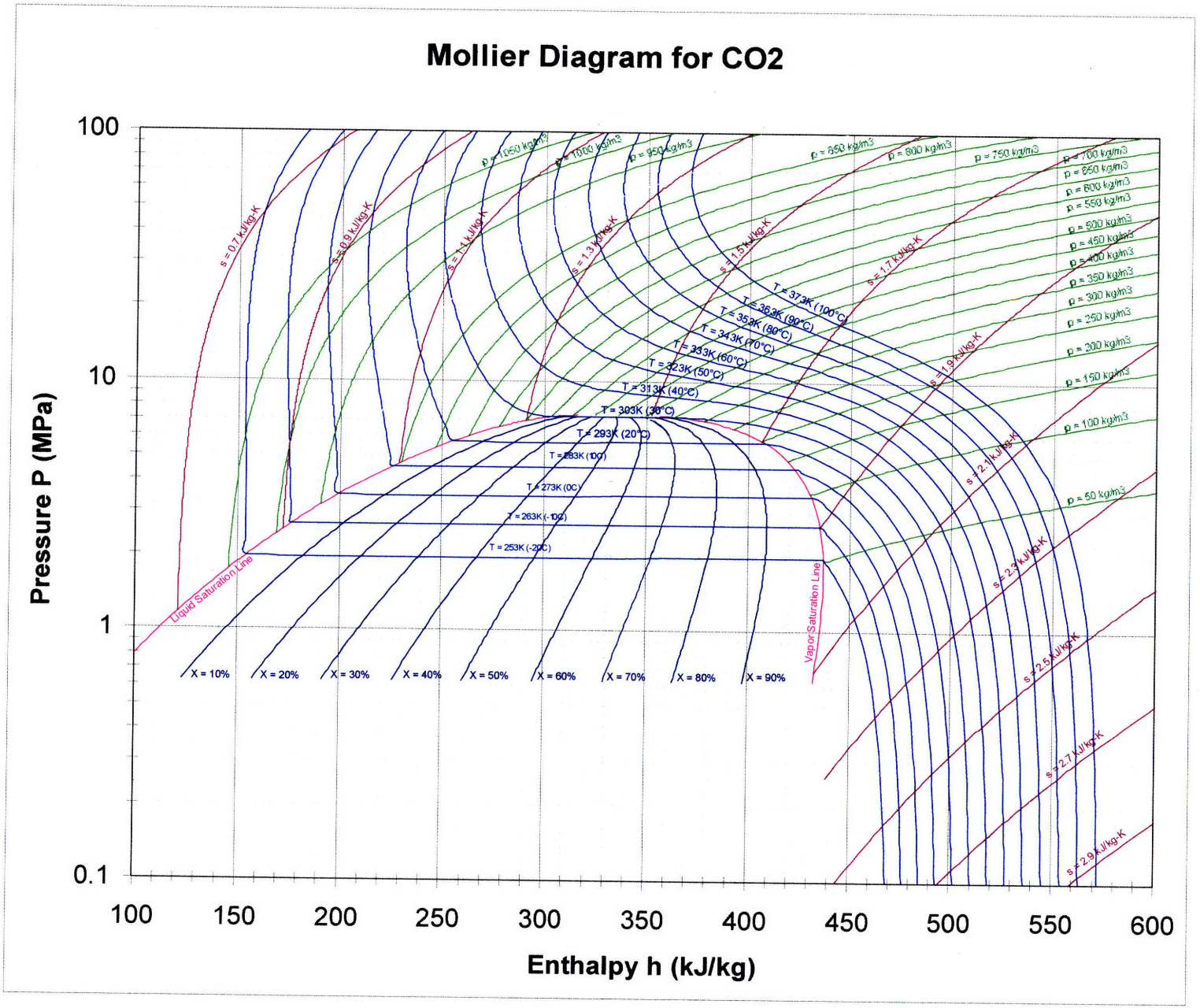

Figure B - 1 Mollier Diagram for CO_2. (Generated in Excel from REFPROP data)

Appendix C

Using SOLID EDGE™ Version 17 [2005], several drawings of a 300 MW_e S-CO_2 PCS (secondary loop only) have been generated to enable the estimation of space requirements for three potential methods of CO_2 storage, as discussed in chapter 2. The systems shown here include an all HPG storage system (figures C-1 through C-4), an all cryogenic storage system (figures C-5 through C-7), and a hybrid of the two containing 100% full-power-PCS-mass in the cryogenic tanks and 50% full-power-PCS-mass in HPG tanks (figures C-8 through C-10).

By using the most conservative estimate of forty-six 10 m^3 tanks, both transfer and storage capability requirements are met when using only HPG storage. Figures C-1 through C-4 show a relative size comparison of the required tank capacity for the 300 MW_e PCS (rounding to 50). The approximate tank dimensions for each 10 m^3 tank are 1 m inner-diameter and 4 m in height with hemispherical domes on the vertical ends. The tanks are banked 5x10 and spaced roughly 32 cm apart within the rack. Each tank has isolation valves for supply and return connections which feed into common headers. Also located on top of each tank is a relief valve. For pumpable HPG storage, only 10 of these tanks per 300 MW_e loop would suffice. The large difference indicates that provision of the compressor is worthwhile.

Preliminary cryogenic storage calculations would allow for the same 150% PCS-full-power-mass storage capability in a single 116 m^3 tank per 300MW_e loop. Figures C-5 through C-7 show a 300 MW_e PCS with the required cryogenic tank. The approximate cylindrical tank dimensions are 5.7 m outer-diameter and 5.7 m height.

Without exogenous compression in the high pressure gas storage system, the cryogenic system provides a large advantage in mass transfer capability. Either way, cryogenic storage has a superior storage capability due to the density ratio of 1.5 when compared to the final HPG ICV density after charging from the PCS (896/617). However, due to the simplicity and rapid response capability of the HPG storage design, a combination of the two storage methods may be advisable. It is assumed that a 0.5% PCS-mass daily CO_2

leak rate may occur. The simple HPG ICV design is adequately capable of providing the make-up from such a small loss on a daily basis (290 kg/day per 300 MW_e loop). This system will also be sufficient for small power level adjustments. However for larger scale plant operations requiring large PCS-mass adjustments, the more complicated cryogenic storage tank system can be at the ready to discharge or load the PCS. It is for this reason that the hybrid system is included; the cryogenic system would be capable of fully charging or discharging the PCS while the HPG storage would contain 50% PCS-full-power mass for smaller power changes and daily leakage make-up. Figures C-8 through C-10 show the 1200 MW_e PCS with a combined configuration without an auxiliary compressor in the HPG system. The piping connections are the same as shown in the 300 MW_e figures (C-1 to C-7). For the four cryogenic tanks in this configuration, the volume is reduced to approximately two-thirds and each dimension (height and diameter) are reduced to approximately 87% ($\sqrt[3]{2/3}$) when compared to the configuration using cryogenic storage only. Additionally, the number of 10 m^3 HPG tanks per loop is reduced by about one-third, with each tank maintaining similar dimensions as described in the HPG-only storage method.

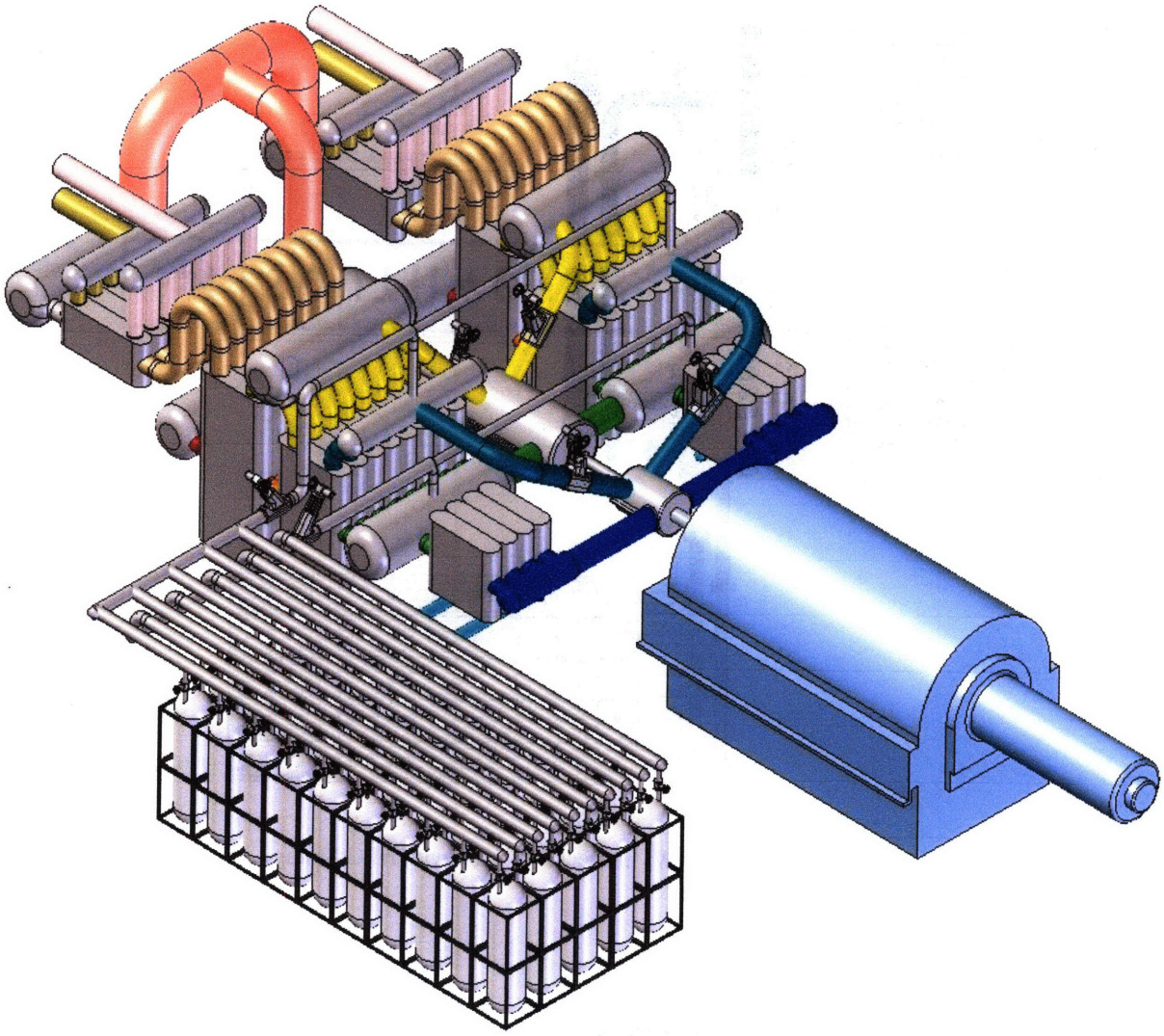

Figure C - 1 Isometric view of the 300 MW_e Indirect Power Conversion System loop with HPG Storage (50 tanks, each 10 m^3)

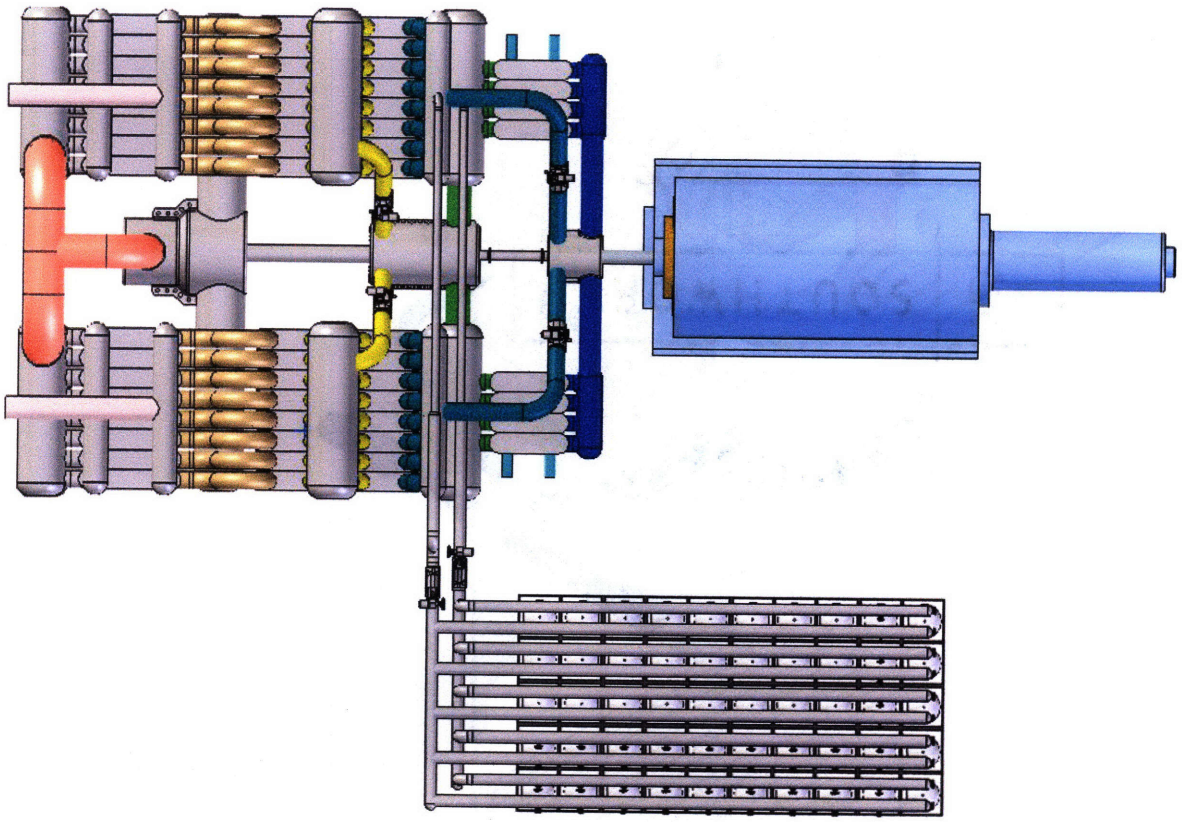

Figure C - 2 Top view of the 300 MW_e Indirect PCS loop with HPG Storage

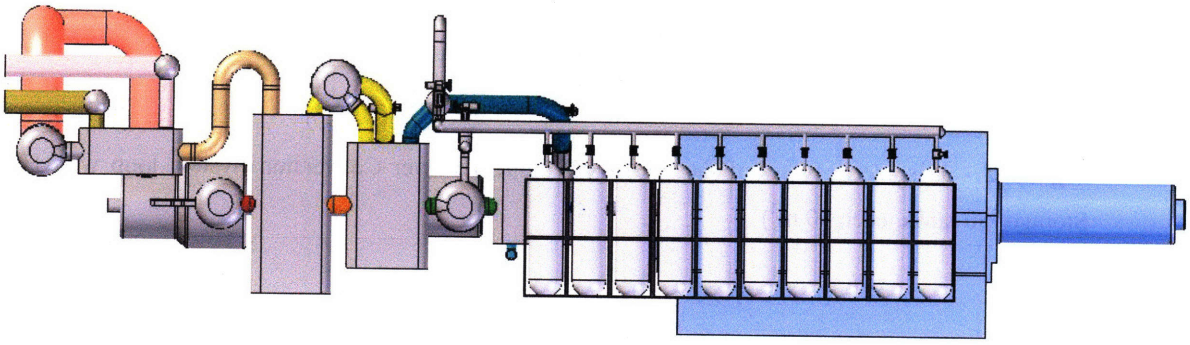

Figure C - 3 Side View of the 300 MW_e Indirect PCS loop with HPG Storage

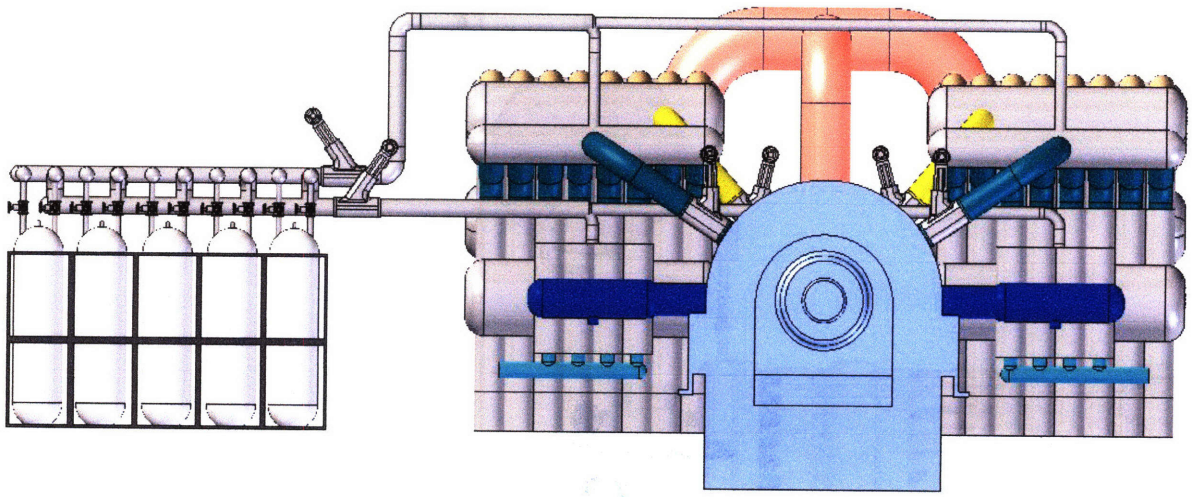

Figure C - 4 Rear View of the 300 MW_e Indirect PCS loop with HPG Storage

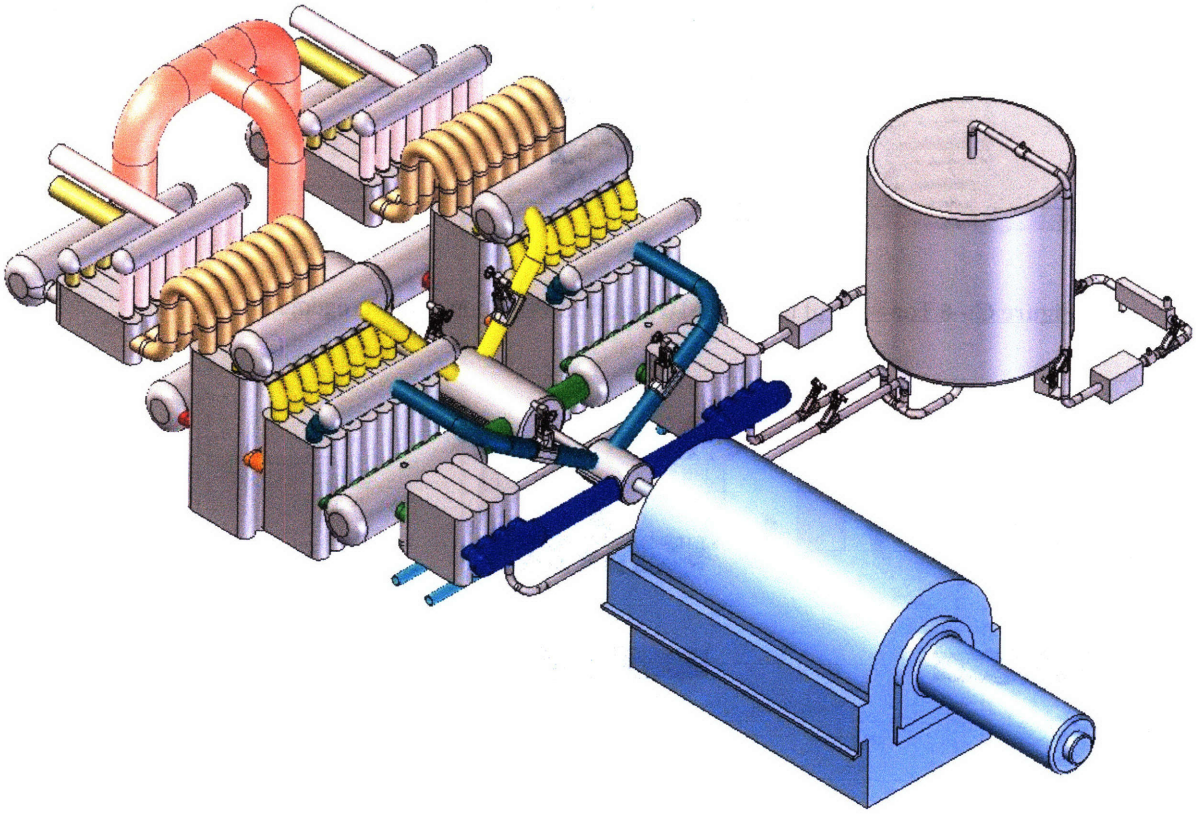

Figure C - 5 Isometric view of the 300 MW_e Indirect Power Conversion System loop with Cryogenic Storage

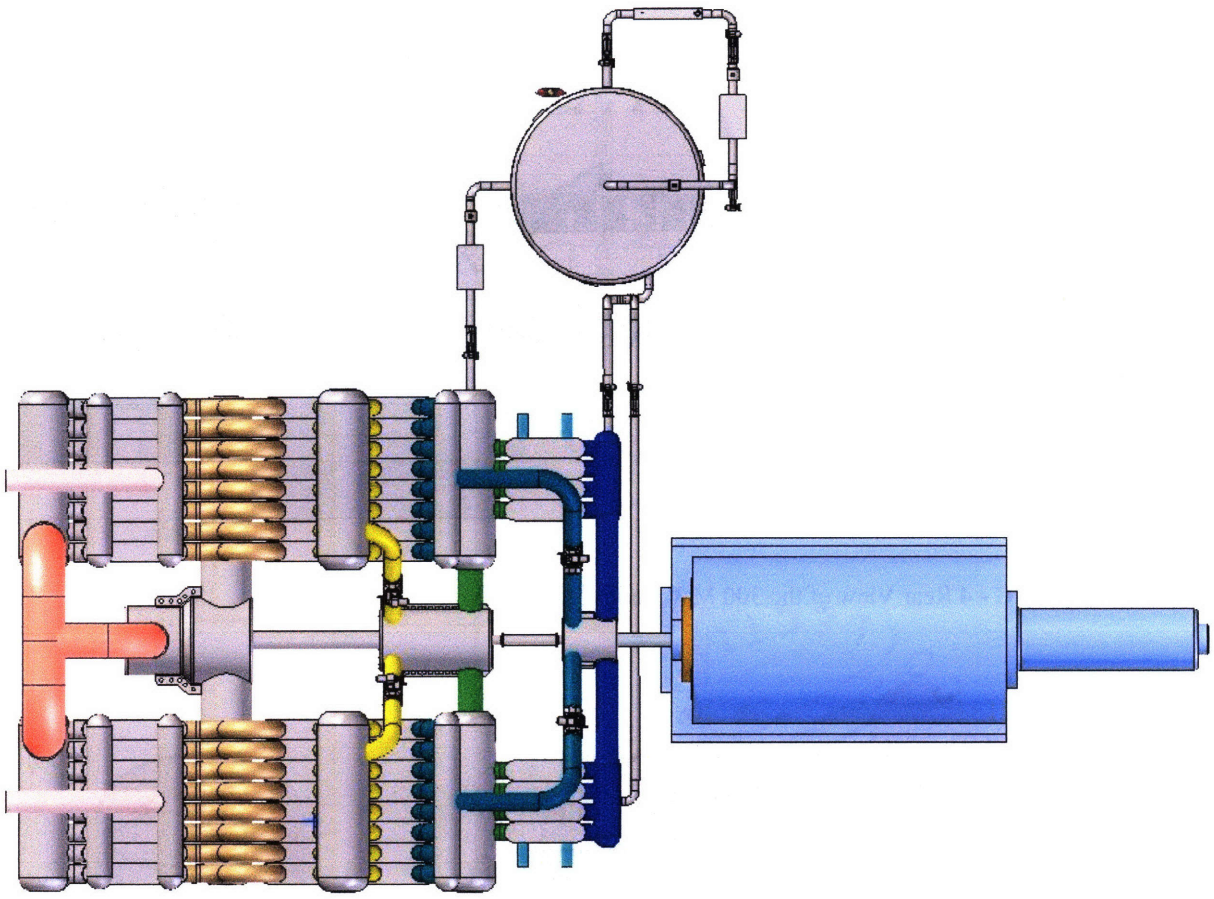

Figure C - 6 Top view of the 300 MW_e Indirect PCS loop with Cryogenic Storage

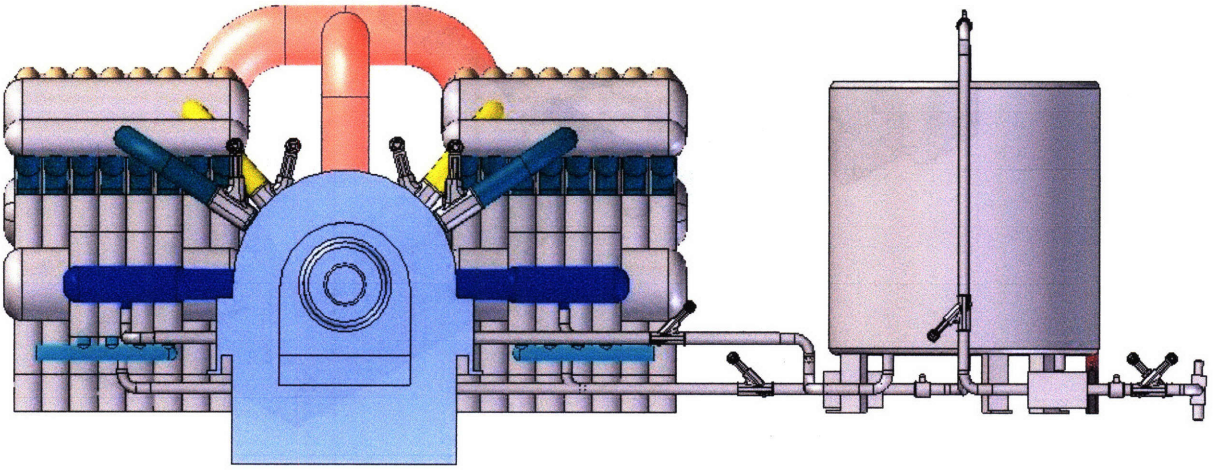

Figure C - 7 Side View of the 300 MW_e Indirect PCS loop with Cryogenic Storage

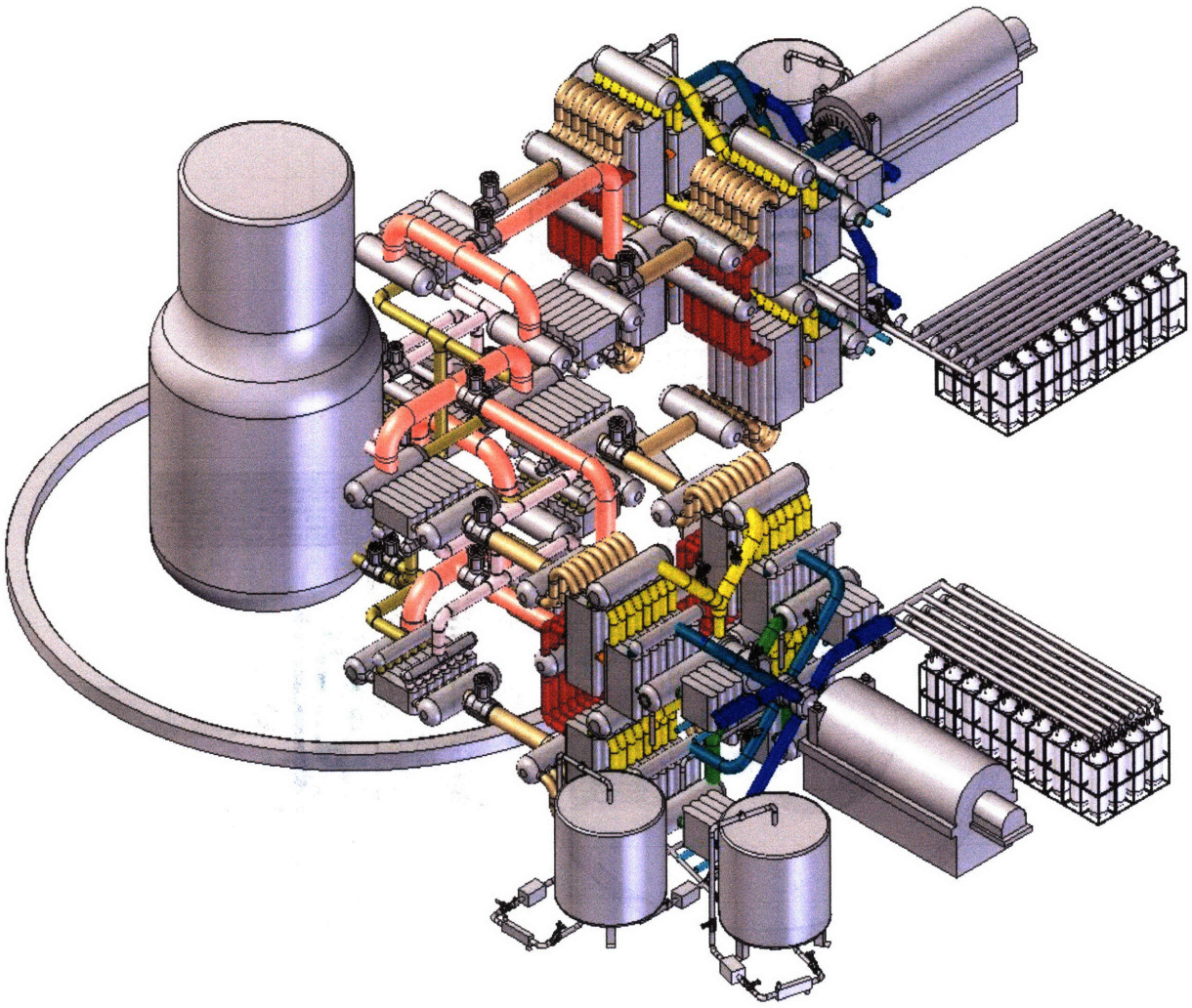

Figure C - 8 Isometric view of the 1200 MW_e Indirect Power Conversion System with Cryogenic and HPG Storage

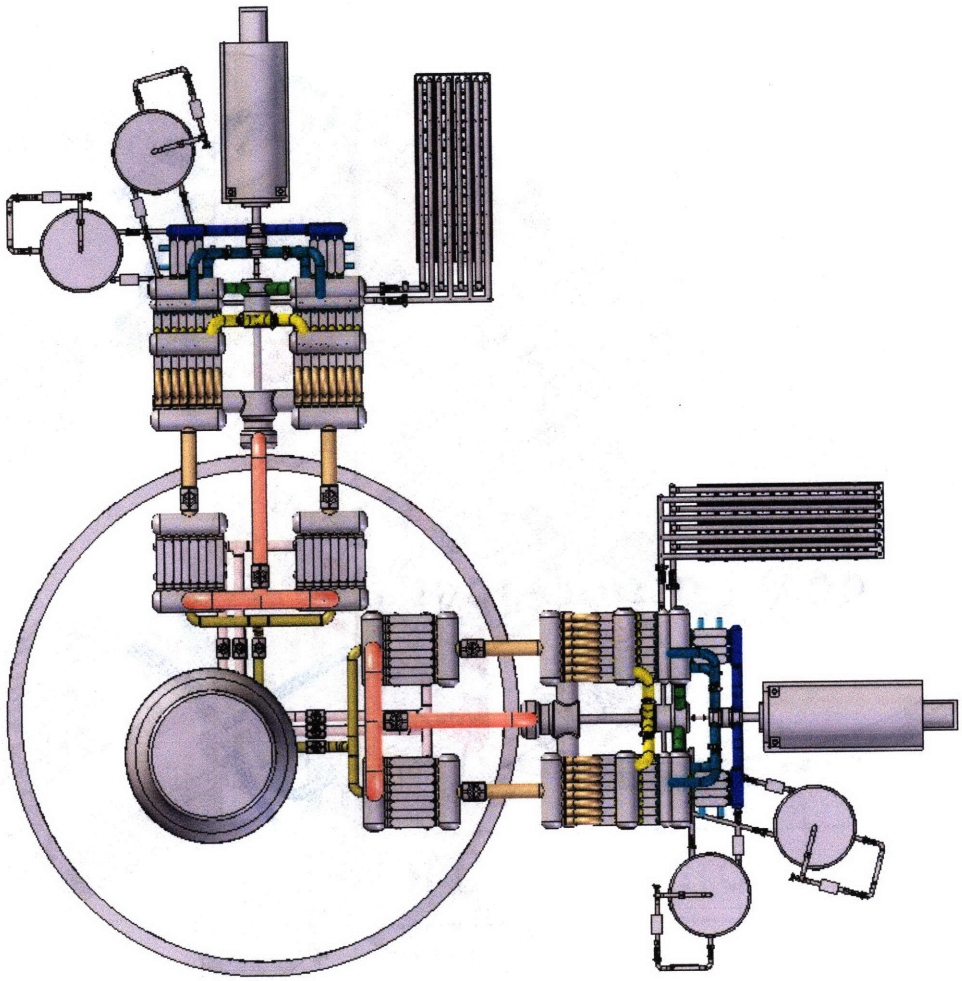

Figure C - 9 Top View of the 1200 MW_e Indirect PCS with Cryogenic and HPG Storage

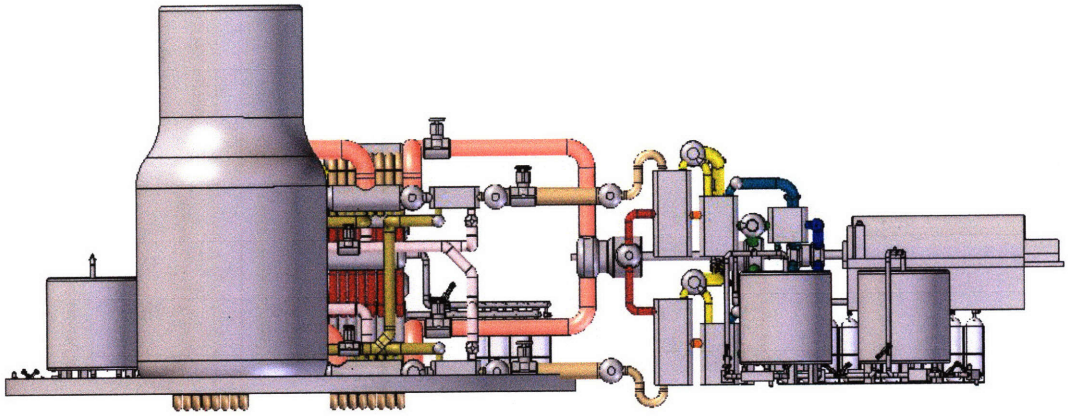

Figure C - 10 Side View of the 1200 MW_e Indirect PCS with Cryogenic and HPG Storage

Appendix D

General Corrosion of Metal Alloys

Metal alloys are the most common materials used throughout the PCS. They make up part of the cladding, structures within the core, pressure vessel, piping, heat exchanger tubing, etc. Different grades of metals offer different temperature dependant strength and corrosion resistance behaviors. The S-CO_2 PCS under development has maximum temperature ranging from 550°C to (at most) 700°C. Low alloy 500 series mild steels simply offer too low a temperature resistance to be suited for these designs. So too do basic 400 series ferritic steels [10.5-27% Cr, <.2%C, <1.5% Mn, <1% Si, <.04% P, <.03% S, 0% Ni] with resistances up to 480°C. However, should the ferritic steels or martinsitic steels be alloyed with small quantities of carbide establishing/strengthening elements, like Mo or V, temperatures of up to 600°C could be used [Thon, 2002]. Nevertheless, 300 series austenitic steels are generally capable of withstanding temperatures up to 700°C (or higher with thicker steels) [Thon, 2002] making them possibly suited for the S-CO_2 PCS.

Austenitic steel materials [Fe-C + >18% Cr, >8% Ni] are close-packed face centered cubic (FCC) structures which have the ability to resist thermal creep but are still subject to irradiation creep, which will be discussed as part of the pressure vessel degradation. Some other characteristics of austenitic steels are that they are very tough and non-magnetic. Austenitic steels also exhibit excellent resistance to general corrosion. It is known that austenitic steels have good high temperature strength with a lack of nil ductility temperature (NDT) (thanks to the Ni). Additionally, higher grade austenitic steels with ~20% Cr can sustain temperatures up to 850°C. Preliminary analyses by Oh et al. [2002] also suggested that Ni-based alloys with 20-30% Cr would exhibit reasonable resistance to degradation by S-CO_2. Fortunately the British AGR uses 300 series [25% Cr, 20%Ni] austenitic steels in the secondary superheater and reheater, so there is information which can be drawn upon. Experience with the British AGRs has shown that corrosion in CO_2 systems is significantly lower than in the conventional Rankine cycle; however, corrosion cannot be considered insignificant to ignore.

Metal alloy corrosion follows the general high-temperature oxidation behavior as shown on an Ellingham diagrams (figures D-1 and D-2), and is very temperature and pressure dependant. This oxidation behavior is somewhat analogous to active-passive kinetics in aqueous corrosion systems, however the reactions are not based on charged particle flow. As such, reaction rates cannot be determined using the Ellingham diagram. During the corrosion process, the reactions (shown below) first form an oxide film. Eventually the film can become saturated and breakaway into the transpassive regime; this process is called breakaway.

$$M^{+} + CO_2 \rightarrow MO + CO$$

$$2M^{+} + CO_2 \rightarrow 2MO + C$$

$$M^{+} + CO \rightarrow MO + C$$

The longevity of the oxide stability is dependant on the metal's ability to absorb the C stripped from CO_2 during the oxidation and not reaching saturation volume fractions of carbide at the metal surface.

Ellingham Diagrams

Key aspects of the high PCS temperatures that should be considered are the effect on the stability of specific oxide layers, and the dissociation of CO_2 to CO, C, and oxygen gas. The best graphical representation used to understand the high-temperature behavior is the Ellingham Diagram (figure D-1). First, a description of how the Ellingham Diagram is meant to be used:

Definitions

The Gibbs free energy (ΔG) of a reaction is a measure of the thermodynamic driving force that makes a reaction occur. A negative value for ΔG indicates that a reaction can proceed spontaneously without external inputs, while a positive value indicates that it will not. The equation for Gibbs free energy is:

$$\Delta G = \Delta H - T\Delta S$$

where ΔH is the enthalpy, T is absolute temperature, and ΔS is entropy.

The enthalpy (ΔH) is a measure of the actual energy that is liberated when the reaction occurs (the "heat of reaction"). If it is negative, then the reaction gives off energy, while if it is positive the reaction requires energy.

The entropy (ΔS) is a measure of the change in the possibilities for disorder in the products compared to the reactants. For example, if a solid (an ordered state) reacts with a liquid (a somewhat less ordered state) to form a gas (a highly disordered state), there is normally a large positive change in the entropy for the reaction.

Construction of an Ellingham Diagram

An Ellingham diagram is a plot of ΔG versus temperature. Since ΔH and ΔS are essentially constant with temperature unless a phase change occurs, the free energy versus temperature plot can be drawn as a series of straight lines, where ΔS is the slope and ΔH is the y intercept. The slope of the line changes when any of the materials involved melt or vaporize.

Free energy of formation is negative for most metal oxides, and so the diagram is drawn with $\Delta G=0$ at the top of the diagram, and the values of ΔG shown are all negative numbers. Temperatures where either the metal or oxide melt or vaporize are marked on the diagram.

The Ellingham diagrams shown (figures D-1 and D-2) are for metals reacting to form oxides (similar diagrams can also be drawn for metals reacting with sulfur, chlorine, etc., but the oxide form on the diagrams is most common). The oxygen partial pressure is taken as 1 atmosphere, and all of the reactions are normalized to consume one mole of O_2.

The majority of the lines slope upwards, because both the metal and the oxide are present as condensed phases (solid or liquid). The reactions are therefore reacting a gas with a condensed phase to make another condensed phase, which reduces the entropy. A notable exception to this is the oxidation of solid carbon. The line for the reaction

$$C+O_2 ==> CO_2$$

is a solid reacting with a mole of gas to produce a mole of gas, and so there is little change in entropy and the line is nearly horizontal. For the reaction

$$2C+O_2 ==> 2CO$$

we have a solid reacting with a gas to produce two moles of gas, and so there is a substantial increase in entropy and the line slopes rather sharply downward. Similar behavior can be seen in parts of the lines for lead and lithium, both of which have oxides that boil at slightly lower temperatures than the metal does.

There are three main uses of the Ellingham diagram:

1. Determine the relative ease of reducing a given metallic oxide to metal;

2. Determine the partial pressure of oxygen that is in equilibrium with a metal oxide at a given temperature; and

3. Determine the ratio of carbon monoxide to carbon dioxide that will be able to reduce the oxide to metal at a given temperature.

Ease of Reduction

The position of the line for a given reaction on the Ellingham diagram shows the stability of the oxide as a function of temperature. Reactions closer to the top of the diagram are the most "noble" metals (for example, gold and platinum), and their oxides are unstable and easily reduced. As we move down toward the bottom of the diagram, the metals become progressively more reactive and their oxides become harder to reduce.

A given metal can reduce the oxides of all other metals whose lines lie above theirs on the diagram. For example, the $2Mg + O_2 ==> 2MgO$ line lies below the $Ti + O_2 ==> TiO_2$ line, and so magnesium can reduce titanium oxide to metallic titanium.

Since the $2C + O_2 ==> 2CO$ line is downward-sloping, it cuts across the lines for many of the other metals. This makes carbon unusually useful as a reducing agent, because as soon as the carbon oxidation line goes below a metal oxidation line, the carbon can then reduce the metal oxide to metal. So, for example, solid carbon can reduce chromium oxide once the temperature exceeds approximately 1225°C, and can even reduce highly-stable

compounds like silicon dioxide and titanium dioxide at temperatures above about 1620°C and 1650°C, respectively. For less stable oxides, carbon monoxide is often an adequate reducing agent.

Equilibrium Partial Pressure of Oxygen

The scale on the right side of the diagram labeled "Po_2" is used to determine what partial pressure of oxygen will be in equilibrium with the metal and metal oxide at a given temperature. The significance of this is that, if the oxygen partial pressure is higher than the equilibrium value, the metal will be oxidized, and if it is lower than the equilibrium value then the oxide will be reduced.

To use this scale, you will need a straightedge. First, find the temperature you are interested in, and find the point where the oxidation line of interest crosses that temperature. Then, line up the straightedge with both that point, and with the point labeled "0" that is marked with short radiating lines (upper left corner of the diagram). Now, with the straightedge running through these two points, read off the oxygen partial pressure (in atmospheres) where the straightedge crosses the "Po_2" scale, and this is the equilibrium partial pressure.

It is possible to reach the equilibrium oxygen partial pressure by use of a hard vacuum, purging with an inert gas to displace the oxygen, or using a scavenger chemical to consume the oxygen.

Ratio of CO/CO_2 Needed for Reduction

When using carbon as a reducing agent, there will be a minimum ratio of CO to CO_2 that will be able to reduce a given oxide. The harder the oxide is to reduce, the greater the proportion of CO needed in the gases.

To determine the CO/CO_2 ratio to reduce a metal oxide at a particular temperature, use the same procedure as for determining the equilibrium pressure of oxygen, except line up the straightedge with the point marked "C" (center of the left side of the diagram), and read the ratio off of the scale marked "CO/CO_2".

Ellingham Diagrams

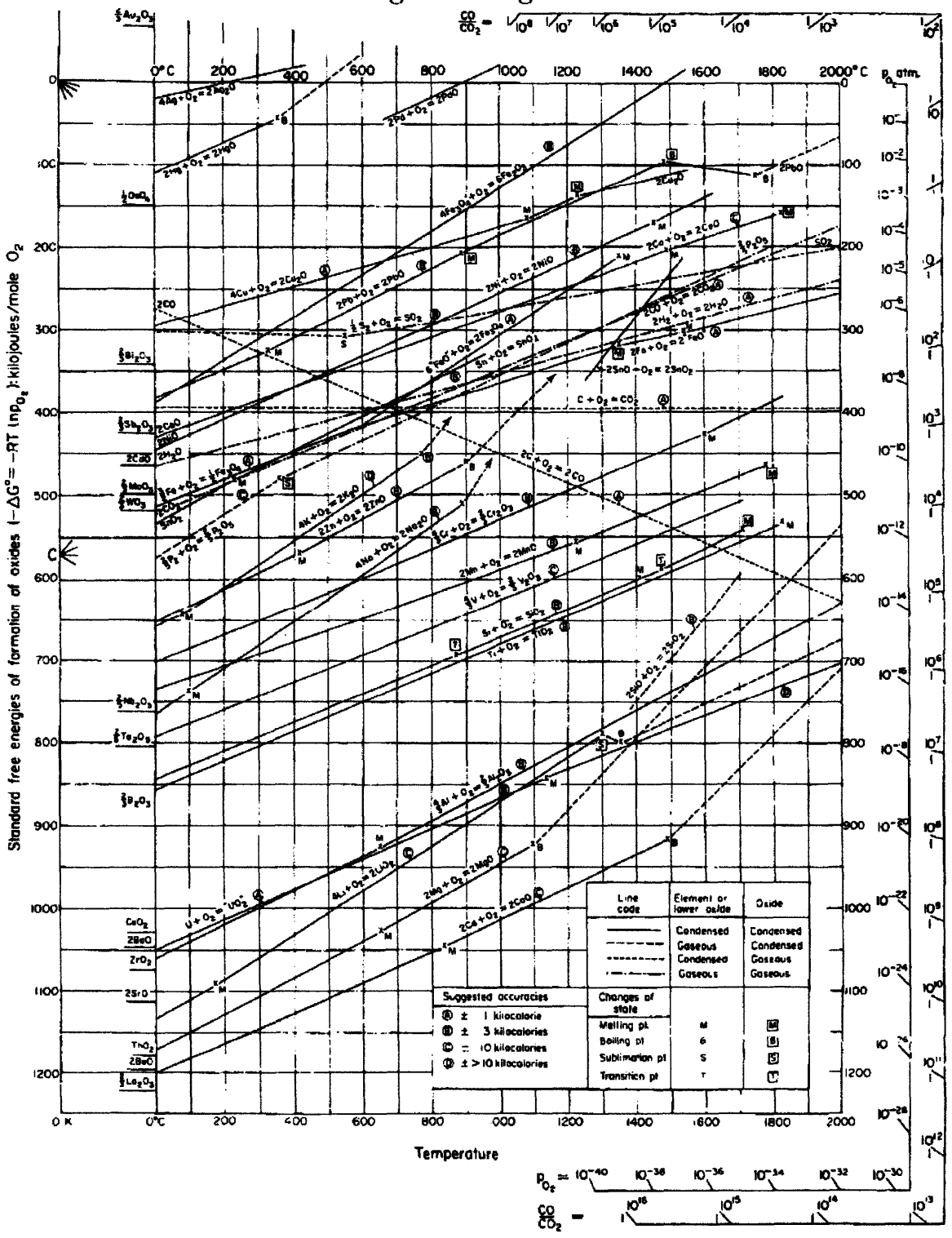

Figure D - 1 Ellingham Diagram for High Temperature Oxidation Corrosion. Solid curves show standard free energies of formation of various oxides from the elements as a function of temperature.

Due to the complexity shown in figure D-1, a more simplified diagram is provided for focus on reactions specifically discussed. Looking at figure D-2, the Gibbs free energy ($\Delta G°$) for formation of the iron oxide (FeO) exceeds that of the carbon dioxide coolant stability at approximately 720°C. Therefore, the reaction $CO_2 + 2Fe \rightarrow C + 2FeO$ proceeds as written at temperatures below 720°C. Above this threshold, the reaction reverses direction causing the breakdown (reduction) of the oxide layer. This effect places an upper limit on the maximum operating temperature for these S-CO_2 PCS designs, if iron based steels are used. Also, nickel and copper based alloys are unsuitable for the high PCS temperatures. However, the aluminum oxide stability (Al_2O_3) seems to exhibit a relative temperature independence with much lower $\Delta G°$, which may help to explain some of the positive test results of aluminum alloy steels such as MA956 which will be discussed later.

CO_2 can be reduced in the presence of hydrogen by $CO_2 + H_2 \rightarrow CO + H_2O$. Other common reaction chains involving CO_2 and CO include:

$$2CO + O_2 \rightarrow 2CO_2$$

$$C + O_2 \rightarrow CO_2$$

$$2CO \rightarrow 2C + O_2$$

Figure D-2 clearly shows that the CO $\Delta G°$ is higher than that of CO_2 at temperatures below about 700°C. This indicates that the first reaction shown involving CO_2 will proceed to the right as shown, in the temperature ranges of interest for the S-CO_2 systems - which is desirable. According to Braker [1971], however, CO_2 is stable to as high as 1700°C (but he doesn't mention the oxygen partial pressure for this stability). The light dash-dot lines shown in this diagram represent constant oxygen partial pressures (in atm) of the gas phase. By following a line up from the system temperature to the constant pressure line, the $\Delta G°$ for a reaction on the Ellingham diagram can be found.

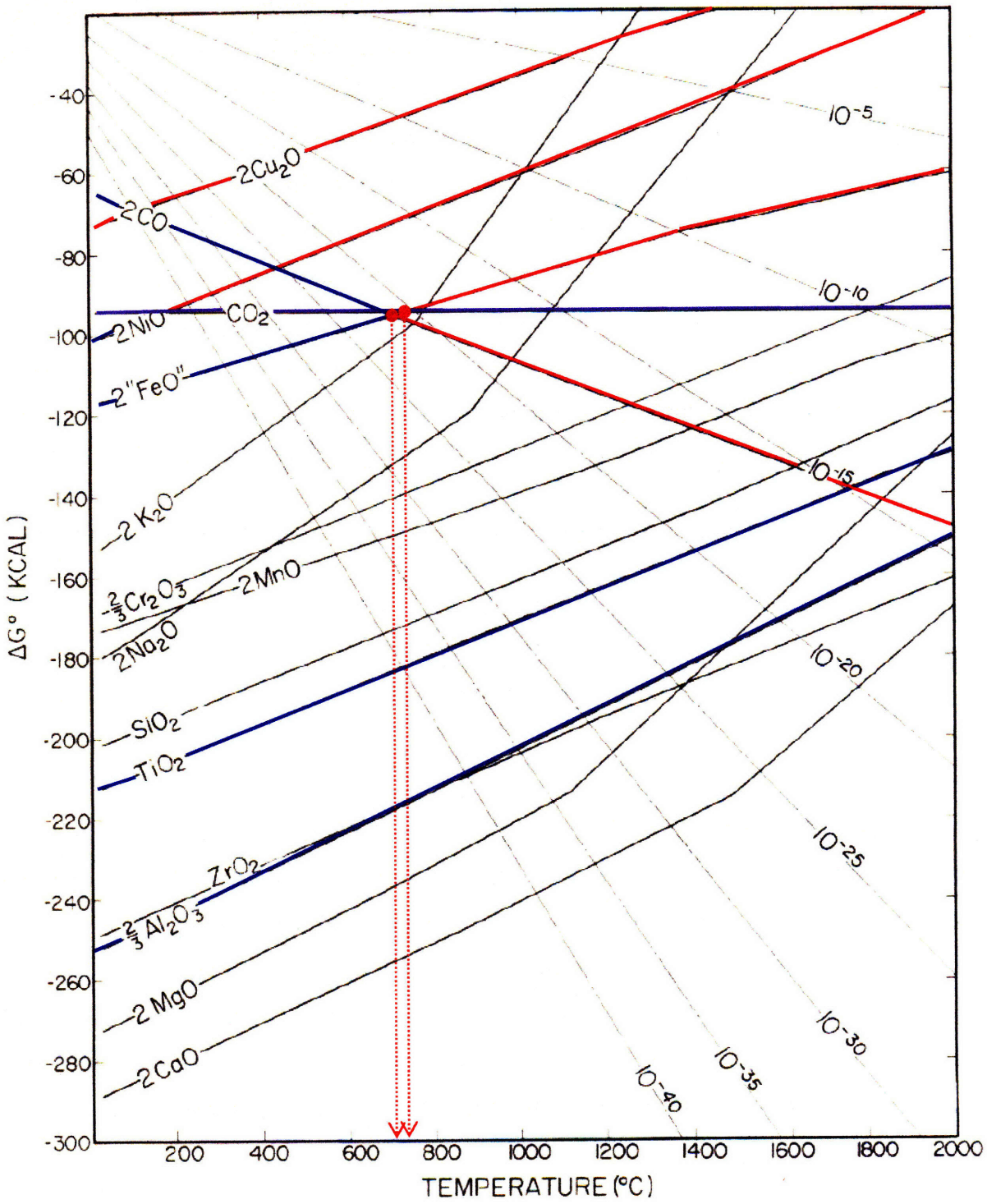

Figure D - 2 Simplified Ellingham Diagram. Solid curves showing standard free energies of formation of various oxides from the elements as a function of temperature, based mainly on data summarized by Coughlin and by Elliott and Gleiser. The curve for Si02 has been drawn on the basis of new data presented by Chipman. Light dash-dot curves are lines of equal oxygen pressures (atm) of the gas phase, as labeled on each curve.

Depending on the plant conditions, the reactions can lead to a build up of oxygen gas. As O_2 continues to buildup in the system, it seems from figure D-2 that the stability of the oxide layer will tend to decrease.

Testing at Idaho National Laboratory

The Gen-IV VHTR is being reviewed primarily for its use in the hydrogen production process. At very high temperatures (1000°C), thermochemical water cracking can be more readily accomplished. By incorporating a secondary CO_2 loop, the overall efficiency of the plant can be to increased. The secondary CO_2 cycle would operate at a pressure of 10 to 20 MPa and be expected to operate for more than 20 years. These extreme conditions prompted INL to perform corrosion testing of two potential materials. [Oh et al., 2006] The two Ni-based alloys selected for testing were oxide dispersion-strengthened (ODS) Incoloy MA 754 and Inconel 617.

The belief was that the 20%Cr in MA 754 would amplify its corrosion resistance and the yttrium oxide, Y_2O_3, would give it high temperature strength and creep resistance while reducing the possibility of spallation due to the higher free energy for oxide formation. Therefore MA 754, a rather new alloy, was tested by Oh et al. [2006] to determine its corrosion resistance for applicability to the VHTR. I-617 was also tested on the basis of corrosion. The higher Cr content (22%) coupled with 9% Mo and 12.5% Co made for an interesting corrosion comparison.

Since at the time of testing Idaho National Labs (INL) had no facilities capable of sustaining the high temperature and pressure conditions needed for their tests, new systems had to be developed. Two CO_2 corrosion systems were made of 304 stainless steel with wall thicknesses sufficient to withstand an internal pressure of 7 MPa at 1000°C for 10,000 hours. One was developed for testing many samples with different surface preparations, as well as three different materials simultaneously without significant cross contamination. The samples were placed in a 1.2 m long 11 mm ID pipe and subjected to ~5 ml/min, single pass laminar flow CO_2. The second system resembled a pipe with higher CO_2 flow rates and significant gradients in temperature and stress for a more "real world" evaluation.

Coarse grained specimens were fabricated with an OD ~ 12.5 mm, ID ~ 4.3 mm for the flowing CO_2. Most focus was on the corrosion behavior of the coarse-grain MA 754. Four coarse-grained samples were exposed to flowing CO_2 for 47, 120, 335 and 500 hours at 1000°C/10 MPa. The fine-grain specimens were only subjected to 1000°C and 7 MPa for 175 hours. After exposure, the samples were cut from the tube at 25 mm intervals along the tube length. These cross-sections were then cut longitudinally to expose the inner corroded surfaces. The samples were then mounted, polished, and analyzed. I-617 underwent the same process as the fine-grained MA 754: 1000C, 7 MPa, for 175 hours. The limited testing of fine-grain MA 754 and I-617 was attributed to time constraints upon completion of the test loop.

Results:

MA 754 formed a black chromium oxide, the only thermodynamically stable compound at 1000°C in the presence of CO_2. Since the exposure times were short, only a quasi steady state corrosion rate of ~ 0.2 mm/yr was determined at 500 hrs of exposure. Figure D-3 shows the results of both the coarse and fine grain specimens of MA 754. The 500 hour corrosion rate still seems to be in a transition state.

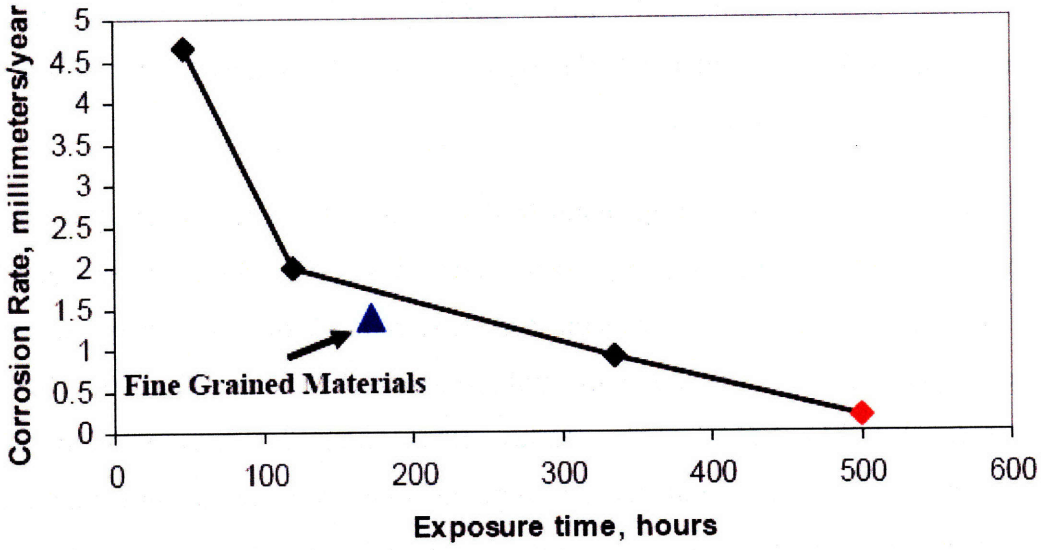

Figure D - 3 Corrosion results for MA 754 at Idaho National Laboratory

MA 754 exhibited relatively uniform corrosion, although near surface porosity developed, presumably from the diffusion of chromium out of the base metal. There was no evidence of spalling or metal dusting, however exposure times were too short to determine the long term behavior. Fine grain showed no discernable difference in corrosion behavior compared to the coarse grain specimens. Overall, they found no evidence that MA 754 is unsuitable for use in CO_2 Brayton cycle, however longer exposure tests are warranted to ensure breakaway corrosion processes, such as spalling or metal dusting, do not become active prior to the end of the intended life cycle.

MA 754 showed a higher corrosion rate than that of the I-617 at ~ 0.25 mm/year after 175 hours of exposure. I-617 also developed a black oxide layer that appeared to be more adhesive than the MA 754's layer. However I-617 had significant intergranular (IG) corrosion in the shorter exposure times. The IG corrosion had reached penetration of ~22 μm. Thus the possibility exists that long term exposure of I-617 could lead to film breakdown, spallation, and rapid corrosion. The tests did not prove this conclusively; therefore it was recommended that more long term tests be conducted.

Testing at MIT H. H. Uhlig Corrosion Laboratory

Prof. Ballinger's team, at MIT's H.H. Uhlig Corrosion Laboratory, has engineered a CO_2 corrosion loop for immersion (relatively stagnant flow) testing of several potential alloys for use in the S-CO_2 PCS. The most recent testing, conducted in July 2007, included the immersion of 316L stainless steel, EP823, MA956, MA957, PM2000, HT9, and T91 in high temperature (650°C) high pressure (12.5 MPa or 22 MPa) supercritical CO_2. To date, three short-term ($\leq$ 1000 hrs) tests have been conducted on these alloys. A summary of alloys tested is shown in table D-2. Future long-term (> 3000 hours) testing is planned with the possible introduction of additional metals. The temperature range will also be expanded to 500-750°C in order to test the chemistry range of CO_2/Fe_3O_4 stability. In the more distant future, the team plans on conducting corrosion and radiolysis experiments on flowing S-CO_2 inside and outside an operating reactor core.

For recent testing, two experimental systems were designed and built. Each system receives CO_2 from supply tanks containing 99.99% instrumentation grade CO_2 which is then

fed through a filter to a gas booster pump. The CO_2 is pumped into an autoclave made of alloy 625 (surrounded by a furnace) where the pressure and temperature are monitored and maintained. The high pressure (22 MPa) autoclave has a 1.0" ID, 3" OD, and is just over 60" long including pipe connections and heat sink. The furnace has three 8" hot zones (for a total of 24") where the CO_2 is heated to 650°C. The low pressure (12.5 MPa) autoclave has a 0.5" ID, 1.5" OD, and is 12" long. The furnace has one 12" heated zone, where about 4" of the CO_2 is uniformly heated to 650°C. Inside each autoclave is a sample train holding ~1 in^2 samples of each alloy to be tested. Both systems are connected to a residual gas analyzer (RGA) which detects the atomic mass of the particles carried in the CO_2 with a detectable range of 0-200 amu/charge.

The team is considering building their own purification system to allow the purchase of lower grade (less expensive) CO_2. Their purification system could include an O_2/H_2O getter like heated titanium, or steel wool as a sacrificial material to scavenge O_2 and H_20; desiccant for moisture absorption; a membrane filter; and/or a bypass loop for distillation using cryogenic sequestration.

Results:

The first test ("test 1") was conducted for 230 hours in the 12.5 MPa autoclave. Only 316L, EP823, MA956, and MA957 were tested. Of these alloys, 316L exhibited the greatest oxidation weight gain rate of 0.4284 mg/cm^2-day, while MA956 exhibited the least weight gain rate of 0.0194 mg/cm^2-day. EP823 and MA 957 fell in the middle with 0.0539 and 0.1386 mg/cm^2-day respectively.

From an X-ray photoelectron spectroscopy (XPS) analysis of SS 316L, EP823, and MA956 and an electron probe micro-analysis (EPMA) of MA957, the compositions of the oxide layers were determined. SS316 developed Si, Mn, and Fe oxides. The cross section also revealed a layer of Fe-Ni-Cr oxide [24.7 at% Fe, 17.6 Cr, 11.8 Ni, 42.8 O, 2.0 Mn, 1.1 Si] under the iron oxide [43.8 at% Fe, 55.3 O, 0.1 Mn, 0.1 Si]. EP823 analysis revealed the presence of Fe, Cr, Si, and Mn oxides. MA956 had Fe, Al, and Cr oxide layers, and MA957 had a dual layer Fe-Cr oxide consisting of a Cr-rich inner layer [15.2 at% Fe, 28.5 Cr, 55.6 O] under a Fe-rich outer layer [30.3 at% Fe, 12.8 Cr, 56.6 O]. From all the scanning electron

microscope (SEM) and atomic force microscopy (AFM) images taken, MA956 had the smoothest surface morphology.

Two additional tests were completed, but the full analysis of the results has not been completed to date. A 1000 hour test ("test 2") was conducted in the 12.5 MPa system, and another 200 hour test ("test 3") was conducted in the 22 MPa system.

Included in the analysis are readings of gas composition using a Residual Gas Analyzer (RGA). So far it seems that the RGA results from test 2 are inconclusive as no significant variance in the compositions of the CO_2 were seen between the autoclave inlet and outlet. The most probable cause for this was the arrangement of the RGA sampling locations. For test 2, the CO_2 was fed into and out of the autoclave via two concentric tubes. It was believed that the systems would stabilize and allow the CO_2 leaving the autoclave to be accurately measured. This arrangement was changed for test 3, with the RGA sampling locations on opposite ends of the autoclave. These test 3 RGA results are shown on figure D-4.

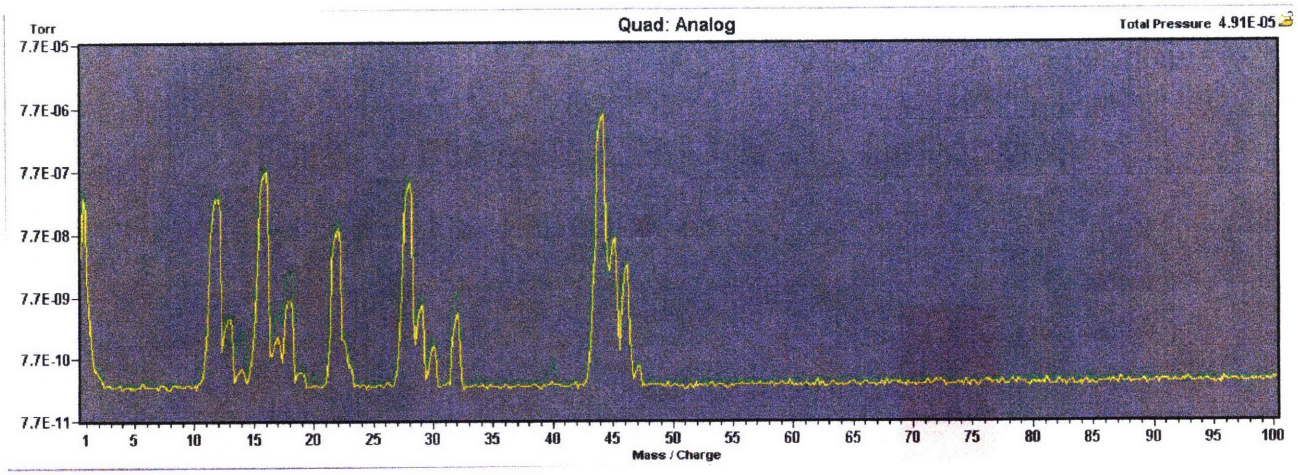

Figure D - 4 Comparison of 15 hour (yellow) data to 180 hour (green) data from corrosion test 3 at MIT H. H. Uhlig Corrosion Laboratory. Test conditions were 22 MPa at 650°C for 200 hours.

Referring to figure D-4, a variance in the autoclave outlet can be seen at two different times since data acquisition began. At 14, 17, 18, 20, 32, and 40 amu, the 180 hour data show a significant increase in counts. The observed changes in the RGA spectra are an indication of possible system contamination and/or reactions of some species (CO_2, CO, H_2O, O_2, etc.) with one mo more of the alloys tested. The possible contaminants causing

these peaks are shown in table D-1. However, these results are largely inconclusive at present. Future tests will include improvements to the system that will reduce the chances of contamination from external sources. Additionally, it may be necessary to run some control tests to see if these compounds are still detected; for example, running the same test without the presence of test samples.

Table D - 1 RGA analysis of corrosion test 3 at MIT H. H. Uhlig Corrosion Laboratory

Significant peak variance (amu/charge)	Possible Contaminants
14	CH_2, oil, solvents
17	OH, NH_3
18	H_2O (light)
20	H_2O (heavy)
32	O_2, CH_3OH (methanol)
40	C_3H_4, oil, solvents

Test 3 also included all seven alloys. By far, HT9 demonstrated the largest weight gain from oxidation formation. MA956 (once again) and PM2000 were nearly tied for the least weight gained. The daily weight gain rates from tests 1, 2, and 3 are plotted on figure D-5 for comparison. Initial conclusions are that the MA956 and PM2000 are very resistant to corrosion.

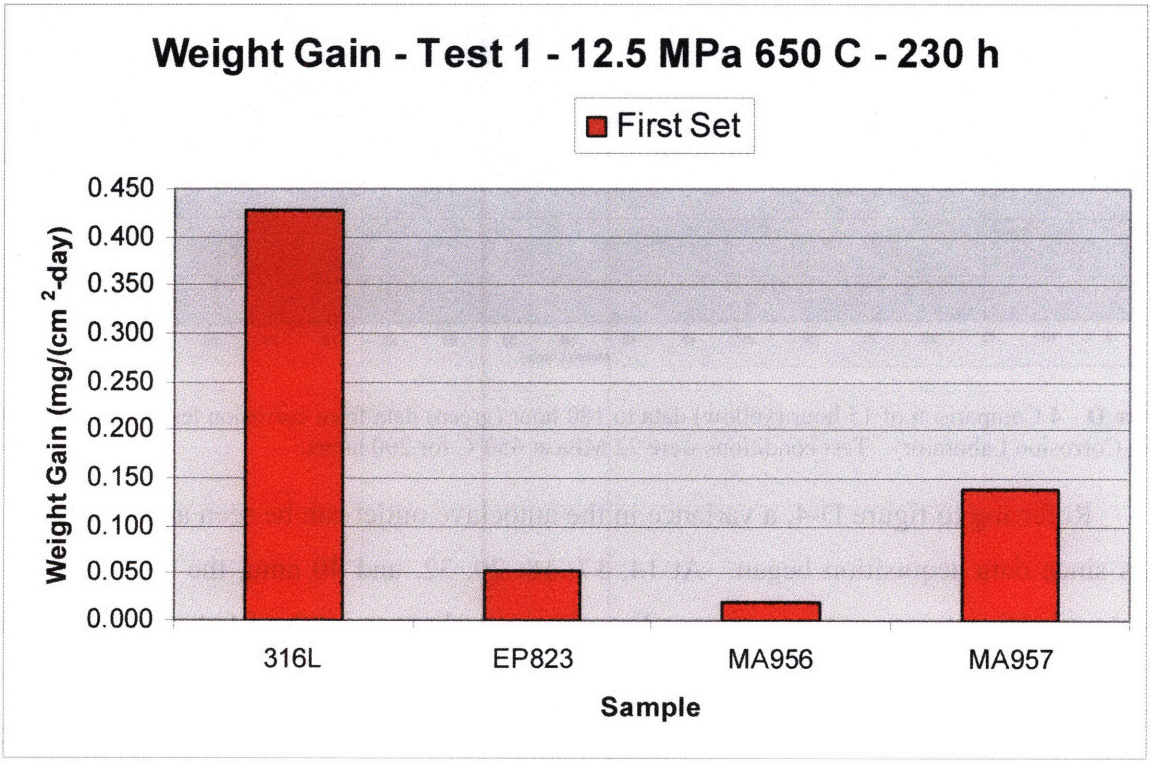

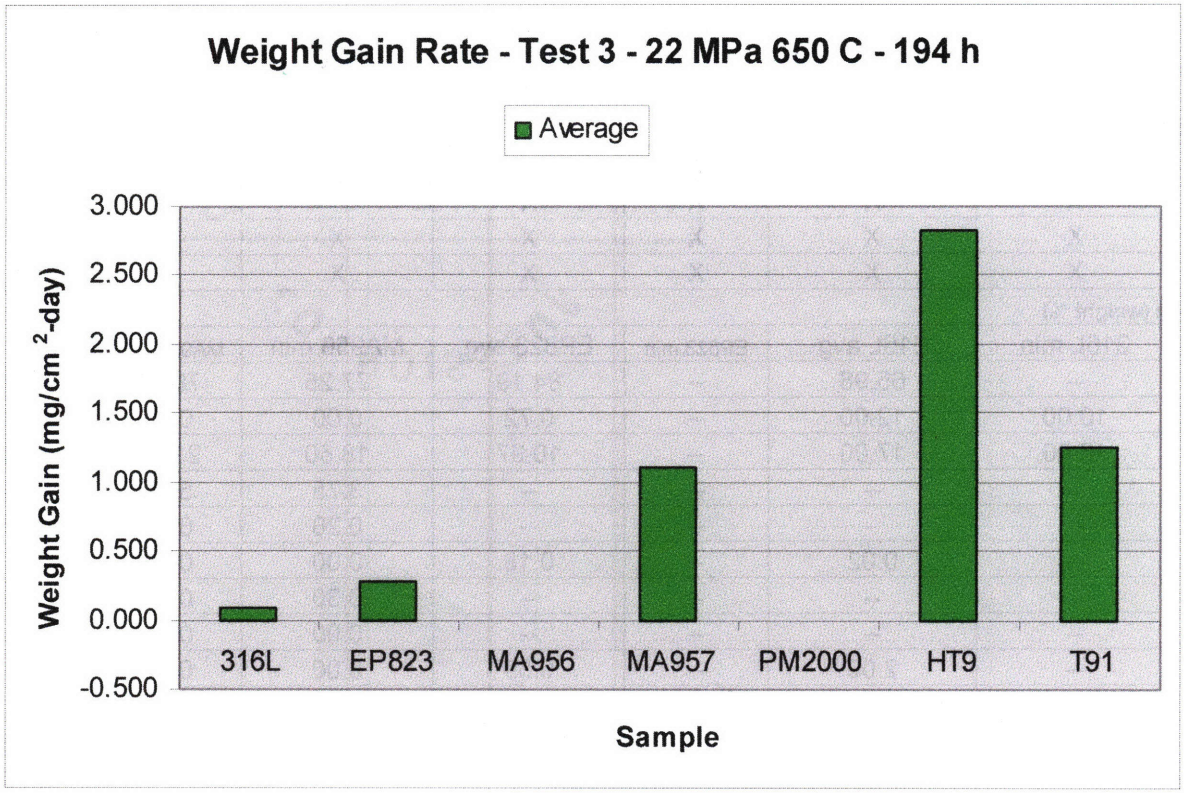

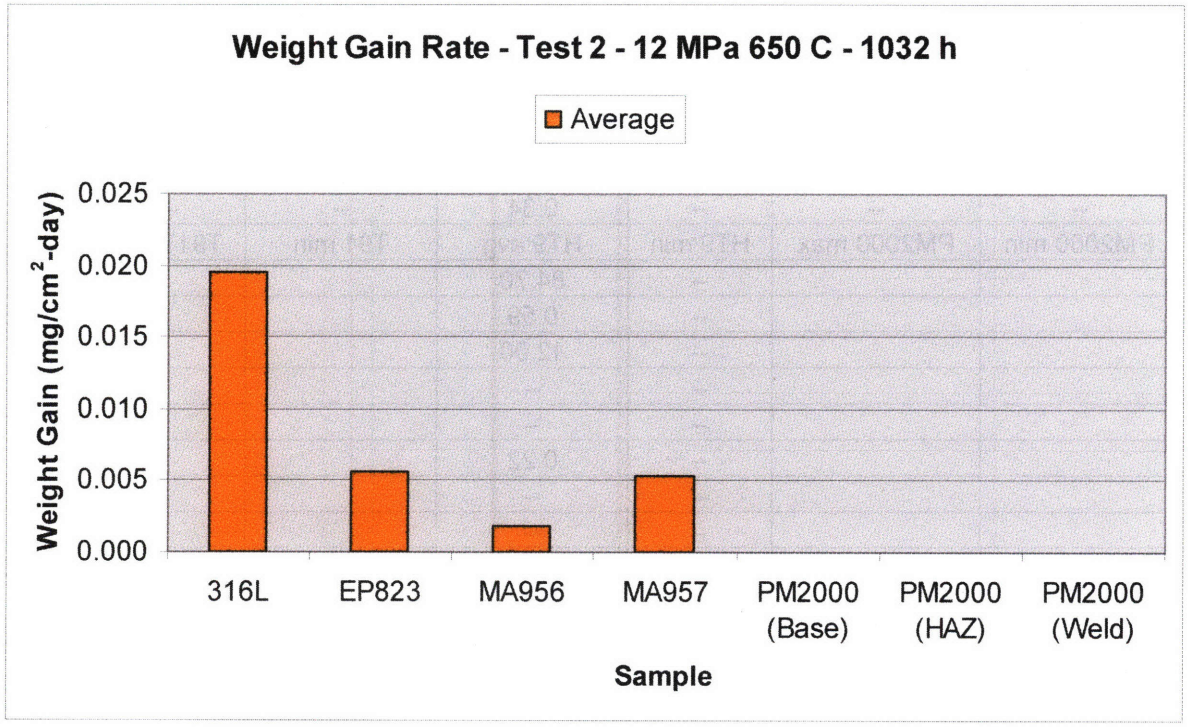

Figure D - 5 Comparison of weight gain rates for testing at MIT H. H. Uhlig Corrosion Laboratory. The alloys from test 1 (12.5 MPa) and test 3 (22 MPa) conducted for ~200 hours, and test 2 (12 Mpa) conducted for ~1000 hours.

Table D - 2 MIT H. H. Uhlig Corrosion Laboratory Testing Summary

Test #	Start Date	End Date	Duration (h)	Pressure (MPa)	Temperature (C)	Autoclave	Comment
1	11/4/05 7:00 PM	11/14/05 9:00 AM	230	12.5	650	small	
2	3/6/07 9:00 AM	4/18/07 9:00 AM	1032	12	650	large	
3	6/14/07 9:00 AM	6/22/07 11:00 AM	194	22	650	large	

Samples Run

Test #	316L	EP823	MA956	MA957	PM2000	HT9	T91
1	X	X	X	X			
2	X	X	X	X	X	X	X
3	X	X	X	X	X	X	X

Composition (weight %)

Element	316L min	316L avg	EP823 min	EP823 avg	MA956 min	MA956 max	MA957 min
Fe	--	65.98	--	84.19	77.25	70.08	84.86
Ni	10.00	12.00	--	0.72	0.00	0.50	0.10
Cr	16.00	17.00	--	10.97	18.50	21.50	13.49
Al	--	--	--	--	3.75	5.75	0.055
Ti	--	--	--	--	0.20	0.60	0.95
C	--	0.02	--	0.18	0.00	0.10	0.012
YO	--	--	--	--	0.30	0.70	0.19
Cu	--	--	--	--	0.00	0.15	--
Mn	--	2.00	--	0.59	0.00	0.30	0.05
Co	--	--	--	--	0.00	0.30	--
P	--	--	--	--	0.00	0.02	0.004
O	--	--	--	--	--	--	0.006
S	--	1	--	--	--	--	0.004
Mo	--	2	--	0.73	--	--	0.28
Si	--	--	--	1.21	--	--	--
W	--	--	--	0.64	--	--	--
V	--	--	--	0.33	--	--	--
Ce	--	--	--	0.1	--	--	--
Nb	--	--	--	0.34	--	--	--
Element	PM2000 min	PM2000 max	HT9 min	HT9 avg	T91 min	T91 max	MA957 max
Fe			--	84.70			83.10
Ni			--	0.59			0.15
Cr			--	12.00			14.19
Al			--	--			0.17
Ti			--	--			1.38
C			--	0.22			0.017
YO			--	--			0.2800
Cu			--	--			--
Mn			--	0.58			0.1200
Co			--	--			--
P			--	--			0.030
O			--	--			0.240
S			--	--			0.006
Mo			--	1.11			0.32
Si			--	0.30			--
W			--	0.50			--

HSC Chemistry® 5.1 Simulations of Core Materials for a Direct S-CO_2 PCS

Simulations of corrosion reactions for material in a 2400 MW_{th} direct S-CO_2 cooled GFR using HSC Chemistry® 5.1 were performed by Handwerk et al. [2007]. Unless otherwise stated, the following information was obtained from their publication.

Fuel

A uranium oxide tube-in-duct (TID) fuel assembly has been proposed for the direct S-CO_2-cooled core, but this type of assembly has never been fully designed, built, and tested. The design's peak fuel temperature is 1770°C. Figure D-6 helps to visualize the geometry of this new assembly design.

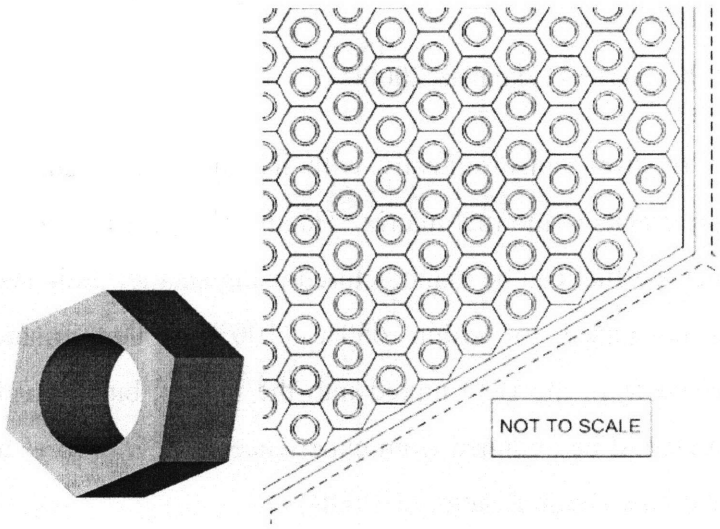

Figure D - 6 UO_2 fuel pellet (left) and quarter cross-section of the TID fuel assembly (right).

This inverted version of the typical triangular lattice pin-type assembly used in current GFRs has a possible Achilles heel; the coolant passes through the circular openings inside the bolt-shaped fuel pellets.

Fuel Material: The chemical reaction considered in the selection of uranium oxide for the fuel (instead of US or UC), was determined unlikely due to a positive Gibb's Free Energy (ΔG) at the expected fuel temperature ranges. HSC Chemistry® 5.1 was used to generate the following overall reaction:

$9UO_2 + 6CO_2(g) \rightarrow U_4O_9 + U_3O_8 + UO_3 + 6CO(g) + 0.5O_2 + UO_3(g)$

ΔG=+215kcal @ 1000C, ΔG=+85kcal @ 2000C

Diluents: Diluents are mixed into the fuel matrix and used for power shaping, similar to burnable poisons, but are neutronically benign. Their purpose is to slightly shift the fast fission neutron energy spectrum into a lower energy state, just slight enough as to reduce the cross section for fission in U^{238} and Pu^{240}. Another suggested purpose of diluents is to increase core heat capacity for increased decay heat removal in case of an accident [Thon, 2002]. Typical diluents are SiC, TiC, and BeO. In the case of the GFR, the BeO is preferred due to its positive ΔG for the reaction,

$3BeO + 3CO_2(g) \rightarrow BeCO_3 + BeO(A) + BeO(B) + 2CO(g) + O_2(g)$

ΔG=+124kcal @ 1000C, ΔG=+117kcal @ 2000C

However BeO tends to grow anisotropically with increased fast neutron fluence, which can lead to microscopic cracks in the fuel matrix. Handwerk suggests two methods of mitigating this problem; either the fuel can be manufactured using smaller grain sizes, or the operating temperature can be raised to within 650°C-1100°C. Unfortunately these characteristics were not derived from the BeO mixed into the matrix, but from pure BeO. Fortunately more information could be obtained from experience of BeO used as a reflector in the Southwest Experimental Fast Oxide Reactor (SEFOR).

Cladding

In the case of the TID fuel assembly discussed, the cladding material selected is an oxide dispersion-strengthened incaloy alloy MA956 [18.5-21.5%Cr, 3.75-5.75%Al, 0.2-0.6%Ti, 0.3-0.7%Y_2O_3]. Incaloy alloy MA956 was first fabricated for use as an aerospace superalloy. It has an outstanding resistance to prolonged exposure to up to 1300°C and melts at a high 1480°C. The alumina layer is also a barrier to carburization and sulfidation. The result is a reduction in carbon diffusion into the metal and adherence to the oxide, and the prevention of nickel sulfide. MA956 tubes are commercially available but tend to exhibit relatively poor circumferential creep strength due to current processing practices resulting in

a fine grain size in the transverse direction. Weldability is also a problem with this material. [M. A. Harper, 2001]

A 550°C core outlet coolant temperature means a cladding hot spot temperature of 700°C. For the 650°C core outlet temperature design, the peak cladding temperature will rise to 810°C -- still well below the capabilities of the incaloy MA956.

Reflectors

Radial: The S-CO_2 travels in the vertical direction through the core. Some of the S-CO_2 is diverted radially around the core and serves as the radial reflector.

Axial: Neutron reflection above and below the core must also be performed to lower the neutron leakage rate. Several elements/compounds were considered for this purpose: Ti, BeO, TiO_2, PbO, $ZrSi_2$, SiO_2, and CaO. Ti was selected based on many factors including its cross section for neutron scattering in the average fast energy spectrum expected (~0.47MeV), its coolant void reactivity (CVR) coefficient, as well as its ΔG for the following reaction:

$$6Ti + 6CO_2(g) \rightarrow TiO_2 + TiO_2(A) + 3C + 2C(D) + CO(g) + Ti_4O_7$$

ΔG=-552kcal @ 500°C, ΔG=-447kcal @ 1000°C, ΔG=-342kcal @ 1500°C

The negative ΔG found for Ti suggests a chemical reaction resulting in the formation of a passive film. Also beneficial, the CO produced will suppress the $CO_2 + UO_2$ reaction.

Pressure Vessel

Reactor Pressure Vessels (RPVs) tend to degrade in the presence of a high neutron fluence due to the production of vacancies, interstitials, dislocations and impurities. These defects tend to harden the material, thereby raising the NDT. The degree to which the NDT shifts is a function of RPV material, fluence, and temperature. This becomes a problem when the ductile to brittle transition temperature increases to a point at or above the shut down system temperatures. The defects also lower the Charpy upper shelf energy, meaning a reduction in the amount of energy the RPV can absorb prior to a ductile failure.

Further evaluation of chromium martensitic [2.25%Cr, 1%Mo] low alloy steels for use in the RPV is recommended due to cost, fabricability, and resistance to irradiation degradation (licensable NRC fast fluence limit of $5x10^{19}$ neutrons/cm^2). Pope, et al. [2006] on the other hand has suggested the possible use of a prestressed cast iron vessel (PCIV) which would require additional testing to protect its steel liner.

Control Assemblies

Boron carbide, is the third hardest material known to man, and it has been selected for use in the control assembly. The B_4C-CO_2 interaction considered was:

$$9.5CO_2(g) + 3B_4C \rightarrow 2B_2O_3 + 6.5C + 5C(D) + 2B_2O_3(G) + 2B_2O_3(A) + CO(g)$$

ΔG=-552kcal @ 500°C, ΔG=-489kcal @ 1000°C, ΔG=-377kcal @ 1500°C

The negative ΔG suggests that the B_2O_3 passive layer will form and thus needs to be analyzed. Analyses of other neutron absorbing materials, including W and Ca_3N_2, gave similar chemical activities. Handwerk suggested a possible method to reducing the likelihood of a chemical interaction between the control assemblies and the coolant is placement of the control assemblies into a shielded inert channel. However, helium gas buildup from the production of B-10 would be harder to accommodate. This topic remains in need of further evaluation.

Appendix E

As part of her 2007 MIT undergraduate research project, Yunzhi Wang provided a set of cryogenic tank specifications including tank sizing to meet the 150% PCS-full-power-mass storage capability, tank construction materials and thicknesses, and a refrigeration loop capable of removing heat from ambient conditions. Table E-1 documents her calculations for the system described in section 2.3 of this thesis, which is shown again here as figure E-1 and described below.

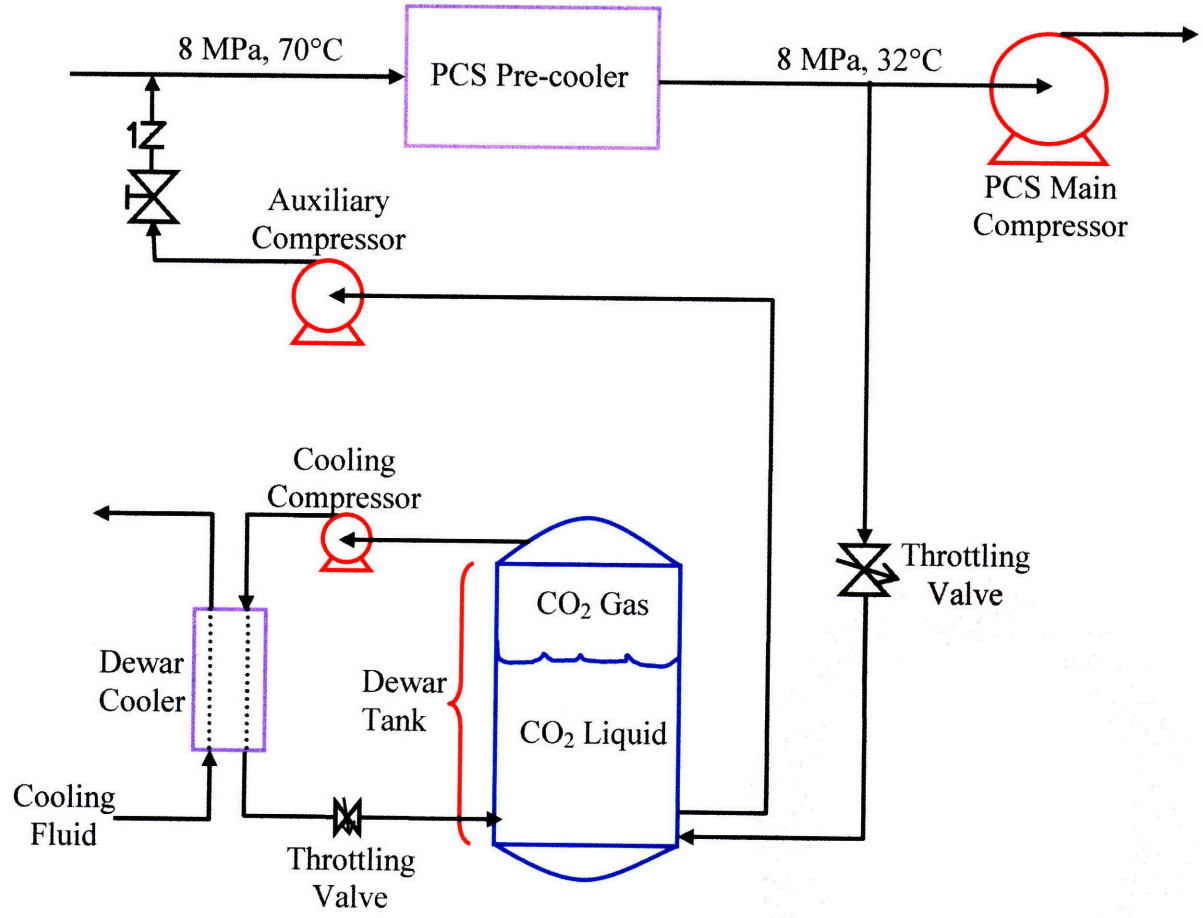

Figure E - 1 Proposed cryogenic system schematic for make-up, inventory control, and refrigeration

In summary, this cryogenic tank design has the capacity to hold 87,000 kg: enough carbon dioxide for a complete discharge or press-up of a 300 MW_e PCS loop plus 100 days of leakage make-up at 290 kg/day (0.5%/day). For a pressure and temperature of ~4 MPa and 5°C, the liquid density is about 896 kg/m^3. Around 3,000 kg of the CO_2 in vapor form

hovers over the liquid with a vapor quality of about 25% (25%(w) vapor, 75%(w) liquid), a density of close to 157 kg/m^3, and an occupied volume of 19.4 m^3 (20% of the tank volume). The 87,000 kg of liquid CO_2 occupies the lower 97 m^3 giving a total tank volume of 116.5 m^3. By optimizing the cylindrical tank dimensions for a minimum surface area to reduce heat losses, the height will need to be about twice the radius. Thus the selected internal tank dimensions are a 2.65 m radius and 5.29 m height. The full tank liquid level is then 4.41 m leaving 0.88 m of vapor height above the liquid.

The main structural component of the tank is steel. For a 0.05 m thick steel wall under these pressure conditions, the steel will experience less than a 230 MPa hoop and 115 MPa longitudinal stresses. Also, to reduce heat losses, the CO_2 held inside the tank is surrounded by polished aluminum sheets, which serve as a reflector. This reflector is perforated which allows pressure to equalize across the plates to prevent overstressing the metal. An insulation layer of 0.15 m thick Polyisocyanurate foam surrounds the aluminum reflector. The approximate cylindrical tank dimensions are 5.7 m outer-diameter and 5.7 m height. Figure E-2 shows a cross section and an isometric view of the cylindrical cryogenic tank.

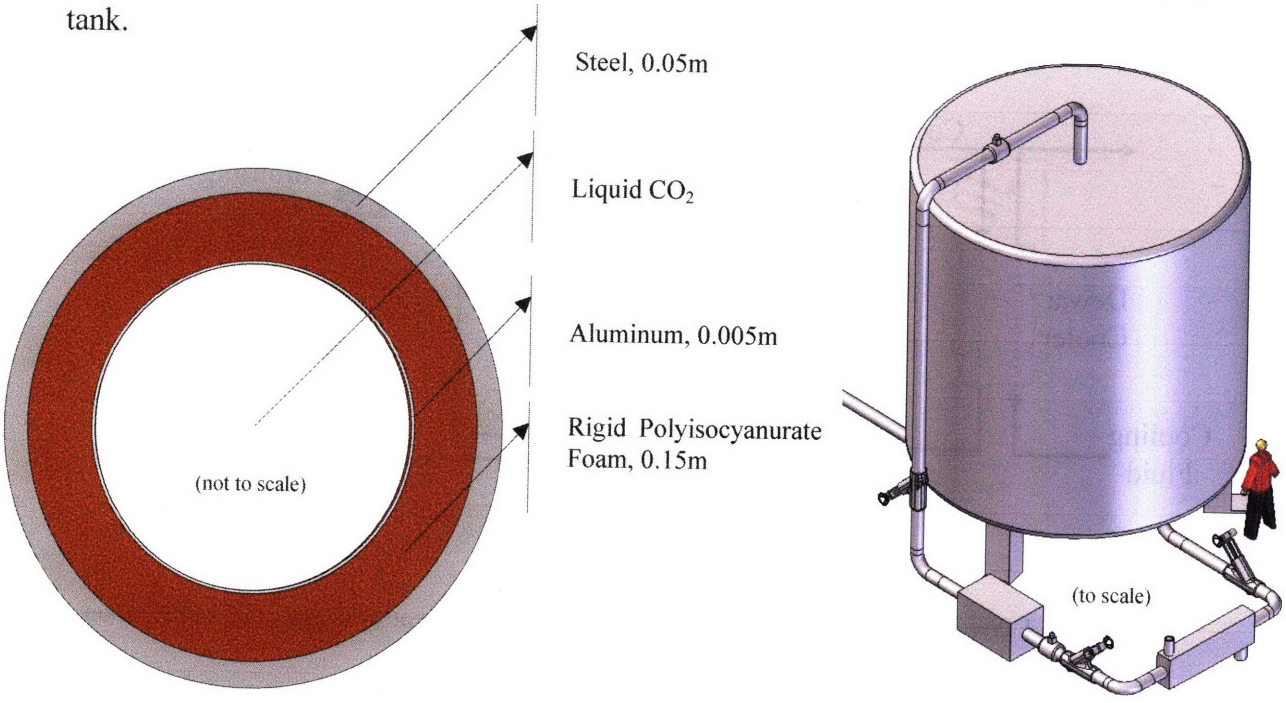

Figure E - 2 Cross section and an isometric view of cryogenic tank. Man is 6 ft tall.

For a tank designed in this manner and placed in a compartment at 0.1 MPa, 30°C ambient conditions, the total heat loss rate would be about 563 Watts. This ambient heat can be removed using a simple refrigeration loop, as shown in figure E-1, with a flow of about 3.7 g/sec. Assuming 80% efficiency, a 563 Watt compressor is required to compress the CO_2 to 7.72 MPa, 55°C. The CO_2 then passes through the cooling condenser where the outlet temperature drops to about 25°C, and is throttled back into the cryogenic tank.

The cooling fluid used in this estimate is R-134a: a very common, cheap, CFC free refrigerant. Also assuming 80% efficiency for the refrigerant loop compressor, rated at 367 W, the R-134a is compressed from 0.1 MPa, -26°C to 5 MPa, 129°C. The refrigerant is then fed into a condenser which removes heat collected in the Dewar cooler (or evaporator). Once the R-134a temperature is lowered to 25°C, it is throttled back to 0.1 MPa, -26°C as a 2-phase saturated liquid with quality of 32%. As the refrigerant re-enters the Dewar cooler, energy is absorbed increasing the quality to a 100% saturated vapor for entry into the compressor.

Based on Carstens' work [2007], the PCS CO_2 removal/addition flow rate does not exceed 10 kg/sec when using inventory control for power changes. Based on the 58,000 kg in the reference 300 MW_e PCS, this allows the removal of about 1% PCS inventory per minute. This flow rate was used to estimate the rating for an auxiliary compressor for re-injection into the pre-cooler inlet. An 80% efficient 427 kW auxiliary compressor is required to press up the CO_2 to the 7.72 MPa pressure at the pre-cooler inlet.

Table E - 1 Details of Cryogenic Tank Design Calculations

External (Ambient) Conditions

Pres	0.1	Mpa
Temp	30	C

Tank Capacity

Need	58,000	kg	for one loop
150%	87,000	kg	

m-dot into pre-cooler	10	kg/sec		**Conversions**

m-dot leakage			1	ft^3/min	equals	0.028316847	m^3/min
	0.5	% per day	1	ft^3/min	equals	0.000471947	m^3/sec
	290	kg/day	1	psi	equals	0.00685	Mpa
	0.003356481	kg/sec	for gas				
m-dot total			20	cfm	equals	4.72E-04	m^3/s
	10.00335648	kg/sec				1.10E+00	kg/s

Fluid Properties in Tank

Storage Conditions

Pressure	4	Mpa				
Temp	5	C		278	K	
Phase	saturated					
dens-l	896.39	kg/m^3	dens-g	156.67	kg/m^3	
h-l	2.12E+05	J/kg	h-g	4.18E+05	J/kg	
s-l	1.0431	J/g-K	s-g		J/g-K	
m-l	87,000	kg	m-g	3041.152	kg	
vol-l	97.05596894	m^3	vol-g	19.41119	m^3	
Quality	0.25393499					
Vol Tot	116.467163	m^3	20% void for evaporator coils			
Shape	Cylinder					
Radius	2.646516113	m				
Height	5.293032226	m				
Vol-liq	97.05596894	m^3				
Height-liq	4.410860188	m				
V-gas	19.41119	m^3				
Height-gas	0.882172038	m				

Tank Properties				
Insulation				
	Material	**Polyisocyanurate Rigid Foam Insulation**		
	k	0.026	W/m-C	(aged-after 6 months)
	thickness	0.15	m	http://www.dyplastproducts.com/ISO-C1-20_physical_prop.htm
	Radius	2.796516113	m	
	Height	5.593032226	m	
	Resist-sides	0.060337844		
	Resist-top	0.234819082		
	Resist-bot	0.234819082		
Structure				
	Material	**Aluminum**		
	k	250	W/m-C	http://www.engineeringtoolbox.com/thermal-conductivity-d_429.html
	emmisivity	0.09		for commercial aluminum sheet:
	Young's Mod	70	GPa	http://www.electro-optical.com/bb_rad/emissivity/matlemisivty.htm
	thickness	0.005	m	
	Radius	2.801516113	m	
	Height	5.603032226	m	
	Resist-sides	2.02965E-07		
	Resist-top	8.11136E-07		
	Resist-bot	8.11136E-07		
	Material	**Steel**	(regular steel)	
	k	46	W/m-C	http://www.engineeringtoolbox.com/thermal-conductivity-d_429.html
	emmisivity			
	Young's Mod			
	thickness	0.05	m	
	Radius	2.851516113	m	
	Height	5.703032226	m	
	Resist-sides	1.07321E-05		
	Resist-top	4.25511E-05		
	Resist-bot	4.25511E-05		

Heat In					
Tank Resistances					
	Rtot-sides	0.06034878			
	Rtot-top	0.23486244			
	Rtot-bottom	0.23486244			
Liquid Resistance				Gas Resistance	
Tank Resistance				Tank Resistance	
	Rsides	0.04667518		Rsides	0.013673604

Fluid Resistance (sides)		
Tside	7	
g	9.8	
Beta	0.00359712	
L	4.41086019	height of liq
L^3	85.8163179	
mu	0.00013933	all properties at Tbulk
rho-liq	896.39	
nu	1.5543E-07	
k	0.10438	
cp	2.7222	
alpha	4.2776E-05	
Tside-Tb	2	
Ra	9.0998E+11	turbulent nat conv
Pr	0.00363369	
psi	0.006622784	
Nu	274.0910957	
h	10.81029827	
Resist	0.001261202	

Gas Resistance (sides)		
Tside	13	
g	9.8	
Beta	0.003663004	
L	0.882172038	height of vapor
L^3	0.686530543	
mu	1.31E-05	all properties at Tbulk
rho-gas	156.67	
nu	8.3711E-08	
k	0.015093	
cp	1.2893	
alpha	7.47198E-05	
Tside-Tb	8	
Ra	31520643954	turbulent nat conv
Pr	0.001120332	
psi	0.002151	
Nu	65.31379	
h	0.372483	
Resist	0.183015	

Air Resistance (sides)		
Text	25.77	
g	9.8	
Beta	0.00330033	
L	4.41086019	
L^3	85.8163179	
mu	1.87E-05	
rho	1.1492	
nu	1.63E-05	
k	2.64E-02	
Cp	1.01E+03	
alpha	2.29E-05	
delta T	4.23	
Ra	3.15E+10	turb nat conv
Pr	7.13E-01	
psi	0.347754169	
Nu	3.34E+02	
h	2.00E+00	
Resist	6.23E-03	

Air Resistance (sides)				
Text	24			
g	9.8			
Beta	0.003663004			
L	0.882172038			
L^3	0.686530543			
mu	0.000018733			
rho	1.1492			
nu	1.63009E-05			
k	0.02644			
Cp	1006.7			
alpha	2.28542E-05			
delta T	6			
Ra	396914588.5	lamnat convec		
Pr	0.713256849			
Turbulent		Laminar		
psi	0.347754	psi	0.347754	
Nu	80.71105	Nu	73.30182	
h	2.41903	h	2.196964	
Resist	0.026155	Resist	0.028798	

Match Q-dot			Match Q-dot			
	fluid to outside surf	433.28264		fluid to outside surf	96.59945176	
	inside surf to air	434.042128		inside surf to air	400.2638464	
	dif	**-0.75948845**		dif	**303.6643946**	
Q-dot-sides	**433.2826397**	**W**				

Q-dot Top and Bottom				Fluid Resistance (top)		
	Fluid Resistance (bottom)			X	0.166548357	
	Ra	1.9656E+11		Ra	8.51057E+11	
	Nu	813.998689		Nu	19.74798028	
	h	38.5254483		h	0.112622124	
	Resist	0.00117965		Resist	0.403531394	

Air Resistance (bottom)			Air Resistance (top)		
Ra	8.51E+09		Ra	13.40E+09	
Nu	2.86E+02		X	0.323572361	
h	2.65E+00		Nu	21.4800335	
Resist	1.48E-02		Resist	0.199168465	

Tank Resistance (bottom)				Tank Resistance (top)			
	Resist	4.26E-05			Resist	0.234862445	
	R-tot	2.51E-01		R-tot	0.837562303		
	Q-dot-bot	99.67693853	W	Q-dot-top	29.84852578	W	
Q-dot total	**562.808104**	**W**					

Tank Mechanical Calculations

Stress

Steel:			Aluminum: (if no perforation)		
hoop stress	228121289	Pa	hoop stress	2.241E+09	Pa
longitudinal	114060644	Pa	longitudinal	4.482E+09	Pa

Refrigeration Loop, Carbon Dioxide side

	Q-dot to remove		562.808104	W

Compressor (assume ideal)

	Inlet Conditions				Outlet Conditions		
	T	5	C		T	55	C
	P	4	Mpa		P	7.72	Mpa
	phase	sat vap			phase	supercrit	
	dens-g	156.67	kg/m^3		dens	193.06	kg/m^3
	h-g	4.18E+05	J/kg		h	4.52E+05	J/kg
	s-g	1.8135	J/g-K	isentropic	s	1.8135	J/g-K

	Power	if ideal	1.26E+02	W
		80% eff	1.57E+02	W

Condenser

	Inlet Conditions			Outlet Conditions		
	T	55	C	T	25	C
	P	7.72	Mpa	P	7.69	Mpa
	phase	supercrit		phase	liq	
	dens	193.06	kg/m^3	dens	767.84	Kg/m^3
	h	4.52E+05	J/kg	h	2.65E+05	J/kg
	s	1.8135	J/g-K	s	1.2085	J/g-K

Throttle

	Inlet Conditions			Outlet Conditions		
	T	25	C	T	5	C
	P	7.69	Mpa	P	4	Mpa
	phase	supercrit		phase	2-phase	
	dens	767.84	Kg/m^3	dens	708.5492	Kg/m^3
	h	2.65E+05	J/kg	dens-liq	896.39	
	s	1.2085	J/g-K	dens-vap	156.67	
				h	2.65E+05	J/kg
				h-liq	2.12E+05	
				h-vap	4.18E+05	
				quality	0.253935	

Q-dot removed

	1.53+05	W/(kg/s)	5.63E+02	W	
m-dot	3.68E-03	kg/s			

Refrigeration Loop, Refrigerant side

Q to remove	562.8081	W
M-dot	1	kg/s
Refrigerant	R-134a	
Heat Removed	1.48E+05	W/(kg/s)
Mass Flow Rate	3.81E-03	kg/s

Evaporator

		Inlet Conditions		Outlet Conditions	
	Pressure	0.1	Mpa	0.1	Mpa
	Temperature	-26.361	C	-26.361	C
	Phase	sat liq		sat vapor	
	Quality	0.320		1	
	Specif Vol	6.65E-02	m^3/kg	6.65E-02	m^3/kg
	liq	0.0072593	m^3/kg		
	gas	0.19256	m^3/kg		
	Density	1.50E+01	kg/m^3	5.19E+00	kg/m^3
	Enthalpy	2.35E+05	J/kg	3.83E+05	J/kg
	liq	1.65E+05	J/kg		
	gas	3.83E+05	J/kg		
	Entropy	1.1490549	J/kg-K	1.7475	J/kg-K
	liq	0.86756	J/g-K		
	gas	1.7475	J/g-k		

Compressor

		Inlet Conditions		Outlet Conditions	
Pressure		0.1	Mpa	5	Mpa
Temperature		-26.361	C	129	C
Phase		sat vapor		supercrit	
Quality		1			
Specif Vol		0.0665374	m^3/kg	0.0035817	m^3/kg
Density		5.1931865	kg/m^3	279.19703	kg/m^3
Enthalpy		3.83E+05	J/kg	4.60E+05	
	liq	1.13E+05	J/kg		
	gas	435.3	J/kg		
Entropy		1.7475	J/kg-K	1.7475	J/kg-K
Power		7.70E+04	W/(kg/s)	power per kg/s mass flow rate	
		9.63E+04	W/(kg/s)	power assuming 80% efficiency	
		366.903	W	for 3.81 kg/sec at 80% efficiency	

Condenser

	Inlet Conditions		Outlet Conditions	
Pressure	5	Mpa	5	
Temperature	129	C	25	C
Phase	supercrit		liquid	
Quality			0	
Density	279.19703	kg/m^3	1230.5	kg/m^3
Enthalpy	4.60E+05	J/kg	2.35E+05	J/kg
Entropy	1.7475	J/kg-K	1.1092	J/kg-K

Throttle

		Inlet Conditions		Outlet Conditions	
Pressure		5	Mpa	0.1	Mpa
Temperature		25	C	-26.361	C
Phase		liq		2-phase	
Quality		0		0.320	
Specific Vol				6.65E-02	m^3/kg
	liq			7.26E-03	m^3/kg
	gas			1.93E-01	m^3/kg
Density		1230.5	kg/m^3	1.50E+01	kg/m^3
Enthalpy		2.35E+05	J/kg	2.35E+05	J/kg
	liq			1.65E+05	J/kg
	gas			3.83E+05	J/kg
Entropy		1.1092	J/kg-K	1.15E+00	J/kg-K
	liq			0.86756	J/g-K
	gas			1.7475	J/g-K

Compressor into the Pre-cooler						
Inlet Conditions				Outlet Conditions		
T	5	C		T	55	C
P	4	Mpa		P	7.72	Mpa
phase	sat vap			phase	vapor	
dens-g	156.67	kg/m^3		dens	193.06	kg/m^3
h-g	4.18E+05	J/kg		h	4.52E+05	J/kg
s-g		J/g-K	isentropic	s		J/g-K

Power	if ideal	34.2E+04	W	for mass flow rate of 10 kg/s
	80% eff	42.7E+04	W	

Cryogenic System Specifications Summary				
Tank Geometry				
	Height	5.293032226	m	
	Radius	2.646516113	m	
Tank Materials		thickness		
	Polyisocyanurate Rigid Foam Insulation	0.15	m	
	Aluminum	0.005	m	
	Steel	0.05	m	
Tank Stresses				
	Steel:			
	hoop stress	228121289	Pa	
	longitudinal	114060644	Pa	
	Aluminum (no perf)			
	hoop stress	2241212890	Pa	
	longitudinal	4482425780	Pa	
Tank Storage Conditions				
	Pressure	4	Mpa	
	Temp	5	C	
	Fluid Quality	0.253934993		percentage gas
	Heat Loss	562.808104	W	
Refrigeration Loop, R-143a				
	Mass Flow Rate	3.81E-03	kg/s	
	Compressor Power	366.903	W	assuming 80% eff
	Compressor Pressure	5	Mpa	
Refrigeration Loop, CO_2				
	Mass Flow Rate	3.68E-03	kg/s	
	Compressor Power	563	W	assuming 80% eff
	Compressor Pressure	7.72	Mpa	
Compressor into Pre-cooler				
	Mass Flow Rate	10	kg/sec	
	Outlet Pressure	7.72	Mpa	
	Power	4.27E+04	W/(kg/s)	Watts per kg/s flow rate, 80% eff
		4.27E+05	W	for 10 kg/sec, 80% eff

Appendix F

There are many grades of CO_2 available from distributors. Minimum purity levels and maximum concentrations for certain impurities are regulated in the United States by the Compressed Gas Association (CGA), and internationally by the International Organization for Standardization (ISO) 9001 2000. Table F-1 is from the CGA Standards Publication G-6.2, Commodity Specification for Carbon Dioxide. It shows the limits on impurities to qualify for certain grades of CO_2, also called quality verification levels (QVL), to meet minimum CGA standards. For blank fields, the concentration is not to be assumed zero; however a maximum level is just not specified for that particular grade. QVLs E through I are liquid CO_2, while J is the dry ice form.

It is the supplier's responsibility to ensure that deliverable CO_2 meets the minimum CGA standards; however it is recommended that the customer regularly review analytical records available from the supplier to ensure quality is maintained. Additional quality tests can also be routinely performed in a laboratory as agreed upon by the supplier and customer. Table F-2 is a compilation of some grades available from a few local distributors, along with some of the impurity levels and costs. Prices currently vary from $0.50 to $40 per kilogram. Keep in mind that CO_2 prices shown are for delivery to the Cambridge area, and can vary dramatically for other intended destinations [Jones, 2007]. Again, for blank fields, the concentration is not to be assumed zero; however a maximum level is just not specified for that particular grade.

The purity specifications offered by a distributor are not the only ones available. It is possible to special order a specific composition of CO_2 and maximum impurities from their processing plant; however the price will obviously fluctuate. CO_2 prices are already quite volatile at present [Jones, 2007].

Table F - 1 Directory of limiting characteristics to meet CGA QVLs. Units in ppm(v) unless otherwise stated. [CGA, 2004]*

Limiting characteristics	E	G	H	I	J
Carbon dioxide min. % (v/v)	99	99	99.5	99.9	
Acetaldehyde		0.5	0.5	0.2	
Ammonia	25			2.5	
Acidity				To pass JECFA test [1)]	
Benzene				0.02	
Carbon monoxide	10 (vapor) [2)]		10	10	
Carbonyl sulfide			0.5	[3)]	
Hydrogen cyanide				None detected [4)]	
Methanol				10	
Nitric oxide	2.5 (vapor) [2)]		5 (total of NO + NO_2)	2.5	
Nitrogen dioxide	2.5			2.5	
Oxygen		50	50	30	
Phosphine [5)]				0.3	
Sulfur dioxide	5		5	[3)]	
Total sulfur		0.5	0.5	0.1 [3)]	
Total hydrocarbon content (as methane)		50	50	50 max including 20 max of nonmethane hydrocarbons	
Hydrogen sulfide	1 (vapor) [2)]		0.5 (vapor)	[2)]	
Color					White opaque
Nonvolatile residues (wt/wt)		10	10	10	500
Oil/grease (wt/wt)				5	
Odor/taste	Free of foreign odor or taste				
Water	200	32	20	20	
Dew point °F	−33	−61	−68	−68	
°C	−36.1	−51.7	−55.6	−55.6	

NOTE—A blank indicates no maximum limiting characteristic.

1) Due to lack of sensitivity, this test is not required if the assay results are acceptable.

2) The use of vapor samples is required for USP. Also, the detection of impurities is determined based on the physical characteristics of the individual impurity and need to accurately represent the physical partitioning of impurities.

3) If the total sulfur content exceeds 0.1 ppm (v/v) as sulfur, then the species shall be determined separately and the following limits apply:

Carbonyl sulfide	0.1 ppm (v/v) max
Hydrogen sulfide	0.1 ppm (v/v) max
Sulfur dioxide	1.0 ppm (v/v) max

4) Applies only to carbon dioxide from coal gasification and combustion sources. Current detection level is 0.5 ppm.

5) Applies only to carbon dioxide from phosphate rock sources.

Table F - 2 Compilation of CO_2 grades, impurity concentrations, and est. cost from a few distributors. Current as of August 2007.

		Maximum Impurity Level (ppm(v) unless otherwise stated)											
Grade	Purity (%)	H_2	O_2	H_20	THC (CH_4 eq)	N_2	CO	Ar	Total Halocarbons	Acetaldehyde	Total Sulfur	Non-volatile Residue	$/kg
Airgas													
G	99.0		50	32						0.5	0.5	10 (%)	
CP	99.9			130									
Bone Dry	99.9			10									0.97
Anaerobic[3]	99.9		10*					10*					2.42
Coolant[2]	99.99		29	30	20	71							
Instrument/Coleman	99.99		20	10	10	70							2.31
Laser	99.99		20	10	10	70							
Laser Plus	99.995		10	5	1								
Research	99.998		1*	3	1	5	1*	1*					12.07
Research Plus	99.999		1	2	½	4							
SFE	99.9995		½*	2	0.5	2	½*	½*					16.83
SFE/SFC	99.9999			250 ppb	10 ppb				1 ppb				21.48
Matheson Trigas													
Commercial (CP)	99.5		860	720		3420							2.02
Bone Dry	99.8		500*			500*						5 ppm(oil)	2.14
Instrument	99.99		20			50							2.83
Ultra High Purity (UHP)	99.995		10	5	5	20							8.30
Research	99.999	1	1	2	4	1	0.2						10.36
SFC	99.999		5	1	4	5			50 ppb				13.45
PraxAir (Middlesex Gas Industries in Massachusetts)													
3.0	99.9												1.39
Anaerobic	99.99		10										
Instrument	99.99		15	10									
Semiconductor Process Gas	99.99		10	10	5	50							
Laser Star	99.995		5	5	1								
Semiconductor Process Gas	99.998	0.5	2	3	4	10	0.5						
Research	99.998		2	3	4	10	0.5						7.36
Supercritical Fluid Chromatography	99.998	0.1	5	1	2&50**	10	0.1						
Supercritical Fluid Extraction	99.999	0.1	2	0.5	2&10**	5	0.1		100 ppb				28.23
Laser Star 5.0	99.999		5	3	1								
Laser Star 5.5	99.9995		5	0.5	10 ppb				100 ppt				

Notes:

1. A blank indicates no maximum limit specified.
2. Airgas Coolant Grade $O_2 + N_2 < 100$ ppm(v)
3. If Airgas uses a dedicated Oxygen analyzer for the Anaerobic Grade, the Ar specification is eliminated
4. * means that total components must be less than limit specified
5. ** means total extractable hydrocarbons (as Dodecane) < given ppb, in addition to 2 ppm limit on THC (as CH_4)

Appendix G

Leak detectors generally use mass spectrometry. Since very few compounds ionize down to a mass of 2, helium is commonly used for leak detection. It has been proposed that He gas added to the S-CO_2 PCS coolant will make leak detection easier due to the faster diffusion and effusion of the helium atoms, and less ambiguous due to the lower average background levels of He.

Helium leak detectors have been designed with an ability to detect He levels from as low as 2 ppm to roughly 300 ppm. Since background levels are generally about 5 ppm, an estimate of 25 ppm detectability was used in this calculation. Using the 1200 MW_e direct S-CO_2 PCS as a reference, one can calculate that less than 0.5 %(v) is more than sufficient for a 25 ppm(v) helium leak detector to detect one day's worth of 0.5% leakage.

According to Pope [2006], the 1200 MW_e direct cycle will have about 330,000 kg CO_2 (including the reactor and four loops). At 0.5% leakage per day, about 1,650 kg will be emptied into the containment building daily. (This calculation ignores the introduction of fresh air by the ventilation system) Once the CO_2 reaches the surrounding atmosphere in the containment (STP conditions), its density will be 1.836 kg/m^3 (assuming ~ pure CO_2) leading to about 900 standard cubic meters of coolant dumping into the containment over the course of one day.

The volume of the containment was also estimated. Using the dimensions shown in figure G-1, the containment volume (neglecting machinery space) is about

$$\pi \cdot r^2 \cdot h + \frac{4}{6}\pi \cdot r^3 = \pi \cdot 30m^2 \cdot 30m + \frac{4}{6}\pi \cdot 30m^3 = 141{,}300 \text{ m}^3$$

For 25 ppm(v) He, or 0.0025% by volume, this means that the helium would need to occupy a total of about 3.54 m^3 dispersed within the 141,300 m^3. If the PCS is supplying 900 m^3 daily due to leakage, then the addition of 0.4% He by volume would provide the 3.54 m^3 needed to be detectable after one day. Therefore by adding at least 0.4 %(v) He to the coolant, any leakage above the expected 0.5% per day could be detected. To add another measure of conservatism, the suggested He addition is rounded to 0.5 %(v).

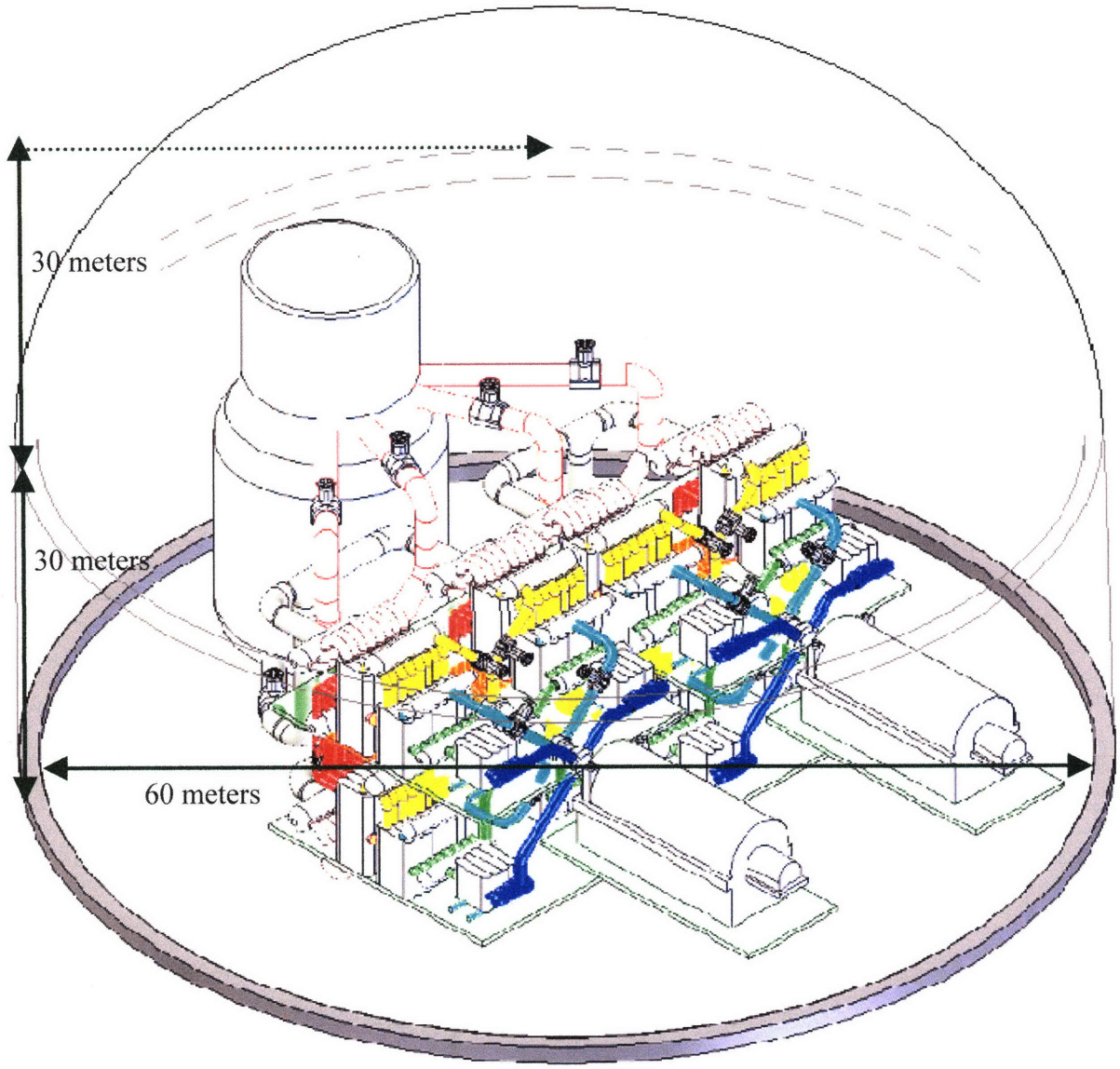

Figure G - 1 Isometric view of the 1200 MW_e direct S-CO_2 PCS with a containment superposition. Measurements for containment are approximate.